ABSTRACT

Title of Dissertation:	GRAIN-SCALE ANISOTROPIC STUDY OF TENSILE VS. SHEAR MECHANICAL CONSTITUTIVE AND FATIGUE BEHAVIOR IN OLIGOCRYSTALLINE SAC305 SOLDER JOINTS
	Abhishek Nitin Deshpande, Doctor of Philosophy, 2021.
Dissertation directed by:	Professor Abhijit Dasgupta, University of Maryland.

Solder joints in microelectronic assemblies experience a multiaxial combination of cyclic extensional and shear loads due to combinations of thermal expansion mismatch and flexure of printed circuit assemblies (PCAs) during thermal cycling or during vibrational loading of constrained PCAs. Although, a significant amount of research has been conducted to study cyclic fatigue failures of solder joints under pure-shear loading, most of the current literature on cyclic tensile loading of solders is on long dog-boned monolithic solder coupons. Unfortunately, such coupon specimens do not capture the critical interactions between key micro-scale morphological features (such as grain orientation, grain boundaries, intermetallic compounds [IMCs] and substrates) that are believed to play important roles in the fatigue of functional solder joints under life-cycle loading. Therefore, Part I of this study uses a combination of experiments and finite element analysis to investigate the differences in mechanisms of cyclic fatigue damage in Sn-3.0Ag-0.5Cu (SAC305) few-grained (oligocrystalline) microscale solder joints under shear, tensile and multiaxial

loading modes at room temperature. Cyclic fatigue durability test results indicate that tensile loads are more detrimental compared to shear loads. Tensile vs. shear loading modes are found to cause distinctly different combinations of interfacial damage vs. internal damage in the bulk of the solder (transgranular and intergranular damage), which correlates with the differences observed in the resulting fatigue durability. The test results also confirm that this type of multimodal fatigue damage cannot be modeled with the traditional approach of a power-law dependence on the cyclic amplitude of equivalent deviatoric strain. Instead, multiaxial fatigue damage results are seen to be affected not only by the cyclic equivalent strain amplitudes, but also by the severity of the stress-triaxiality, as hypothesized in models such as Chaboche model.

Estimating the true deviatoric strains and triaxiality ratios at the failure sites is not a trivial task in typical oligocrystalline SAC305 solder joints, because the strong anisotropy of the individual grains - and the interactions of such grains with surrounding grains as well as with the interfacial boundaries - make the strain field unique in each joint. Thus, the current approach of modeling solder joints as homogenous isotropic structures, are clearly inadequate because they fail to capture the true grain-scale stress fields at the failure sites. The joint-to-joint variation in the grain morphology leads to variability in fatigue damage accumulation rates under cyclic loading. Part II of this study thus focuses on grain-scale study of the fatigue results presented in Part I, by: (a) characterizing multi-scale anisotropic elastic-plastic properties of SAC305 single crystals, using a hybrid combination of experiments and finite element simulation, (b) applying a grain-scale parametric study to explain the variability seen in Part I, in the bimodal fatigue failures under multiaxial cyclic loading.

The anisotropic elastic-plastic properties in Part IIa were determined by conducting monotonic tensile and shear tests on SAC305 single crystal specimens. The anisotropic elastic behavior is modeled using anisotropic elastic stiffness constants for SAC305, whereas anisotropic plasticity is modeled using Hill's potential in conjunction with a Holloman-type power-law plastic constitutive model. Microstructurally motivated scaling factors are empirically developed, to assess the effect of dendritic and eutectic microstructural features on single-crystal stress-strain properties. This facilitates extrapolation of constitutive properties across different cooling rates and different isothermal aging protocols. Additional empirical scaling factors are also developed to account for the influence of characteristic grain sizes and grain aspect ratios (relative to principal loading directions). The parametric study in Part IIb, was conducted using the anisotropic properties of Part IIa, to quantify the effect of grain anisotropy on variability in cyclic mechanical fatigue curves of SAC305 solder. This study demonstrates an efficient computational approach for determining variability in mechanical response and fatigue behavior of Sn-rich solder joints, thereby reducing the time and costs associated with physical testing.

GRAIN-SCALE ANISOTROPIC STUDY OF TENSILE VS. SHEAR MECHANICAL FATIGUE IN OLIGOCRYSTALLINE SAC305 SOLDER JOINTS

by

Abhishek Nitin Deshpande

Dissertation submitted to the Faculty of the Graduate School of the
University of Maryland, College Park, in partial fulfillment
of the requirements for the degree of
Doctor of Philosophy
2021

Advisory Committee:
Professor Abhijit Dasgupta, Chair
Professor Bongtae Han
Professor Patrick McCluskey
Dr. Michael Osterman
Professor Sung Lee (Dean's Representative)

Dedication

To

My father Mr. Nitin Deshpande and my mother Mrs. Aboli Deshpande for their patience, support, love and hard work which has brought me here.
My lovely wife Sneha Karandikar for her love, encouragement, faith and sacrifices throughout this hard journey.
My father-in-law Mr. Sudhakar Karandikar and my mother-in-law Mrs. Anita Karandikar for their love and support.

Acknowledgments

I feel deeply fortunate to have Dr. Abhijit Dasgupta as my Ph.D. advisor. I am indebted to him for mentoring and nurturing me with his vast knowledge, wisdom and experience during this challenging journey. My work wouldn't have been accomplished if it weren't for Dr. Dasgupta's scientific approach, sanity checks and timely advice. I am sincerely grateful to him for providing a supportive, collaborative and intellectual research environment, which helped me improve my research and social skills. I thank him for his quality guidance and career counseling. He has made me a better researcher and engineer.

I would like to thank my dissertation committee members Prof. Bongtae Han, Prof. Patrick McCluskey, Dr. Michael Osterman and Prof. Sung Lee. I would like to thank them for serving in my dissertation committee and providing valuable suggestions to improve my dissertation research. In addition, I thank Dr. Ulrich Becker from Robert Bosch Gmbh, for his valuable feedback and for funding the project through these years.

I am grateful to Prof. Hugh Bruck for assisting with his DIC system, Prof. Sarah Penniston-Dorland for letting me use her cross-polarized microscope, Dr. Jiancun Rao for helping me with EBSD analysis. I would like to thank Dr. Robert Utter and Mr. Majid Aroom for their valuable guidance during my experiments throughout my doctoral studies. I am deeply grateful to Dr. Sandeep Tonapi for inspiring me to pursue a career in the field of electronics packaging.

I thoroughly enjoyed the support and company of awesome CALCE lab-mates over the years- Dr. Qian Jiang, Dr. Jonathan Kordell, David Leslie, Dengun Chen, Dr. Hao Huang, Dr. Subramani Manoharan, Dr. Saurabh Saxena, Guruprasad Pandian, Nripendra Patel, Manuel Bascolo, Aniket Bharamgonda, Idowu Olatunji, Biehan Zhao, Prabhat Janamanchi, Xiao Lin and Neil Dalal. I would also like to thank all the interns (Christoph, Marc, Dennis, Sebastian, Roman, Hannah and Mohamed) who assisted me in my experimental work over the years. It wouldn't have been possible without their hard and painstaking efforts with fabricating specimens and grinding-polishing those specimens. My lab mates and interns have helped me smoothly cruise through my graduate studies.

Table of Contents

List of Tables

List of Figures

Chapter 1 : Introduction

This chapter consists of background, problem statement, literature review, gaps in literature and scope.

1.1.Background and Problem Statement

Complex electronic packaging designs based on SysMoore (or 'more-than-Moore') have driven heterogeneous integration (HI) of different components and functionality into a single package. Heterogeneous integration has led to miniaturization of different components as well as multiple levels of micro-scale solder interconnects within the HI package. This trend is expected to continue for at least the next few decades. As solder joints play a crucial role of providing electrical, mechanical and thermal connections between different packaging levels, the durability of solder joints is of utmost importance for developing reliable electronics package technologies. Highly anisotropic nature of Sn, along with the fact that now lead-free Tin-based solder joints (like the SnAgCu family of solders, termed SAC solders) have shrunk to a length-scale where a joint consists of a one (monocrystalline joint) to at most a few grains (oligocrystalline joint) within a solder joint, has only exacerbated the challenge of accurately characterizing and modeling the mechanical behavior of solder alloys.

Solder joints in microelectronic assemblies are known to experience a multiaxial combination of extensional and shear loads due to combinations of thermal expansion mismatch and flexure/warpage of printed circuit assemblies (PCAs) during thermal cycling or during vibrational loading of constrained PCAs. However, the

majority of research tends to investigate the cyclic fatigue failures of solder joints under pure-shear loading as the CTE mismatch induced shear is the most dominant cause of failure of solder joints. The damage contributions due to cyclic extensional loads on solder joints is often overlooked and least studied in the literature. Hence, Chapter 2 carefully examines and compares the effect of cyclic tensile vs. shear stress states on fatigue durability of Sn3.0Ag0.5Cu (SAC305) solder joints. A bimodal empirical multiaxial fatigue damage model is proposed in this study to capture the two different fatigue failure modes seen in solder joints experiencing cyclic shear vs tensile loading.

Traditionally, solder joints have mostly been modeled using isotropic constitutive material models, as proposed by numerous researchers [1][2][3][4]. However, given that SAC solder joints now consist of only a few highly anisotropic grains, each joint has a unique mechanical and thermomechanical response leading to piece-to-piece variation in their performance when subjected to external loads during the service life. Therefore, it is of utmost importance to determine anisotropic plastic and creep properties of each grain, to capture the true mechanical response of solder joints. Anisotropic plastic properties were primarily needed in this work to understand the effect of grain orientation in solder joints subjected to cyclic mechanical fatigue loads presented in Chapter 2. Chapter 3 of this dissertation provides anisotropic plastic behavior of solder joints. Anisotropic elastic stiffness constants and creep properties for SAC305 have been previously established by [5].

Engineers often use finite element simulations to quantify stresses and strains in the critical solder joint, by modeling the solder joints as homogeneous isotropic

domains. Solder strains (or other similar damage metrics, such as work density) are used to construct fatigue durability curves from fatigue test data and to predict failures under life-cycle loading conditions. In reality, as discussed earlier, each SAC solder joint consists of few highly anisotropic grains and is neither homogeneous nor isotropic. As a result, homogeneous, isotropic finite element models erroneously misrepresent the true material behavior and neglect the resulting stress concentrations at grain boundaries and triple corners between mis-oriented grains and IMC interfaces. Due to piece-to-piece variability in the grain structure of tested joints, a simple homogeneous isotropic representation leads to significant piece-to-piece uncertainty in predicting the strain levels (and hence the fatigue durability) of each solder joint at any given level of applied loads. A typical approach for dealing with this variability is to test a large number of samples at each loading level and use confidence intervals to determine the statistical variability. However, such a process is resource-intensive and time-consuming. Therefore, Chapter 4 quantifies the role of the grain structure on the variability in fatigue durability predictions, based on a simulation-based 'virtual-testing' alternative. In addition, this study also draws attention to the limitations of modeling solder joints as homogeneous isotropic domains. The approach consists of parametric, grain-scale, anisotropic FEA simulations. Findings of this study can enable more accurate 'digital twins' and empower engineers to obtain more accurate, faster and cheaper *a-priori* estimates about stochastic fatigue reliability predictions.

1.2.Literature Review

This section discusses prior work on- tensile mode monotonic and fatigue characterization of solder, anisotropy of β-Sn and microstructural heterogeneity of SAC solder, impact of solder cooling rates and aging on solder microstructure and grain-scale modeling methodologies.

1.2.1. Tensile Mode: Monotonic and Fatigue Characterization

Researchers have used different types of specimens to characterize cyclic mechanical fatigue durability of solder alloys. Examples include both joint-scale specimens (such as straddle board specimens and lap shear specimens [6][7]), as well as conventional dog-bone bulk solder-material specimens [8][9]. Most of the studies on joint-scale specimens investigated the influence of shear cycling, while the influence of tensile cyclic loads has been studied mostly with macro-scale dog-bone specimens of bulk solder materials. Andersson, et.al. investigated tensile fatigue durability using a bulk solder dog-bone specimens and shear fatigue durability of joint-scale solder specimens [10]. The joint-scale specimens displayed lower fatigue life compared to bulk solder specimens at high strains, possibly due to differences in micro-architecture, grain structure, stress states, and strain rates. The micro-architectural differences stem from the fact that dog-bone bulk solder specimens have neither the right length-scale effects (arising from the ratio of characteristic grain-size to overall characteristic structure size) nor the microstructural features observed in actual solder joints, such as the interfacial layer of intermetallic compound (IMC). As documented in the literature,

mechanical response of solder joints made from lead-free Tin-rich solder alloys such as SnAgCu (SAC) display strong length-scale effects due to (i) their oligocrystalline structure consisting of a few strongly anisotropic body-centered tetragonal (BCT) β-Sn grains [11]; (ii) the complex dendritic structure of the pro-eutectic β-Sn and the interspersed eutectic Ag-Sn eutectic material [12], and (iii) the interfacial IMC layers [5]. The details regarding the β-Sn properties and SAC305 microstructure are provided in the next section.

A few studies have reported the effect of tensile loads on solder joints of various height (ranging from 25μm to 1mm), but for monotonic uniaxial tensile behavior and not for cyclic fatigue durability [14] [13]. These studies established that the failure mode tends to shift from plastic deformation and ductile damage within the bulk of the solder material, to interfacial damage, near or within the IMC layer, as joint height decreases (< 150μm). This transition is believed to be caused by the fact that, the interfacial region of tensile hydrostatic stresses (generated by mismatch of mechanical properties between the solder and the IMC layer at the interface) becomes the weakest link in joint scale specimens.

One of the few studies to study cyclic fatigue behavior of joint-scale solder specimens was conducted on Sn-4Ag/Cu solder joints [15]. This study examined the effects of both monotonic and cyclic tensile loading and reported the effect of isothermal aging on IMC growth and its consequence on decrease in the tensile strength and tensile fatigue durability of the solder joint. However, this study did not provide: (i)

comparison with shear fatigue durability; and (ii) proper quantification of the effect of microstructure and solder strains.

1.2.2. β-Sn Anisotropy and SAC305 Microstructure

The SAC solder joint consists of heterogeneous oligocrystalline microstructure with a few coarse SAC grains [16]. SAC305 consists of 96.5% β-Sn. β-Sn has a body-centered tetragonal crystal lattice (a = 0.58 nm, c = 0.317 nm and c/a = 0.545). The ß-tin has a very strong anisotropy of the thermal expansion coefficient and the modulus of elasticity as shown in Figure 1-1 [18]. The modulus of elasticity in the [001] direction at 20 °C at 68 GPa is considerably larger than the [100] direction, which has a modulus of elasticity of about 24 GPa. The coefficient of thermal expansion in the [001] direction is 30 ppm/°C and almost twice as large as in the [100] direction which amounts to 15 ppm/°C. Such anisotropic behavior leads to stress concentrations due to the different coefficients of thermal expansion along the grain boundaries.

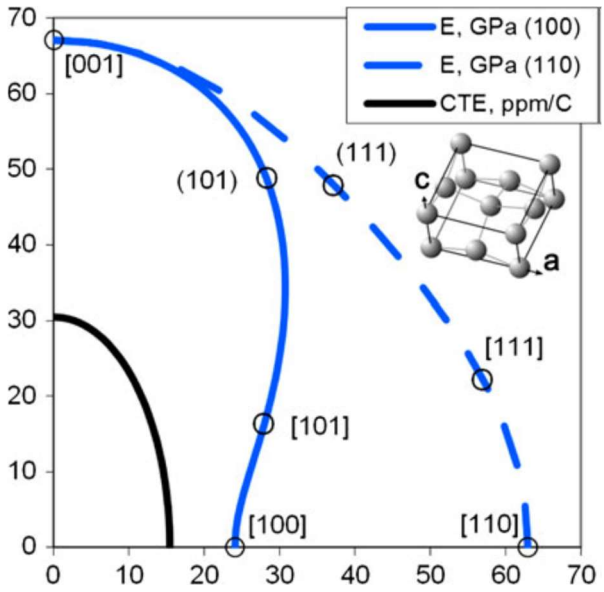

Figure 1-1 Elastic modulus and CTE of Sn in different crystal directions [18]

The anisotropic elastic stiffness constants used for defining the anisotropic elastic response of β-Sn has been characterized by several researchers in the past [19][20] and used Sn elastic constants in lieu of SAC properties. Jiang et. al quantified the elastic stiffness constants for SAC305 shown in Table 2-1 by incorporating the microstructural variations between SAC grain and Sn grain.

Table 1-1 Elastic stiffness constants for SAC305 [5] (Unit: 10^{10} Pa)

C_{11}	C_{22}	C_{33}	C_{44}	C_{55}	C_{66}	C_{23}	C_{13}	C_{12}
7.32	7.35	8.93	2.23	2.23	2.42	3.64	3.63	5.96

Apart from highly anisotropic behavior of SAC, another source of variation in SAC305 properties is its heterogeneous microstructure. The entire composition of SAC305 from macro-scale to nanoscale length-scales has been classified in different tiers by Mukherjee et. al [11] using as shown in Figure 1-2. Tier 4 consists of

macroscale solder joint specimen. Tier 3 consists of grain-scale solder joint that has few grains (<3), which is also called as oligocrystalline microstructure. Tier 0-2 consists of single grain and its microstructure. A SAC grain consists of pro-eutectic β-Sn dendrites which are surrounded by a eutectic Sn-Ag phase and Cu_6Sn_5 phase. This is referred as Tier 2. The Tier 1 eutectic phase consists of nanoscale Ag_3Sn IMC particles distributed in β-Sn matrix. These IMCs block the dislocation motions which lead to dispersion strengthening of the solder alloy. Another challenge in characterizing the mechanical behavior of solder joints arises from the length scale effect of the solder joint specimen used for testing. As the aspect ratio of solder joints increases, the global triaxial stresses significantly increase the yield strength of the solder joint during tensile loading. The global triaxial stresses are generated in the solder, due to the constraint provided by Copper and IMC layers, preventing the shrinkage of the solder due to Poisson's transverse deformation [16][17]. Therefore, the mechanical properties of solder joints must be evaluated using the specimen which has similar length-scales.

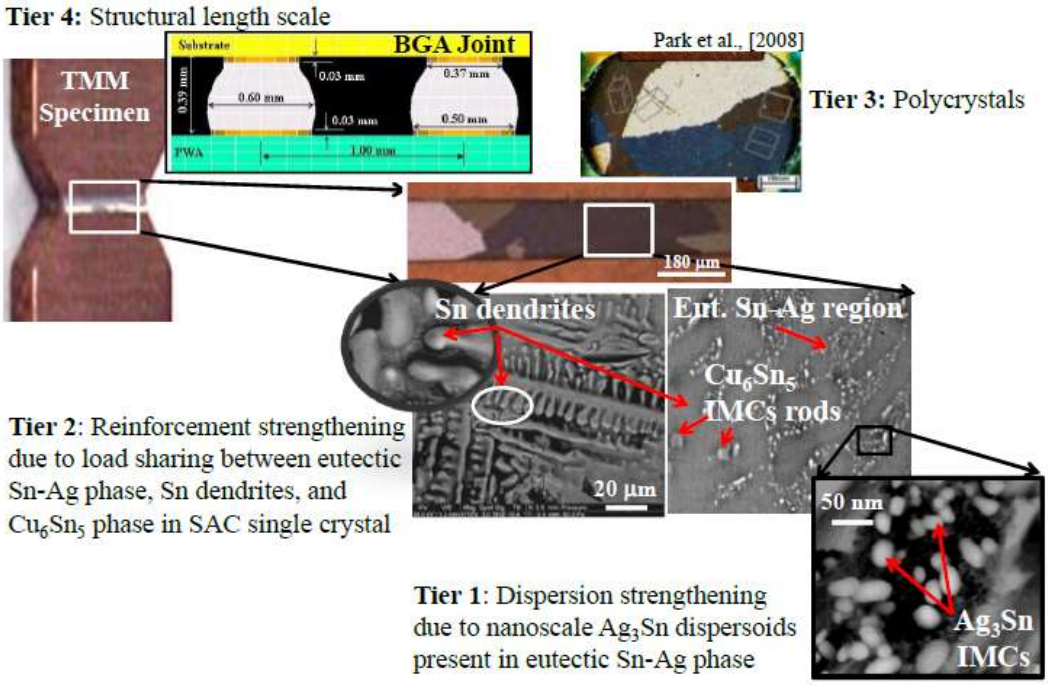

Figure 1-2 SAC miscrostructure classified in different tiers across different length-scales [11]

Owing to this extent of microstructural variation in solder joints, many researchers have studied the impact of solder microstructure on failures. Matin et al. investigated deformations in solder joints subjected to thermal cycling using SEM and correlated those microscopic observations with stress fields obtained from elastic anisotropic FE analysis [21]. High stress concentrations were observed in FEA along the Cu-solder interface and also along high angle grain boundaries due to CTE mismatch resulting from Sn anisotropy. The failure locations in test specimens also matched with the high stress regions in FEA, effectively determining vulnerable sites in the solder joints. In addition, Park et al. [22] [23] characterized strain fields in eutectic SAC solder balls with single grain and multiple grains, using cross-polarized

microscopy and DIC to measure localization of von Mises strain under thermal cycling. The highest strain concentrations and cracking were along the grain boundaries and pad-solder interfaces in few-grained solder joints as shown in Figure 1-3. Whereas, von Mises strains were uniform in a single grained SAC solder ball.

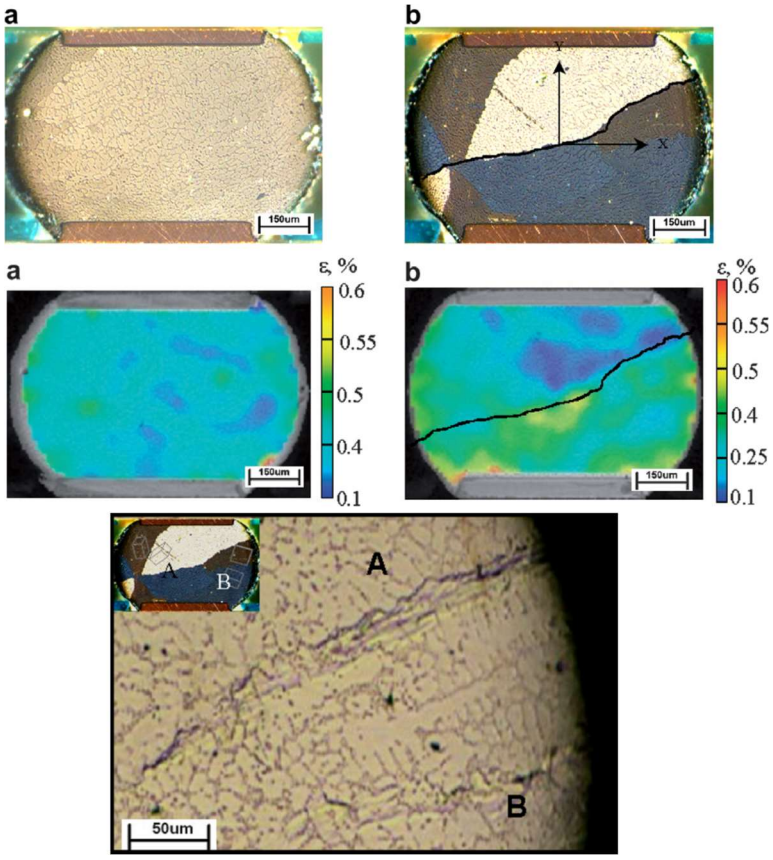

Figure 1-3 Strain concentrations and inter-granular cracks in single vs. multi-crystal solder ball [23]

Arfaei et. al [24] studied the effect of number of grains and their orientation on cyclic mechanical fatigue of solder balls under shear mode. Fatigue lifetimes for multi-grained (2 to 3 grains) solder ball was found to be longer than single grain solder balls.

Early failures were observed in single grain solder joint with grain oriented along [001], [010] and [110] directions. Similarly, Bieler et. al. [12] looked at the effect of Sn grain size and orientation on thermomechanical reliability of solder joints. OIM analysis clearly indicated that the severity of damage correlated with the orientations that had very high CTE values ([001] direction). Maximum CTE mismatch is observed when the crystal c-direction is oriented parallel to the substrate and is a worst-case scenario. This demonstrates that the single grain solder joints are less reliable than multi-grain solder joints, since up to a quarter of the solder joints may have worst case crystal orientations. Xu et. al [25] examined the grain structure in BGA solder balls and correlated that with fatigue failures. The grain structure of different solder balls within a BGA package was found sensitive to the joint location and cooling rate. Polygranular solder balls were found to have better fatigue resistance and reliability than oligocrystalline solder balls.

In summary, highly anisotropic nature of Sn leads to considerable misorientation between the different grains in the solder joint. Higher degree of misorientation can cause the higher internal stress concentrations along the material heterogeneities such as grain boundaries and IMCs rendering these sites vulnerable to fracture. Therefore, accurate understanding and quantification of solder microstructure is needed for modeling anisotropic grain-scale behavior of solder joints.

Several factors affect the microstructure of the lead-free solder alloys such as composition, solder cooling rates, time above liquidus, aging conditions and surface

plating materials. Next section explores in detail the effect of cooling rate and aging on mechanical properties of solder joints.

1.2.3. Effect of Cooling Rate and Aging on Microstructure, Mechanical Behavior and Reliability of SAC305 Solder Joints

The cooling rate during the assembly process impacts the solder microstructure and thermo-mechanical behavior of lead-free solder joints. However, a limited literature explores the effect of cooling rate on SAC solder. Wei et.al [26] studied the effect of cooling rate on microhardness of SAC305 solder joints. Different cooling methods such as furnace cooling (0.14 K/s), air cooling (1.7 K/s) and water cooling (~100 K/s) were used to control the cooling rate. Figure 1-4 shows the resultant microstructure obtained by employing different cooling methods. The β-Sn dendrite size and arm spacing was seen to decrease as the cooling rate increased. Similarly, slower cooling also leads to significant coarsening of Ag_3Sn IMC particles. In addition, Vickers microhardness was also seen to increase with the rapid solidification rates. Faster cooling rates lead to finer microstructure which consists of uniformly distributed Ag_3Sn particles resulting in severe dispersion strengthening.

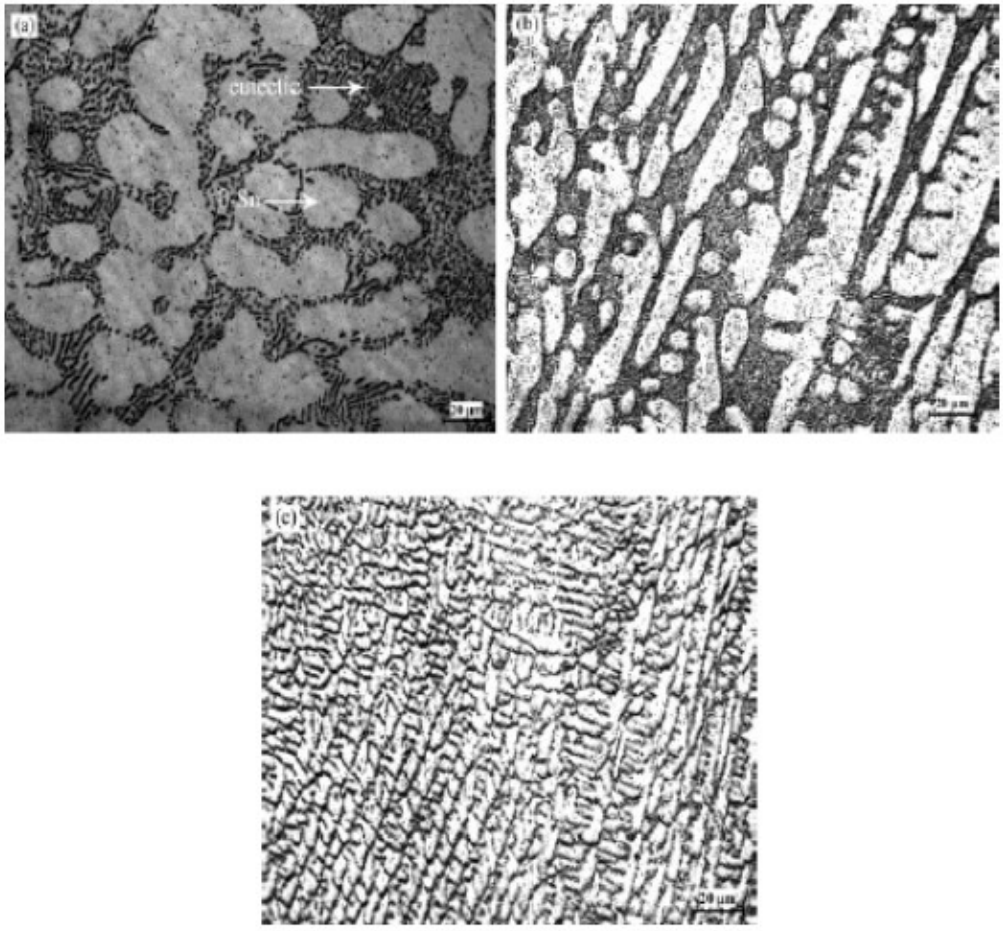

Figure 1-4 Solder microstructure as a functions of different cooling rates: (a.) furnace cooling; (b.) air cooling; (c.) water cooling. [26]

Similarly, Lee et. al. [27] studied the SAC305 microstructure under different cooling rates- 2.5ºC/s, 9ºC/s, 21ºC/s and 63ºC/s. The β-Sn dendrite size (620μm^2, 550μm^2 ,380μm^2 and 30μm^2) and volume fraction (55.3%, 50.2%, 42.5% and 27.8%) decreased as the cooling rate increased monotonically. The Ag_3Sn IMC was shaped like a leaf at lowest cooling rate and changed to particle shape at highest cooling rate. In addition, the strength and hardness of SAC305 was also found to vary depending

upon the cooling rate. The tensile strength was seen to reduce by 34% between highest cooling rate (60.8 MPa) to lowest cooling rate (39.5 MPa). Mueller et al. [28] analyzed the effect of cooling rate, composition and solder volume on the microstructure of lead-free solder joints. Cooling rates used in this study were 0.14K/s, 1.1K/s and 10.9K/s. Increase in cooling rate was seen to reduce the size of IMC particles and spacing between β−Sn dendrites, whereas the area fraction of eutectic Ag3Sn phase was seen to increase. Mutuku et. al. [29] investigated the effect of cooling rate, aging time on microstructure and shear fatigue lifetimes of different SAC solder joints. The mechanical properties of lead-free solder joints were found to be in in direct correlation with the distribution of dispersoids in the joint. The solder joint strength and shear fatigue life increased as the number of Ag_3Sn IMC particles increased (with increasing cooling rate).

As cooling rate influences the solder microstructure and mechanical properties, so does the post-reflow aging temperature and duration. Numerous researchers have studied the evolution of mechanical behavior of solder joints as it undergoes aging. Solder microstructure continuously evolves throughout its life starting from assembly process to its end of life. It's important to understand the evolution of the stress-strain response of SAC305 since its degradation or enhancement can both influence its reliability. Chauhan and Mukherjee [30], quantified microstructural parameters such as size, volume fraction and spacing of nanoscale Ag_3Sn, Cu_6Sn_5 IMCs and Sn dendrites in SAC305 solder alloy during 24-1000 Hrs. of aging at 100ºC. The microstructural parameters were used in mechanical multi-scale creep model to predict the effect of aging on creep behavior of SAC305 solder joints. The Ag_3Sn IMC particle size and spacing was seen to monotonically increase with increasing aging duration. In contrast,

evolution of microscale Cu_6Sn_5 phase wasn't sensitive to aging duration and exhibited a non-monotonic trend. Volume fraction of pure Sn dendrites increased monotonically from 59% to 72% from as soldered condition to 1000 Hrs. of aging. Secondary creep resistance of SAC305 was seen to decrease with aging, since the increased Ag_3Sn particle spacing reduced the dispersion strengthening of the alloy.

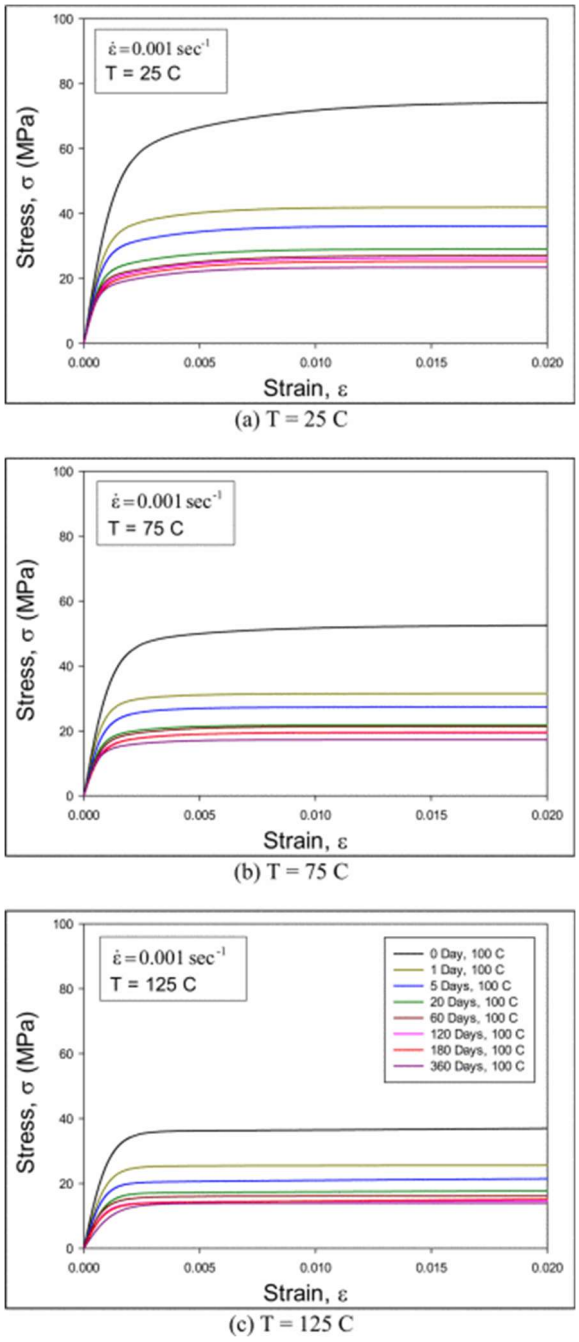

Figure 1-5 Effect of aging and test temperature on uniaxial monotonic stress-strain behavior of water quenched SAC305 specimens [31]

Lall et. al. [31] conducted uniaxial tensile tests at different test temperatures (25 ºC, 75 ºC, 100ºC and 125ºC) and at different strain rates (1E-3, 1E-4 and 1E-5 s^{-1}) on miniature SAC305 bulk solder specimens aged at 100ºC for different durations (0-12 months). Specimens with two cooling methods were used in this study- reflowed and water quenched. For both kinds of specimens, the yield strength and ultimate tensile strength of the solder was seen to decrease significantly with the duration of aging and test temperature. Figure 1-5 shows effect of aging and test temperature on uniaxial monotonic stress-strain behavior of water quenched SAC305 specimens. Similar trends were also observed for reflow cooled specimen as well. Fu et. al. [32] studied the effect of long-term aging of SAC305 and SAC405 solder specimen on its cyclic stress-strain response. The solder specimens were fabricated using two cooling methods- reflow and water-quenching. The tests were conducted at 25 ºC and 1E-3 strain rate. The test specimens were subjected to two aging temperatures- 25 ºC and 125 ºC for various aging periods (0, 5, 10, 20, 30, 45, 60, 80, 110, 150, 200, 260, and 360 days). A microscopic examination of fixed region of a sample was conducted at the end of each aging period. The stress-strain hysteresis area ΔW reduced significantly in first few days of aging and then stabilized. This was correlated with the coarsening of Ag_3Sn IMC particles and weakening of pure tin dendritic structure. Fu and Wu [33] [34] in different studies have quantified the evolution of microstructure at different intervals during the aging period. The Ag_3Sn particle size and number was measured at a fixed location in the specimen by analyzing the SEM images using image processing tools.

For example, Figure 1-6 shows evolution of IMC particles during aging of reflowed SAC305 specimen.

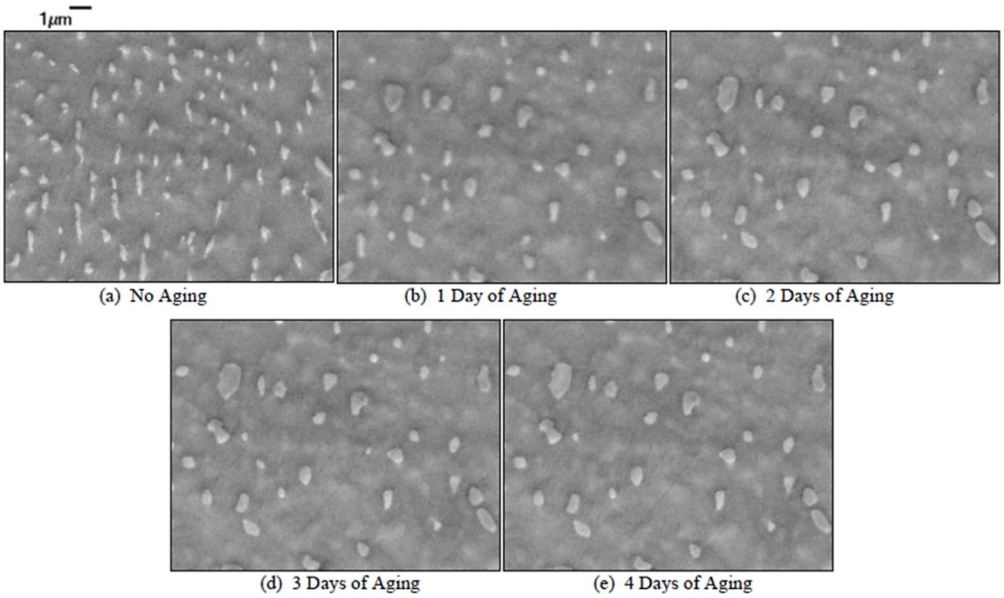

Figure 1-6 Evolution of Ag_3Sn IMCs with aging (at 125°C)

1.2.4. Grain-Scale Modeling of Solder Joints

Solder joints are traditionally modeled as a homogenous isotropic inelastic volume in finite element analysis to gain understanding of the stresses and strains leading to failure of the joint. Researchers used time-dependent plasticity models and unified viscoplasticity models such as Anand's model and Chaboche model, to describe monotonic, cyclic and creep loading of homogenous isotropic inelastic solder joints. Chaboche model accounts for the influence of stress triaxiality on durability of solder joints and is hence well suited for studying the effect of multiaxial stress states. Modeling the solder joint with this assumption is a common practice, because of the impracticality of obtaining grain orientation information of every single solder joint in

actual electronic components. However, coarse-grained lead-free SAC solder joints are far different from homogeneous isotropic structures. Instead, they have few highly anisotropic SnAgCu (SAC) crystals, which creates local mismatches and incompatibilities along the grain boundaries and triple corners, generating stress concentration sites, especially between mismatched grains and interfacial IMC layers. Most of the research studies neglected the influence of such heterogeneities on the observed fatigue failures leading to inaccuracies in quantifying the severity in failures. Therefore, to improve the accuracy of constitutive models, some researchers implemented crystal-plasticity/crystal-viscoplasticity finite element analysis approach (CPFEA) which accounts for grain orientation and slip system behavior in solder joints [12][18]. For example, Zamiri et. al [35] evaluated the stress-strain response of a solder joint due to thermomechanical load caused by 165°C temperature change using crystal-plasticity modeling. C-axis of the crystal orientated parallel to the solder-IMC interface was seen to have largest thermal expansion mismatch and plastic work. Darbandi et. al [18] presented a crystal plasticity (CP) model to simulate mechanical deformation in a tri-crystal solder ball with different orientations. Lap-shear tests on solder joints were used to calibrate the CPFEA model. The model demonstrated that the CP model was able to simulate deformation in the solder ball in reasonable agreement with the experimental results. Implementing crystal plasticity FEA on every solder joint can be quite challenging and computationally inefficient. Mukherjee [11] and Jiang [36] have provided a hybrid crystal viscoplasticity (CV) based anisotropic continuum modeling approach. This approach uses anisotropic dislocation mechanics based multi-scale

crystal viscoplasticity method. The microstructural features of SAC from tiers 0-2 (described in previous section) are used to model anisotropic creep behavior of solder joints. The CV model outputs are converted to continuum creep models (Hill's potentials and Norton power law creep model) for SAC grains. This methodology is relatively simple and computationally efficient to adopt, compared to traditional crystal plasticity finite element analysis.

However, implementing crystal plasticity FEA on every solder joint can be quite challenging and computationally inefficient. As an alternative, researchers have also attempted to model grain-scale solder joints using anisotropic continuum Hill's plasticity approach. Hill's yield strength ratios for different crystal directions, were determined using Sn single crystal uniaxial tensile test data in selected crystal directions. Hill's model was relatively easy to implement and was able to predict stress-strain response of solder joint reasonably well [37] [38]. Unfortunately, corresponding Hill's model and single grain stress-strain experimental data for SAC305 was not present in the literature. Therefore, the part-I paper essentially proposes a set Hill's yield stress ratios and Hill's stress-strain curves, which were calibrated using uniaxial monotonic tensile and shear tests conducted on single grain SAC305 solder joint specimens. Such a grain-scale modeling approach can be used to evaluate the stress concentrations and mechanical response on few-grained solder joints, however, the available literature lacks such information.

1.3.Gaps in Literature

Following gaps in the literature were observed based on the literature review conducted-

i. Cyclic tensile fatigue characterization and its comparison with cyclic shear fatigue of solder joints is not available.

ii. Differences in failures modes in solder joints subjected to cyclic tensile vs. shear loads are not well understood.

iii. Multiaxial fatigue damage models which can account for the different damage modes under combined tensile and shear cyclic loads in solder joints are not available.

iv. Uniaxial tension and shear monotonic elastic-plastic stress-strain data for single grain SAC305 solder joint specimens is non-existent.

v. The effect of grain size on the elastic-plastic stress-strain behavior of oligocrystalline SAC solder joints is not well understood.

vi. Hill's yield criterion and Hill's stress-strain curves for modeling anisotropic plastic properties of SAC305 solder alloy are not available. In addition, effect of cooling rate, aging and grain sizes on Hill's stress-strain curves in not available in the literature.

vii. Method for predicting stochastic variability (caused by grain anisotropy) in plasticity dominated cyclic mechanical fatigue of oligocrystalline solder joints is not available.

1.4.Scope of Dissertation

Based on the missing gaps encountered in the literature, this dissertation aims to fill these gaps through following chapters-

i. Chapter 2 focuses on experimental fatigue characterization of solder joints in tensile and shear modes, failure analysis to identify the resulting failure modes and development of multiaxial mechanism-based solder fatigue damage model.

ii. Chapter 3 describes the fabrication of monocrystalline and oligocrystalline solder joint specimens along with uniaxial monotonic elastic-plastic tests conducted on those specimens. Anisotropic elastic-plastic properties for SAC305 single-crystal for different cooling rates and grain sizes are determined in this chapter.

iii. Chapter 4 demonstrates the application of anisotropic scaled properties (obtained in Chapter 3) by providing simulation-based explanation of the variability observed (in Chapter 1) in fatigue damage model constants, due to grain anisotropy in oligocrystalline solder joint specimens. Similar approach is used to demonstrate proactive prediction of mechanical fatigue variability that can be expected in a typical BGA solder interconnect.

Chapter 2 : Role of Nominal Stress State on Cyclic Fatigue Durability of SAC305 Grain-scale Solder Joints

2.1.Abstract

Solder joints in microelectronic assemblies experience a multiaxial combination of extensional and shear loads due to combinations of thermal expansion mismatch and flexure of printed circuit assemblies (PCAs) during thermal cycling or during vibrational loading of constrained PCAs. Although, a significant amount of research has been conducted to study cyclic fatigue failures of solder joints under pure-shear loading, most of the current literature on cyclic tensile loading of solders is on long dog-boned monolithic solder coupons. Unfortunately, such specimens do not capture the critical interactions between key micro-scale morphological features (such as grain orientation, grain boundaries, IMCs and substrates) that are believed to play important roles in the fatigue of functional solder joints under life-cycle loading. Therefore, this paper uses a combination of experiments and finite element analysis to investigate the differences in mechanisms of cyclic fatigue damage in Sn-3.0Ag-0.5Cu (SAC305) few-grained (oligocrystalline) microscale solder joints under shear, tensile and multiaxial loading modes at room temperature. Cyclic fatigue durability test results indicate that tensile loads are more detrimental compared to shear loads. Tensile vs. shear loading modes are found to cause distinctly different combinations of interfacial damage vs. internal damage in the bulk of the solder (transgranular and intergranular damage), which correlates with the differences observed in the resulting fatigue durability. The

test results also confirm that the traditional approach of assuming a power-law dependence on equivalent deviatoric strain amplitude is inadequate for modeling cyclic fatigue durability of solder interconnects experiencing multiaxial loading. Instead, multiaxial fatigue damage results are seen to be affected not only by the cyclic equivalent strain amplitudes, but also by the severity of the stress-triaxiality, as hypothesized in models such as Chaboche model.

2.2.Introduction

Solder interconnects in electronic assemblies are required to perform both mechanical and electrical functions with excellent reliability. Miniaturization of modern electronic devices has also driven a corresponding miniaturization of the solder interconnects, creating new reliability challenges for solder joints. Solder interconnect failures may occur during pre-market storage or during operational applications [6], not only in consumer electronics but also in electronics for harsh environments, such as in automotive, aerospace, military, industrial applications [39]. Realistic life-cycle conditions of the types schematically shown in Figure 2-1, subject solder joints to multiaxial stresses that consist of both transverse shear (τ_{xy} and τ_{yz}) and out-of-plane tensile loading (σ_{zz}). Shear load is induced by in-plane thermal expansion mismatch between the component and the substrate, while out-of-plane tensile peeling forces are induced by flexure of the substrate (due to external loading and clamping forces as well as due to internal thermo-mechanical warpage).

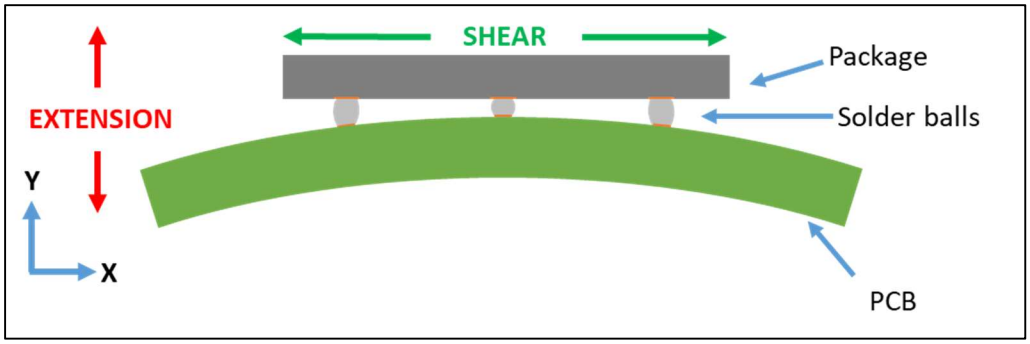

Figure 2-1 Schematic of solder joints subjected to multiaxial stresses

One such example of reliability challenges due to multiaxial stresses in solder interconnects is in electronics for Engine Control Units (ECU) used in automotive applications which must function under harsh operating conditions [40]. Printed Wiring Boards (PWBs) in ECUs may warp and/or stretch due to temperature excursions, as well as flex due to vibration loading. As another example, commonly used consumer electronics such as cellphones, laptops [41][42], etc. may experience repeated actuation of keys [43], power/thermal cycling and drop loads which potentially cause similar multiaxial solder stresses in Printed Wiring Assemblies (PWAs) [44]. In addition, mechanical stress is also induced in PWA solder joints during mounting of the PWBs using clamping screws. The resulting complex PWB deformations can induce a mixture of nominally tensile and shear loads on the solder interconnects. Since functional solder joints experience such multiaxial loading, this study assesses mechanical behavior and fatigue degradation under both tensile and shear cyclic loading.

Researchers have used different types of specimens to characterize cyclic mechanical fatigue durability of solder alloys. Examples include both joint-scale

specimens (such as straddle board specimens and lap shear specimens [6] [7]), as well as conventional dog-bone bulk solder-material specimens [8][9]. Most of the studies on joint-scale specimens investigated the influence of shear cycling, while the influence of tensile cyclic loads has been studied mostly with macro-scale dog-bone specimens of bulk solder materials. Andersson, et.al. investigated tensile fatigue durability using a bulk solder dog-bone specimens and shear fatigue durability of joint-scale solder specimens [10]. The joint-scale specimens displayed lower fatigue life compared to bulk solder specimens at high strains, possibly due to differences in micro-architecture, grain structure, stress states, and strain rates. The micro-architectural differences stem from the fact that dog-bone bulk solder specimens have neither the right length-scale effects (arising from the ratio of characteristic grain-size to overall characteristic structure size) nor the microstructural features observed in actual solder joints, such as the interfacial layer of intermetallic compound (IMC). As documented in the literature, mechanical response of solder joints made from lead-free Tin-rich solder alloys such as SnAgCu (SAC) display strong length-scale effects due to (i) their oligocrystalline structure consisting of a few strongly anisotropic body-centered tetragonal (BCT) β-Tin grains [11]; (ii) the complex dendritic structure of the pro-eutectic β-Sn and the interspersed eutectic Ag-Sn eutectic material [12], and (iii) the interfacial IMC layers [5]. A few studies have reported the effect of tensile loads on solder joints of various height (ranging from 25μm to 1mm), but for monotonic uniaxial tensile behavior and not for cyclic fatigue durability [13][14]. These studies established that the failure mode tends to shift from plastic deformation and ductile damage within the bulk of the solder

material, to interfacial damage, near or within the IMC layer, as joint height decreases (< 150μm). This transition is believed to be caused by the fact that, the interfacial region of tensile hydrostatic stresses (generated by mismatch of mechanical properties between the solder and the IMC layer at the interface) becomes the weakest link in joint scale specimens.

One of the few studies to study cyclic fatigue behavior of joint-scale solder specimens was conducted on Sn-4Ag/Cu solder joints [15]. This study examined the effects of both monotonic and cyclic tensile loading and reported the effect of isothermal aging on IMC growth and its consequence on decrease in the tensile strength and tensile fatigue durability of the solder joint. However, this study did not provide: (i) comparison with shear fatigue durability; and (ii) proper quantification of the effect of microstructure and solder strains.

In summary, there is inadequate understanding about the differences in cyclic durability and degradation mechanisms under tensile and shear loading of oligocrystalline joint-scale solder specimens. Therefore, this study aims to fill this gap and provide a simple engineering approach to quantify fatigue damage under multiaxial loading (tensile, shear and combinations) in grain-scale solder joints.

2.3.Cyclic Testing Methodology

This section provides details about test specimens, test setup, testing method, results and failure analysis conducted in this study.

2.3.1. Test Specimens

Three types of specimens were used in this study for applying cyclic tensile, shear and multiaxial loads on the solder joints, as seen in Figure 2-2. The joint-scale shear specimen (termed the M0 specimen because the loading axis (Y-axis) is aligned with the interface between the solder and the substrate) used in this study was initially proposed by Haswell, et. al. [45]. The design was inspired by Iosipescu's shear specimen with two 90° notches, to generate a uniform shear stress field in the solder joint. The design of the tensile specimen (termed the M90 specimen because the loading axis (Y-axis) is orthogonal to the interface between the solder and the substrate), developed in this study is inspired by traditional dog-bone shaped specimens used for uniaxial tensile tests [46]. M45 specimen was developed in this study for applying multiaxial (simultaneous tensile + shear) loads on the solder joint. The solder-substrate interface is oriented at 45° to the loading axis (Y-axis). Details of specimen geometry and dimensions are described in Figure 2-2. The Copper-IMC-SAC305-IMC-Copper sandwiched structure acts like a spring in series and experience the same instantaneous load level. Therefore, any loss of load carrying capacity either in the bulk solder or near the IMC-solder interface will lead to loss in the specimen stiffness.

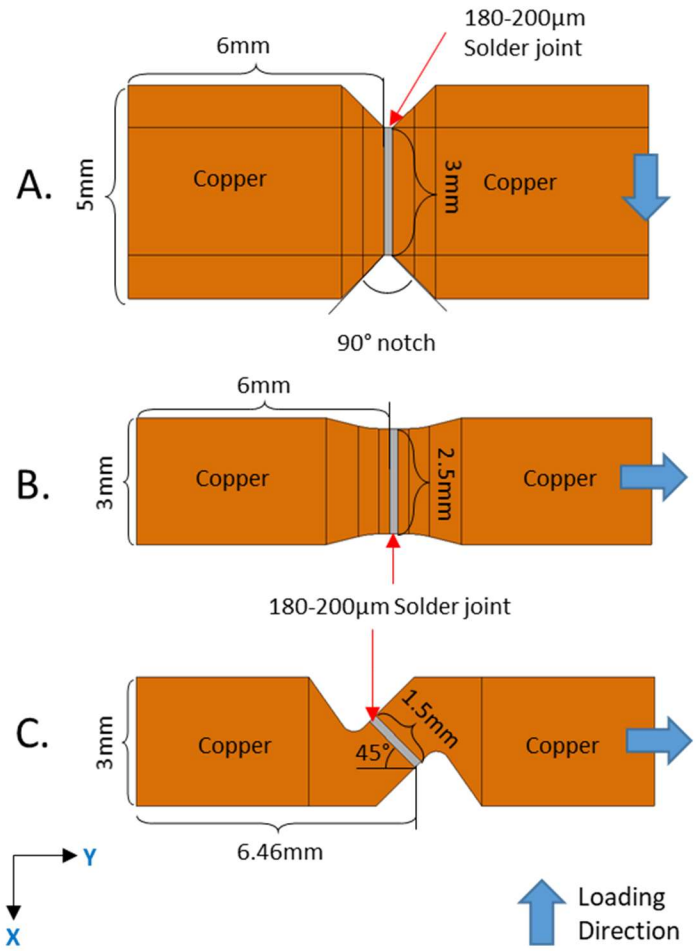

Figure 2-2 TMM specimens- A.) M0 (Shear) Specimen; B.) M90 (Tensile) Specimen; C.) M45 (Multiaxial) Specimen [47]

All the specimens used in this study are fabricated by manually soldering two symmetric platens of unplated Oxygen-Free High Conductivity Copper (OFHC) together using Kester 331 flux-cored SAC305 solder wire, as shown in Figure 2. The flux is mildly corrosive so the residues were immediately cleaned with isopropyl alcohol. The platens are fabricated using Electro-Discharge Machining process, since it can cut platens without creating blunt or sheared edges. The soldering surface of the

platens is roughened using 600 grit silicon carbide paper. Copper platens are selectively paired for dimensional consistency, aligned in a soldering fixture and then placed on a hotplate for soldering [48]. A spacer is inserted between the two copper platens in order to maintain 180-200μm solder joint height for each specimen. Temperature profile used for soldering is shown in Figure 2-3. The excess pool of solder is ground off from the specimens and the final thickness of the specimens is approximately 1mm. All specimens are aged for 63 Hrs. at 125°C before testing (consistent with previously used aging protocols for all specimens tested in this group), to partially stabilize the microstructure and to relieve the residual stresses generated during soldering and grinding steps. Cross-polarized images and associated SEM images during this study have revealed that the test specimens have oligocrystalline structure, with each grain having dendritic structure and intermetallic morphology (both in the eutectic region in the bulk of the solder material, as well as at the interfaces), that are comparable to those observed in functional solder joints, shown in Figure 2-4 [49][50]. Each test specimen has a unique grain structure (and hence, unique mechanical response), as commonly observed in functional solder joints.

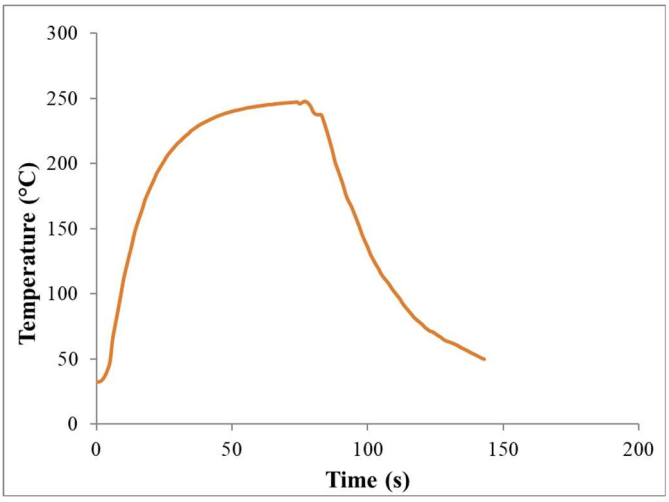

Figure 2-3 Soldering temperature profile

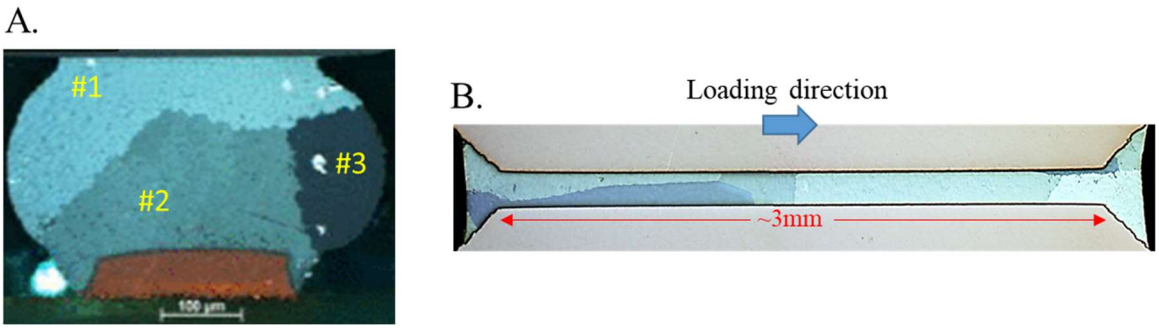

Figure 2-4 A.) Ball grid array solder joint [49]; B.) TMM Shear M0 specimen [50]

2.3.2. Test Setup

Cyclic mechanical tests were conducted on a custom Thermo-Mechanical Microscale (TMM) test system (Figure 2-5) developed by Haswell, et. al. [45]. The TMM system, when initially developed, was built with shear grips and hence could only apply shear loads on M0 solder specimens. For the purpose of this study and to enhance the testing capabilities of the TMM setup, new set of tensile grips were

designed for gripping M90 (tensile) and M45 (multiaxial) specimens. The test system consists of a piezo-electric stack actuator which loads the specimen with closed-loop displacement control, using a displacement transducer (LVDT). The load is measured by a load cell [48]. The average tensile or shear stress (force divided by cross-sectional area) is calculated for each specimen after measuring the dimensions of the solder joint. The red box shows the location and orientation of the specimens when mounted on the grips. In order to accurately measure the real-time deformation field in the solder joint, a Digital Image Correlation (DIC) system, consisting of camera and image processing software, has been added to the TMM setup in this study. As shown in Figure 2-6, the DIC system uses virtual extensometers placed across the top and bottom interfaces of the solder joint near the center of each specimen, to measure the average deformation across the solder layer. The length of extensometer gages along Y and Y' axes is approximately equal to the height of the solder joint, whereas gages along X and X' axes are approximately 400μm long. The DIC field of view is about 1x1mm. As, the solder alloy is more ductile and yields at about 35-45MPa compared to pure copper (yield stress > ~300MPa), the plastic deformation is concentrated in the solder.

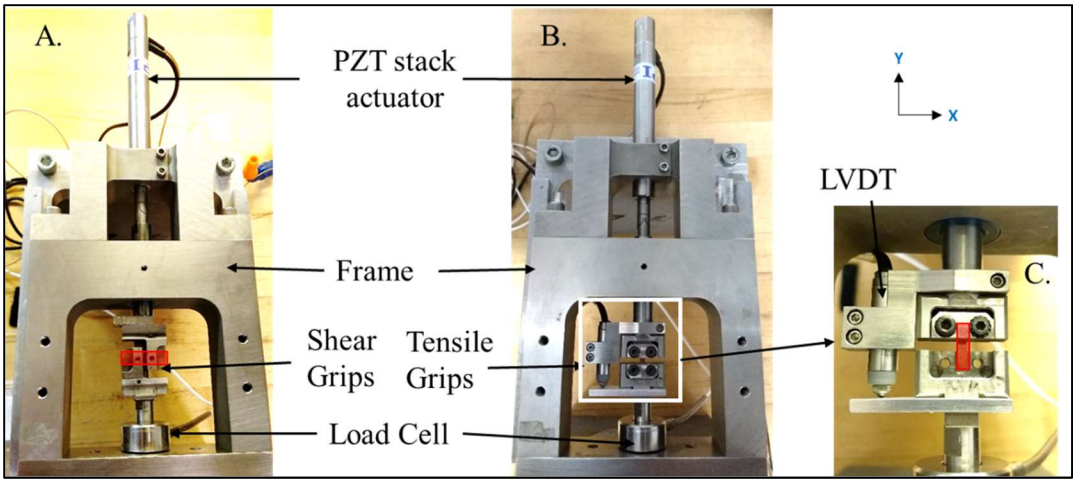

Figure 2-5 A.) TMM test frame with shear grips; B.) TMM test frame with tensile grips; C.) Specimen mounted in tensile grips.

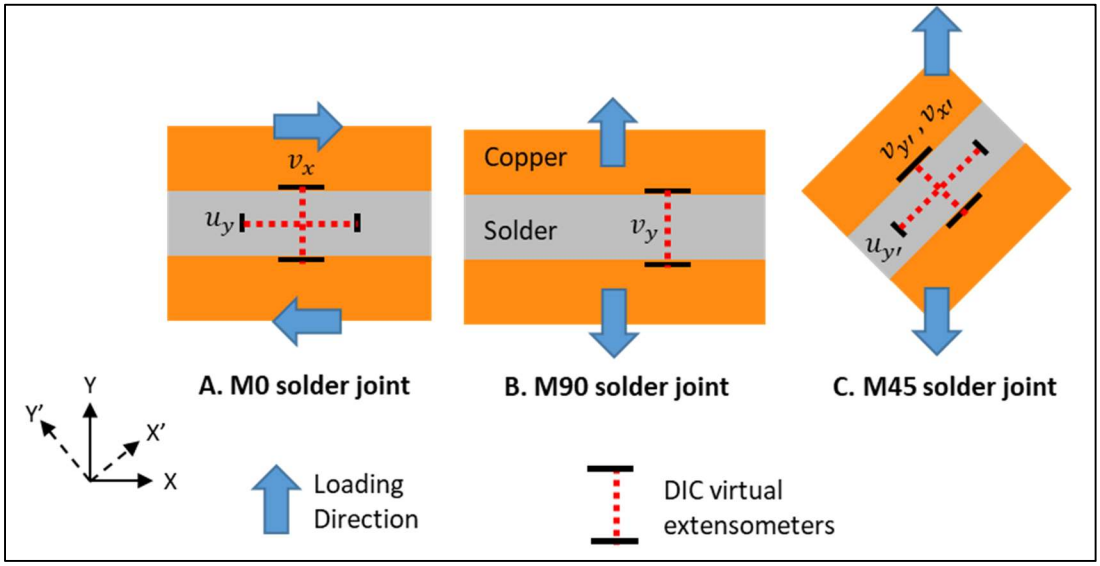

Figure 2-6 DIC virtual extensometer locations in- A.) M0 solder joint; B.) M90 solder joint and; C.) M45 solder joint.

Cyclic tensile and shear tests were conducted at room temperature on these OFHC-SAC305 TMM solder joint specimens at different displacement-controlled loading levels. The specimens were loaded at a displacement rate of 1μm/s (which resulted in a nominal average strain rate in the solder of approximately ~1E-3/s). The tests were terminated after achieving 20% drop in maximum cyclic force level at the max cyclic applied displacement. The average deformation of the solder joint, between two Copper interfaces, is measured using the DIC extensometer discussed above. The in-plane engineering strains (ϵ_{xx}, ϵ_{yy}, γ_{xy}) are derived from the measured displacements. The average axial solder strain (ϵ_{yy}) is measured with DIC, while out-of-plane (ϵ_{zz}) transverse strain is estimated using the effective Poisson's ratio. However, in-plane (xx-direction) transverse strain is assumed to be negligible, considering that the x-dimension is much larger than the y-dimension. The average shear strain (γ_{xy}) was calculated from deformation gradient components ($\partial v/\partial x$ & $\partial u/\partial y$) which were also measured using DIC. Total equivalent cyclic strain range ($\Delta\epsilon_{eq}$) for tensile, shear and multiaxial specimens are estimated with Eq. 2-1-Eq. 2-4.

$$\Delta\epsilon_{eq}^{tensile} = \frac{1}{\sqrt{2}\,(1+\nu)}\sqrt{(\Delta\epsilon_{yy})^2 + (\Delta\epsilon_{yy} - \Delta\epsilon_{zz})^2 + (\Delta\epsilon_{zz})^2} \quad \text{Eq. 2-1}$$

$$\Delta\epsilon_{zz} = \nu\Delta\epsilon_{yy} \quad \text{Eq. 2-2}$$

$$\Delta\epsilon_{eq}^{shear} = \frac{1}{\sqrt{3}}\Delta\gamma_{xy} \quad \text{Eq. 2-3}$$

$$\Delta\epsilon_{eq}^{multiaxial} = \frac{\sqrt{2}}{3}\sqrt{(\Delta\epsilon_{yy})^2 + (\Delta\epsilon_{yy} - \Delta\epsilon_{zz})^2 + (\Delta\epsilon_{zz})^2 + 6(\frac{\Delta\gamma_{xy}}{2})^2} \quad \text{Eq. 2-4}$$

Eq. 2-5

$\Delta\epsilon_{zz}$, $\Delta\epsilon_{yy}$ and $\Delta\gamma_{xy}$ are average cyclic magnitudes of engineering total strains in the solder, ν is solder effective Poisson's ratio. The Poisson's ratio used in this study is 0.3 for elastic deformation and 0.5 for plastic deformation. The effective Poisson's ratio was: (i) 0.3-0.4 for M90 tensile specimens (depending on the plastic strain contributions); (ii) 0.5 for M0 shear and M45 multiaxial specimens due to large plastic strains.

2.3.3. Cyclic Fatigue Durability Results

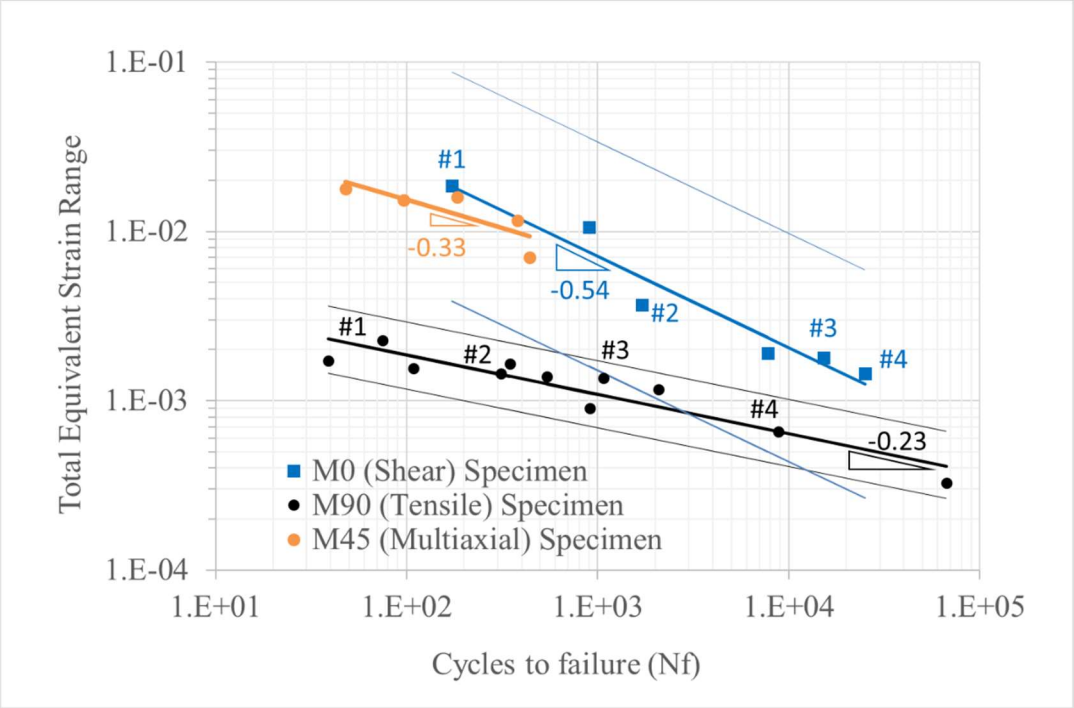

Figure 2-7 Comparison of equivalent total cyclic strain range vs. life (SN) plots (using log-log scale) for solder joints subjected to nominally tensile, shear and multiaxial loads. Specimen numbers provided here are same as the specimen numbers used later in Figure 8.

As shown in Figure 2-7, tensile durability clearly tends to be an order of magnitude lower than shear durability, for comparable levels of cyclic equivalent total strain range. Due to the contributions of both tensile and shear loads, multiaxial durability datapoints appear to be bounded between tensile and shear durability data. However, more datapoints are needed to arrive at a statistically significant conclusion. The different slopes of the tensile, shear and multiaxial durability plots show that the

shear mode failure is less sensitive to the applied strain level, and points towards different failure mechanisms in each case. There is more statistical scatter in the shear results, compared to that in tensile results. The 90% confidence bounds in the shear results are wider than in tensile results, in part because there are significantly fewer shear data points (compared to tensile data points); and in part because there is larger variability in the shear damage mechanisms. In addition, the SN curve developed using total equivalent strain range does not yield a master fatigue model for same solder joint configuration. This confirms that the popular method of modeling fatigue durability using a Coffin-Manson power-law dependence on equivalent deviatoric strain range is inadequate for quantifying the fatigue damage mechanisms observed under different loading modes in joint-scale solder specimens. Therefore, a more general and unifying fatigue damage modeling approach for solder joints loaded under multiaxial stress states is proposed in this paper. The details of the proposed model are provided in Section 2.5.

2.3.4. Failure Analysis: Degradation Mechanisms

Tested specimens were subjected to destructive post-failure analysis using optical microscopy under cross-polarized light, as well as Scanning Electron Microscopy (SEM). As shown in Figure 2-8 and Figure 2-9, OFHC-SAC305 M90 tensile specimens undergo degradation predominantly by cracking along the interface between the IMC layer and bulk solder. In a few specimens, two types of cracking were observed within the solder material: (i) shallow inter-granular cracks at triple points,

where 3 grains meet each other; and (ii) shallow trans-granular cracks. The term 'shallow' here implies that these damage modes were localized near the surface and did not extend into the interior of the specimen in the thickness (z) direction as shown in Figure 2-10.

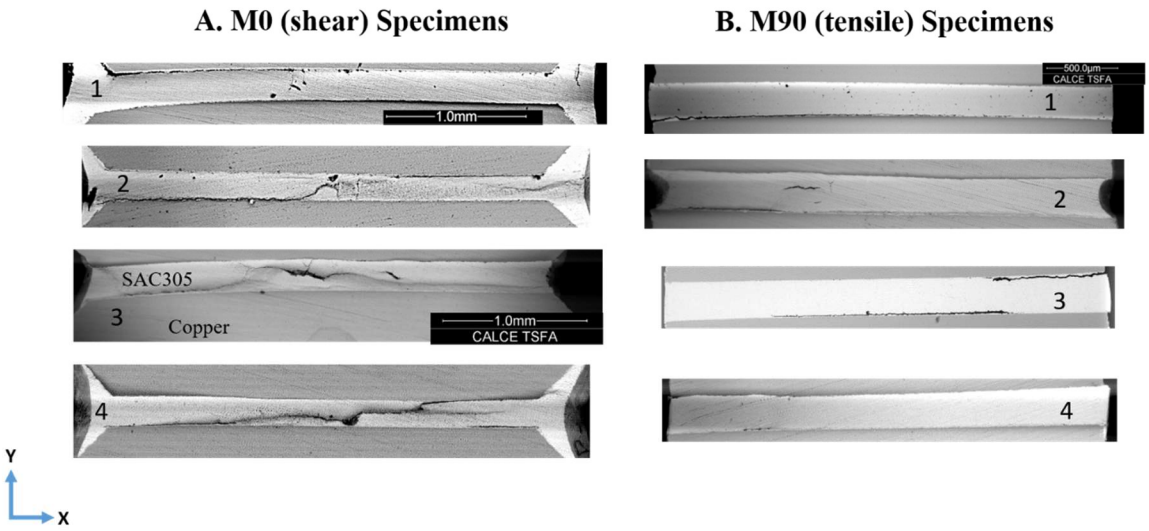

Figure 2-8 SEM images showing failure modes in A. M0 specimens and; B.) M90 specimens. Loading history of each specimen can be found in Figure 7.

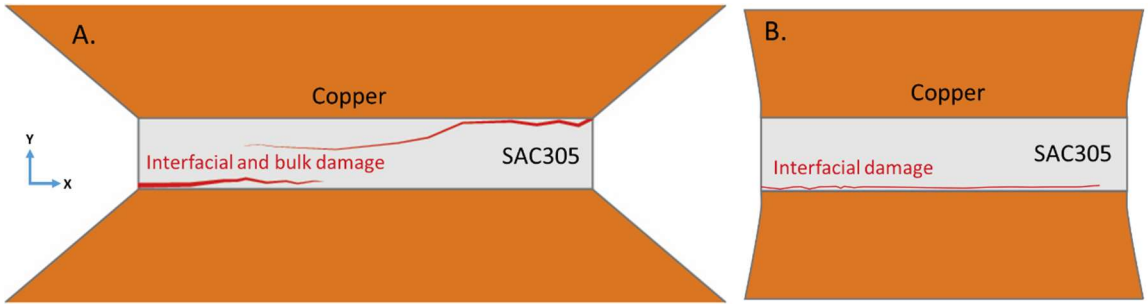

Figure 2-9 Schematic of failure modes observed in A.) M0 specimen; B.) M90 specimen.

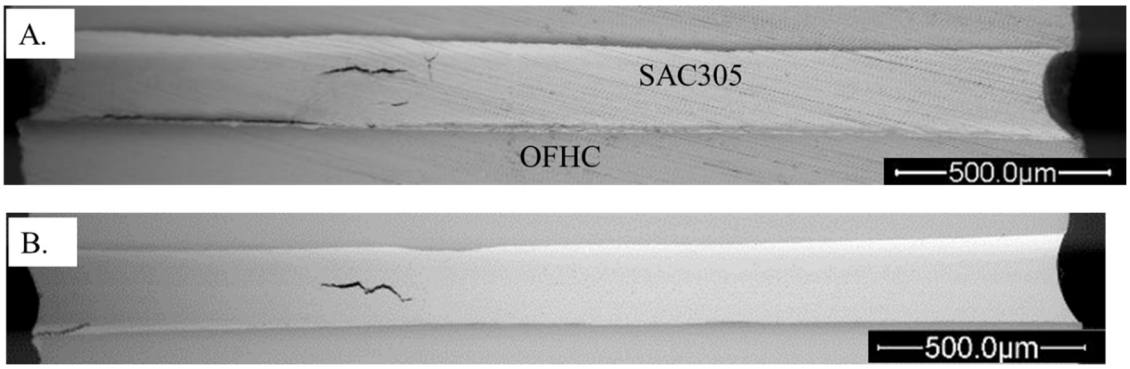

Figure 2-10 M90 Tensile Specimen A.) Before Polishing; B.) After Polishing.

In M90 tensile specimens, transverse deformation (in the x and z directions) of the solder layer is constrained by Copper and IMC layers, preventing Poisson's shrinkage of the solder during tensile loading. This mismatch becomes even more significant past the solder yield stress, when the solder experiences large inelastic isochoric deformation (with Poisson's ratio ≈0.5). As discussed before, this mismatch of properties between the solder and the IMC layer generates significantly higher global triaxial stresses near the IMC-solder bulk interface, under tensile loading, compared to that under shear loading. Higher triaxial stresses are known to allow the material to carry higher loads before it [51][13]. Therefore, the region around IMC-solder bulk interface effectively behaves like a more brittle material and favors brittle damage at the IMC-solder interface, compared to ductile deformation/damage within the bulk of the solder material.

Failure analysis of OFHC-SAC305 M0 shear specimens, as shown in Figure 2-8 and Figure 2-9, revealed a combination of different damage mechanisms. In addition to cracks along IMC-solder interface, there is considerably higher amount of

plastic deformation and ductile microstructural damage in the bulk of the solder, compared to that in M90 tensile specimens. The ductile damage is in the form of inter-granular cracks along grain boundaries, exacerbated by transgranular strain localization in certain grains in the form of shear bands on favorable slip systems. Thus, nominal shear stresses contribute to ductile bulk solder damage. The interfacial IMC-solder cracks first initiate at diagonally opposite corners of the solder joint due to local concentrations of bending stresses and then propagate inwards along the length of the solder joint, sometimes meandering into the solder bulk. Hence, damage in M90 (tensile) specimens is dominated by brittle interfacial damage, while damage in M0 (shear) specimens is due to a mixture of ductile solder damage and brittle interfacial damage. The drop in relative contribution of interfacial brittle damage (relative to bulk ductile solder damage) increases the fatigue durability of the M0 specimens, relative to the M90 tensile specimens. Since, ductile deformation of bulk solder is significantly higher in M0 shear specimens, their degradation and failure are more sensitive to the solder microstructure, compared to the degradation of M90 tensile specimens. This effect of microstructure on damage and failure is evident from the fact that shear durability test results show higher degree of statistical scatter across multiple specimens that have stochastic variability of grain structures. On the other hand, M90 tensile specimens which have significantly less bulk solder damage, show relatively low piece-to-piece variability in durability test results and lesser dependence of degradation/failure mechanism on solder grain structure.

M45 multiaxial specimens failed by a combination of the brittle interfacial and bulk ductile damage modes, consistent with those seen in the M90 tensile and M0 shear damage mechanisms. An example of failure analysis of OFHC-SAC305 M45 specimens is shown in Figure 2-11. As expected, M45 specimens were seen to experience a higher percentage of bulk solder damage than M90 tensile specimens, and a higher percentage of IMC-solder interfacial damage than M0 shear specimens.

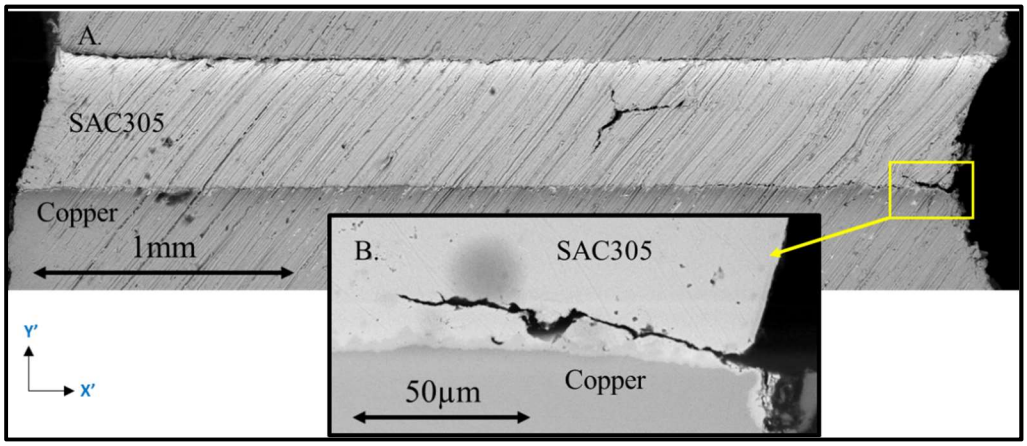

Figure 2-11 Failure analysis of M45 Specimen: A) SEM image before polishing; B) Zoomed SEM image after polishing

In summary, clearly, the damage and failure modes observed in solder joint specimens under multiaxial loading are sensitive to the nominal state of stress. Introduction of nominal tensile loading tends to lower the fatigue durability behavior of OFHC-SAC305 solder joints compared to nominal shear loading. This difference in failure modes suggest different fatigue failure mechanisms in nominally tensile vs.

shear loading. Stress analysis is conducted in the next section for more detailed insights into the stress states in both M0 shear and M90 tensile specimens.

2.4.Finite Element Analysis of M0 And M90 Specimens

To gain an understanding of the impact of tensile and shear loads on damage modes observed in solder joint specimens used in this study, an elastic-plastic finite element analysis (FEA) was conducted. The primary goal of this FEA is to qualitatively understand and compare the relative amounts of deviatoric deformation and volumetric deformation in the solder, under shear and tensile loading. In addition, this analysis was also used to estimate hydrostatic strains which will be used later for multiaxial damage model, as explained later in Section 2.5.

As shown in Figure 2-12, the model is a half-symmetry representation of the exposed portion of the test specimen that spans between the loading grips. The solder joint was modeled as a homogenous isotropic block of solder material sandwiched between the two copper substrates. The bottom face of the specimen was fixed and small cyclic displacements, ranging from 0.5 to 1.7μm, were applied on the top face along appropriate directions, to represent tensile and shear loads. 8-noded linear brick element with reduced integration (C3D8R) was used for modeling the entire specimen. Copper substrate was modelled as a linear elastic isotropic material (E=110GPa, ν=0.35). The solder properties used in the FE analysis (Figure 2-13- #3 dashed curve) were obtained by averaging the 1st half-cycle monotonic portion of the apparent stress-strain curves from the tested M0 shear (Figure 2-13- #4 curve) and M90 tensile

specimens (Figure 2-13- #2 curve). As discussed in the literature [13][14], this difference in the apparent stress-strain curves under tensile and shear loading in joint-scale specimens stems in part from the plastic transverse Poisson's constraint that is present under tensile loading but not under shear loading. In addition, as discussed in Section 6, there are important anisotropic grain-size effects in joint-scale specimens of high aspect ratio, that produce different behavior in tensile vs. shear loading. Not surprisingly, this average stress-strain curve identified from the experiments conducted in this study is consistent with properties reported in the literature from uniaxial tests on long SAC305 solder rods [52]; and falls within the range of properties from unaged condition (Figure 2-13- curve #1 [52]) to aged condition (Figure 2-13- curve #5 [52]). The aging was conducted for 4500 hours at 125^{o}C and nominal strain rate during the test was 0.001/s.

The FEA model based on this average SAC305 isotropic stress-strain behavior is validated in Figure 2-14 by comparing the predicted structural response of the tensile and shear specimens with experimental measurements. As expected, the normalized load-displacement curves (the average stress-strain response) predicted by the FEA (red curve) under-predicts the measured plastic hardening in tensile specimens (black curve in Figure 2-14A) and over-predicts the measured plastic hardening in shear specimens (black curve in Figure 2-14B). Section #2.7 contains further discussions on some of the fundamental limitations regarding experimental validation of FEA models that represent anisotropic grain-scale solder joints with simplified homogeneous isotropic material models.

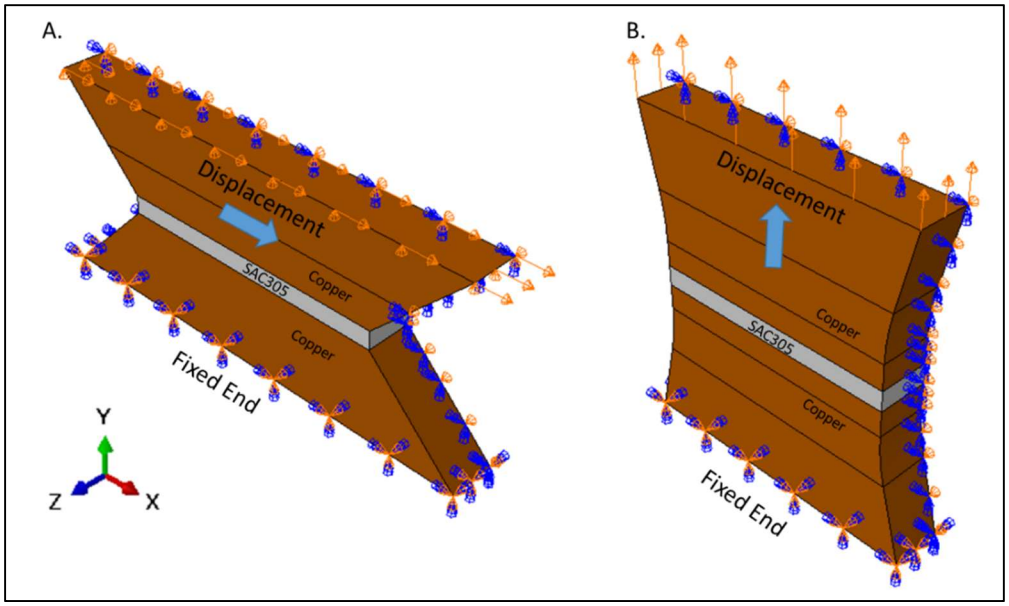

Figure 2-12 FEA Model and Boundary Conditions: A. M0 (shear) specimen; B. M90 (tensile) specimen

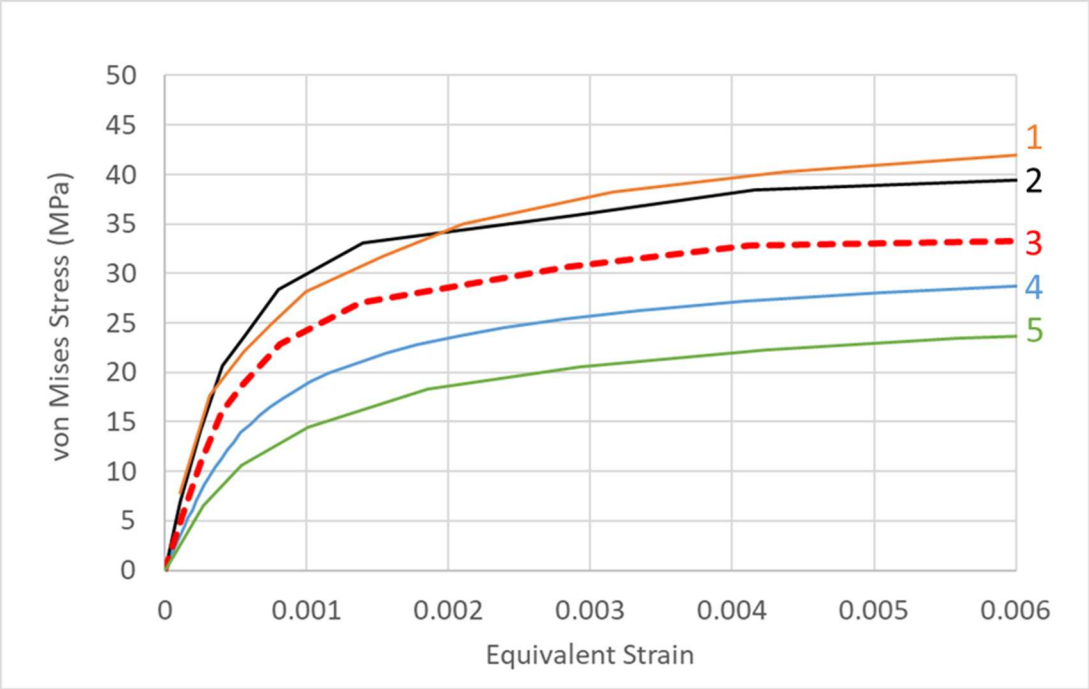

Figure 2-13 SAC305 von Mises true stress-strain curves for: (1) Unaged specimen [52]; (2) M90 tensile tests; (3) Average of M90 tensile and M0 shear tests; (4) M0 shear tests; (5) Aged specimen [52].

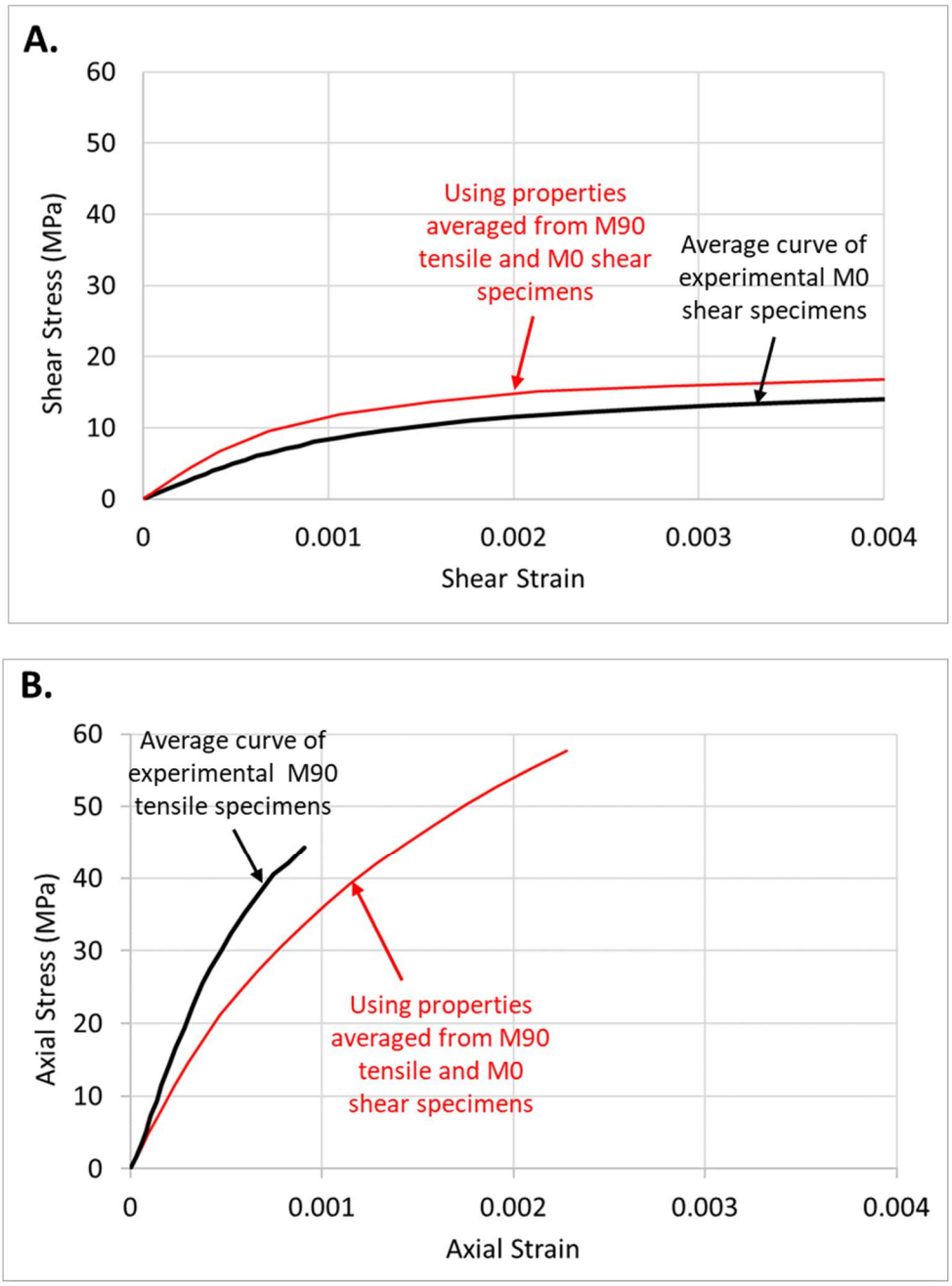

Figure 2-14 A.) M0 shear specimen stress-strain validation; B.) M90 tensile specimen stress-strain validation

The predicted strain field are very instructive, even for this simplified homogeneous isotropic representation. As an example, Figure 2-15 shows comparison of von Mises strain, equivalent plastic strain and hydrostatic strain (as computed by ABAQUS finite element software) in solder layers of M0 (shear) and M90 (tensile) specimens when subjected to 1μm displacement. M0 (shear) specimens have uniform distribution of von Mises stress and equivalent plastic strain in the bulk of the solder; and the average magnitudes of the von Mises stress and equivalent plastic strain are significantly higher than in M90 (tensile) specimen, for comparable deformation levels. This is consistent with the higher level of bulk solder damage observed in M0 (shear) specimens, compared to that in M90 (tensile) specimens. In addition, the significantly higher IMC-solder interfacial damage in the M90 tensile specimen can be explained by the high hydrostatic strains at the interfacial layers of the M90 tensile specimen, compared to that in M0 shear specimen (for comparable deformation levels). The results also confirm that volume-averaged ϵ_{xx} in-plane transverse strain was less than 20% of the volume-averaged axial strain ϵ_{yy} for M90 (tensile) specimens.

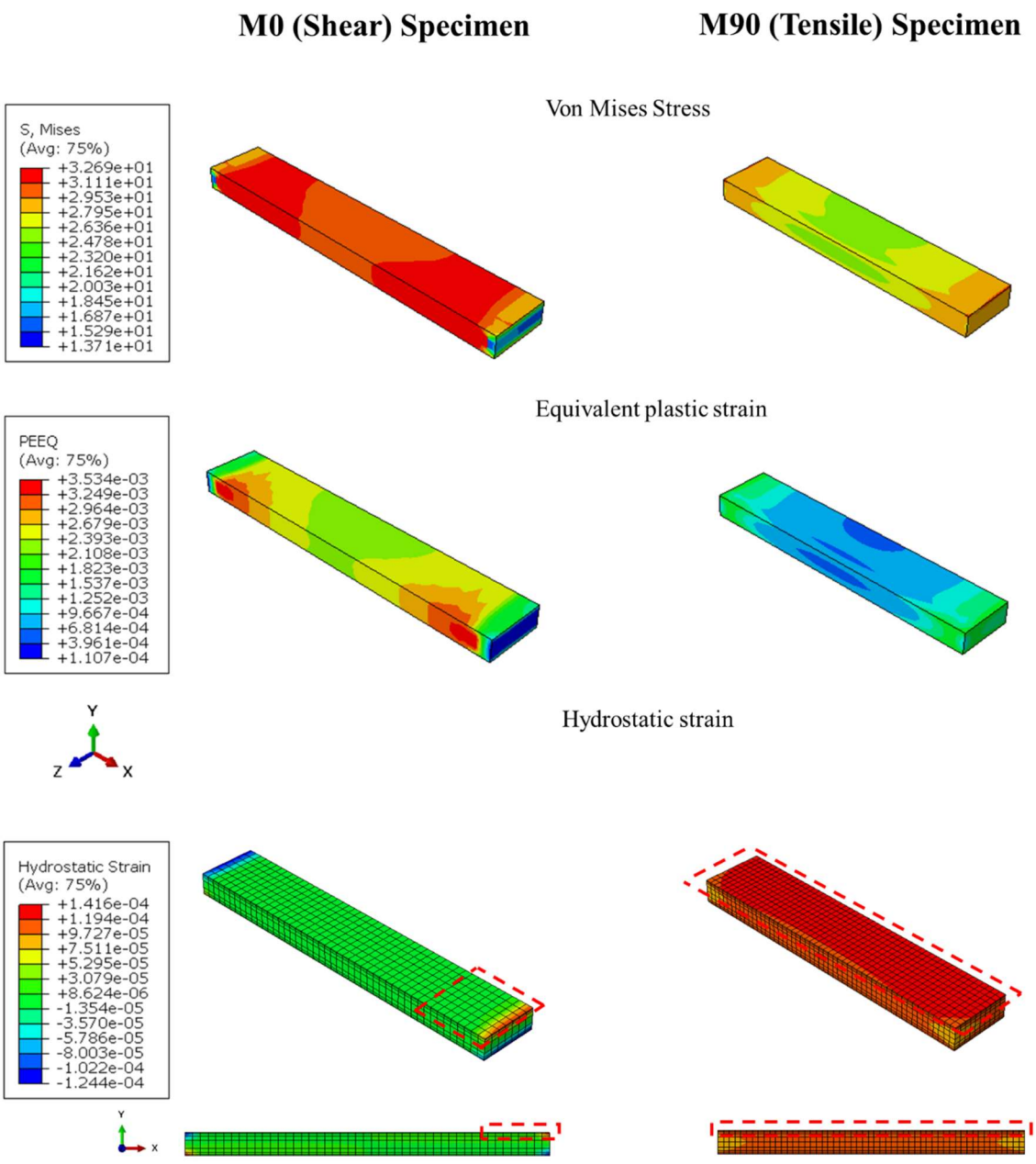

Figure 2-15 von Mises stress, equivalent plastic strain and hydrostatic strain contour plots of solder layer in shear and tensile specimen for 1 μm displacement.

2.5.Multiaxial Fatigue Damage Model

As mentioned in earlier, the fatigue durability plots in Figure 2-7 demonstrate that for a given joint configuration (material and geometry), the total equivalent strain range is not a sufficiently comprehensive metric for establishing a universal fatigue durability model that is applicable under all possible multiaxial stress states. In other words, the cyclic equivalent strain range is not a sufficient descriptor of all relevant damage mechanisms that compete under different multiaxial stress states. Therefore, a linear damage superposition multi-mode approach similar to that developed in the past [53], is proposed as a means for unifying quantification of the fatigue damage across different multiaxial stress-states.

The damage mode for each multiaxial loading combination is treated as a combination of some degree of interfacial damage at the IMC layer and some degree of bulk solder damage (transgranular and intergranular damage). As an example, the M90 (tensile) loading produces predominantly interfacial damage. In contrast, the M0 (shear) and M45 (multiaxial) loading produces varying combinations of interfacial damage as well as damage in the bulk of the solder.

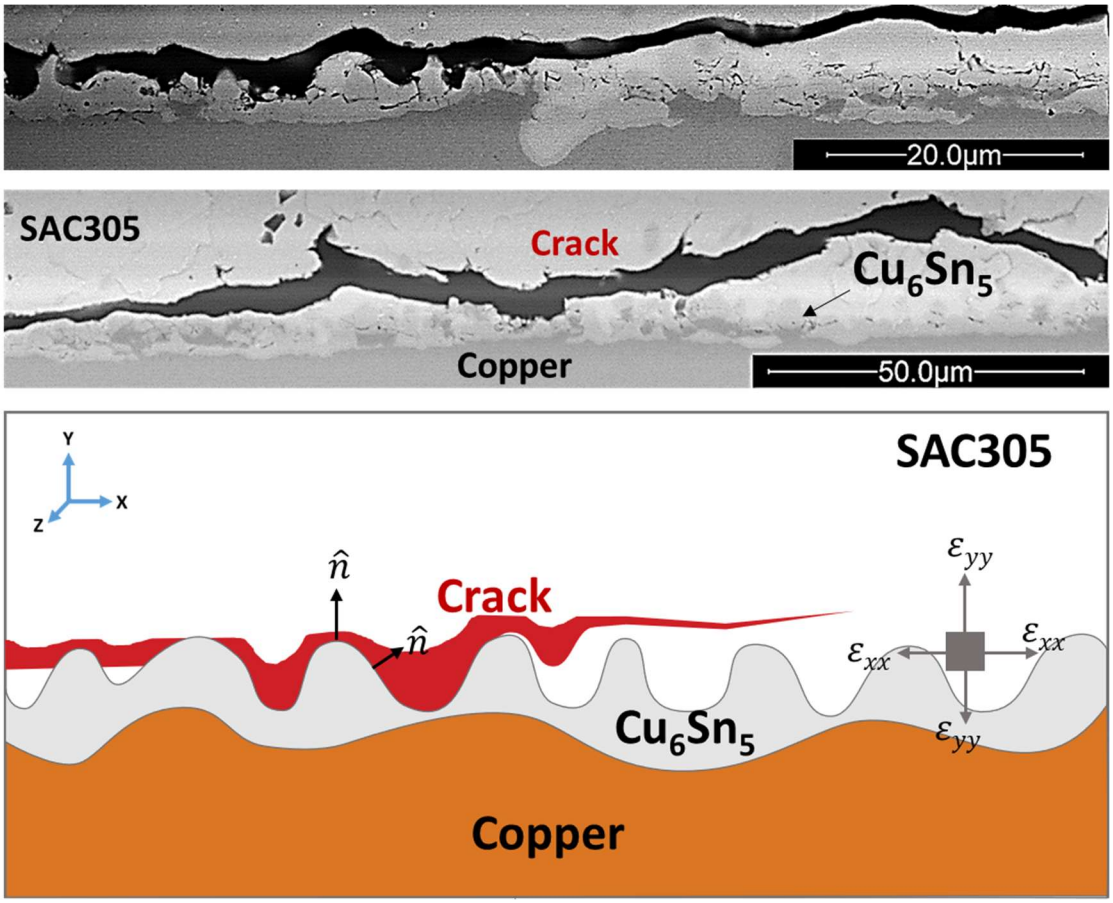

Figure 2-16 Damage near IMC layer in M90 and M0 specimens

The interfacial damage mode near the IMC layer is assumed to be driven predominantly by the interfacial positive hydrostatic strains. Positive hydrostatic strains occur during tensile portion of M90 (tensile) solder joint and at diagonally opposite edges of M0 (shear) solder joint. Even though peel strains drive mode-I interfacial ductile damage during tensile loading, the wavy and scalloped shape of the IMCs leads to locally wavy damage path and complex locally multiaxial strain states in the damage zone, as shown in Figure 2-16. Therefore, it is more appropriate to correlate interfacial ductile damage mechanism to interfacial positive hydrostatic

strains rather than to peel strains. At the interface (where the tensile failures are predominantly localized), the positive hydrostatic strain is estimated by considering both the axial strain in the loading direction as well as the transverse strains caused by the Poisson ratio mismatch between the substrate and the solder (details of this process are discussed later in this section). In contrast, the equivalent strain in the solder bulk is correlated to intergranular and transgranular damage. The respective damage contributions due to the interfacial damage and intergranular/transgranular solder damage were approximated from the SN plots obtained in this study from the M90 (tensile) and M0 (shear) specimens, respectively. The solder bulk and the interfaces in the joint are considered to act like nonlinear springs in series, both forms of damage (damage in the bulk and damage at the interface) contribute to loss in the load-carrying capacity of the joint (and therefore can be treated as instantaneous increase in the compliance of each spring in this series network). Hence, these two damage contributions are treated additively and are linearly superposed in Eq. 2-8 below, to provide an approximate estimate of the total loss of load carrying capacity. This loss in load carrying capacity is used as the failure criterion in the fatigue damage measurements in Section #2). This damage superposition scheme is shown in Eq. 2-6-Eq. 2-9.

$$\epsilon_{\mathrm{h}}^{\mathrm{interface}} = A_1 D_1^{m_1} \qquad \text{Eq. 2-6}$$

$$\Delta\epsilon_{eq}^{bulk} = A_2 D_2^{m_2} \quad \text{Eq. 2-7}$$

$$D_t = D_1 + D_2 = \left(\frac{\epsilon_h^{interface}}{A_1}\right)^{\left(\frac{1}{m_1}\right)} + \left(\frac{\Delta\epsilon_{eq}^{bulk}}{A_2}\right)^{\left(\frac{1}{m_2}\right)} \quad \text{Eq. 2-8}$$

$$N_t = \frac{1}{D_t} \quad \text{Eq. 2-9}$$

Where, A_1, m_1 are power-law fatigue durability model constants for interfacial fatigue damage and are dependent on interfacial features such as IMC species (which in turn depends on the solder material, substrate plating) and waviness of the IMC layer (which in turn can depend on the surface roughness of the substrate). A_2, m_2 are corresponding damage constants for damage in the solder bulk and depend on the solder material. In addition, all four model constants also depend upon the soldering profile and thermal aging history. The values for these damage model constants (given in Table 2-1) are estimated from the hydrostatic and equivalent strain vs. damage plots shown in Figure 2-19 and Figure 2-20. $\epsilon_h^{interface}$ is the tensile amplitude of cyclic hydrostatic strains at the interface (compressive portion of the cyclic hydrostatic strain is ignored as it does not cause damage propagation at interface) and $\Delta\epsilon_{eq}^{bulk}$ is the cyclic range of equivalent strain in the bulk solder. D_1 and D_2 are metrics of continuum damage, for interfacial damage and intergranular/transgranular solder damage, respectively. D_t is the total continuum damage due to combinations of interfacial and solder damage contributions under multiaxial loading and is an indirect indicator of the

load carrying capacity of the specimen. N_t, the corresponding cycles to failure under multiaxial stress state, is estimated as the reciprocal of D_t.

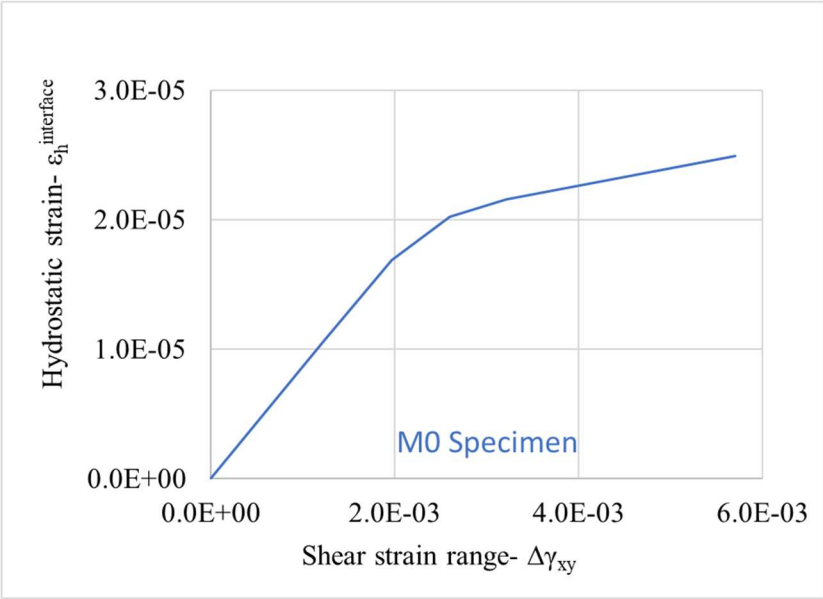

Figure 2-17 Relationship between interfacial hydrostatic strain (locally averaged near diagonal corners) and shear cyclic strain range (averaged over the entire solder region) estimated using FEA for M0 specimen.

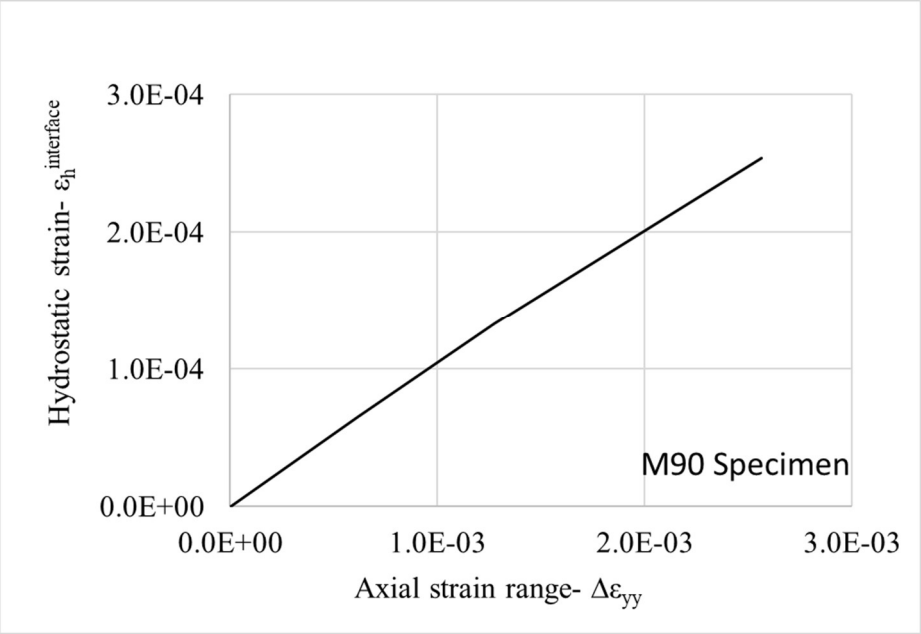

Figure 2-18 Relationship between interfacial hydrostatic strain and axial strain range (averaged over the entire solder region) estimated using FEA for M90 specimen.

The hydrostatic strain $\epsilon_h^{interface}$ is estimated at the substrate-solder interface using a hybrid approach. Axial strain range $\Delta\epsilon_{yy}$ and shear strain range $\Delta\gamma_{xy}$ are experimentally measured from M90 and M0 cyclic tensile tests, while hydrostatic strain $\epsilon_h^{interface}$ is estimated using finite element analysis because hydrostatic strain cannot be directly measured experimentally. The details of the finite element analysis are provided in Section 2.4. Equivalent strain range $\Delta\epsilon_{eq}^{bulk}$ was estimated from experimentally measured shear strain range $\Delta\gamma_{xy}$ during entire cycle of M0 shear fatigue tests, as shown in Eq. 2-3. Finite element models of M90 and M0 specimens were used to determine the relation between volume averaged hydrostatic strain $\epsilon_h^{interface}$ in the interfacial region to average axial strain range $\Delta\epsilon_{yy}$ in the solder for

M90 specimen and shear strain range $\Delta\gamma_{xy}$ in the solder for M0 specimen as shown in Figure 2-17 and Figure 2-18. The finite element models assume interfacial IMCs as a flat layer instead of a wavy surface for simplification. Thus, the current model constants should be treated as appropriate model constants for the level of IMC waviness seen in the tested specimens. The role of this interfacial waviness needs to be examined in future studies by testing specimens of varying the IMC waviness and combining the test results with global-local finite element modeling approach to capture the effect of IMC morphology on local hydrostatic strains. The interfacial elements used for calculating hydrostatic strains and their locations in the M90 and M0 specimens are marked in red boxes in Figure 2-15. The size of the red box depends on the concentration of hydrostatic strains in the interfacial layer of tensile and shear specimens. In M90 tensile specimens, volume averaged hydrostatic strain is calculated from the elements along the entire solder-IMC interface in M90 tensile specimens during tensile portion of the cycle, as damage is distributed along the entire interfacial region. In contrast, in M0 shear specimens, the diagonally opposite corners experience local concentrations of hydrostatic tensile strain during half of the load cycle. Therefore, elements in the area marked by red box in Figure 2-15 (which is 15% of the total surface area of entire interface) close to the corner edge were used for volume averaging corresponding to the interfacial damage zone in M0 shear specimens.

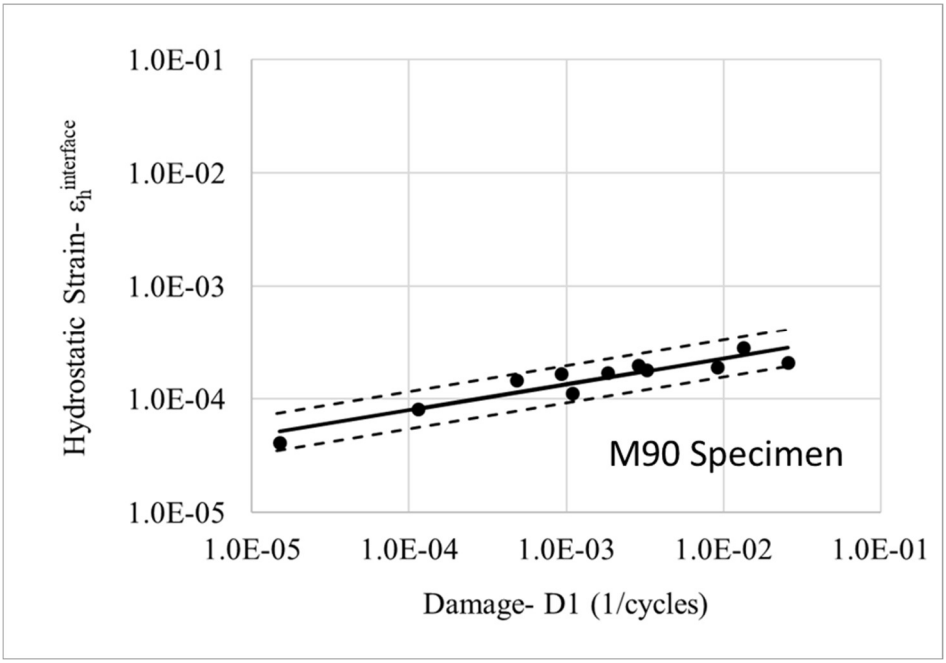

Figure 2-19 Hydrostatic strain vs. interfacial damage plot for M90 (tensile) specimen with 90% confidence intervals.

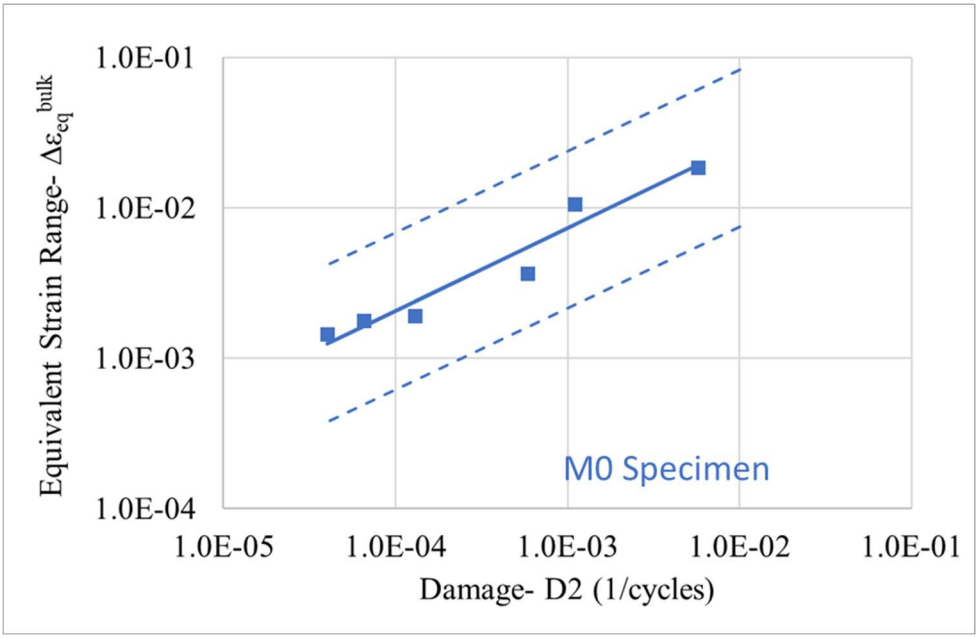

Figure 2-20 Equivalent strain range vs. bulk damage plot for M0 (shear) specimen with 90% confidence intervals.

Table 2-1 Power Law Fatigue Model Constants with 90% confidence bounds

Parameter	**IMC interface damage**		**Bulk solder damage (Intergranular and transgranular damage)**	
A [cycles]^m	6.57E-4	Upper bound: 9.5E-4	3E-1	Upper bound: 10E-1
		Lower bound: 4.5E-4		Lower bound: 0.9E-1
m	0.23		0.54	

The fatigue life predicted by the proposed damage model for cyclic tensile (M90), shear (M0) and multiaxial (M45) test data is plotted in Figure 2-21 to

demonstrate the ability of this damage modeling approach (given earlier in Eq. 2-6-Eq. 2-9), to describe the fatigue degradation observed under different multiaxial stress states explored in this study. The average experimental trends, for all tested loading combinations, appear to be well described with this power-law linear damage superposition approach. This linear damage superposition approach presents an easily implementable method to predict the average fatigue life of solder joints where the geometry can be approximated as a series combination of deformation at the interface and deformation in the solder bulk (e.g. in ball grid array (BGA), quad flat pack (QFP), small outline packages (SOP), quad flat no-lead (QFN), etc.) subjected to multiaxial cyclic stress states. However, there is significant stochastic variability seen in the test results, due to the piece-to-piece variation in the grain structure. This stochastic uncertainty will be addressed and quantified in a future paper with grain-scale analysis.

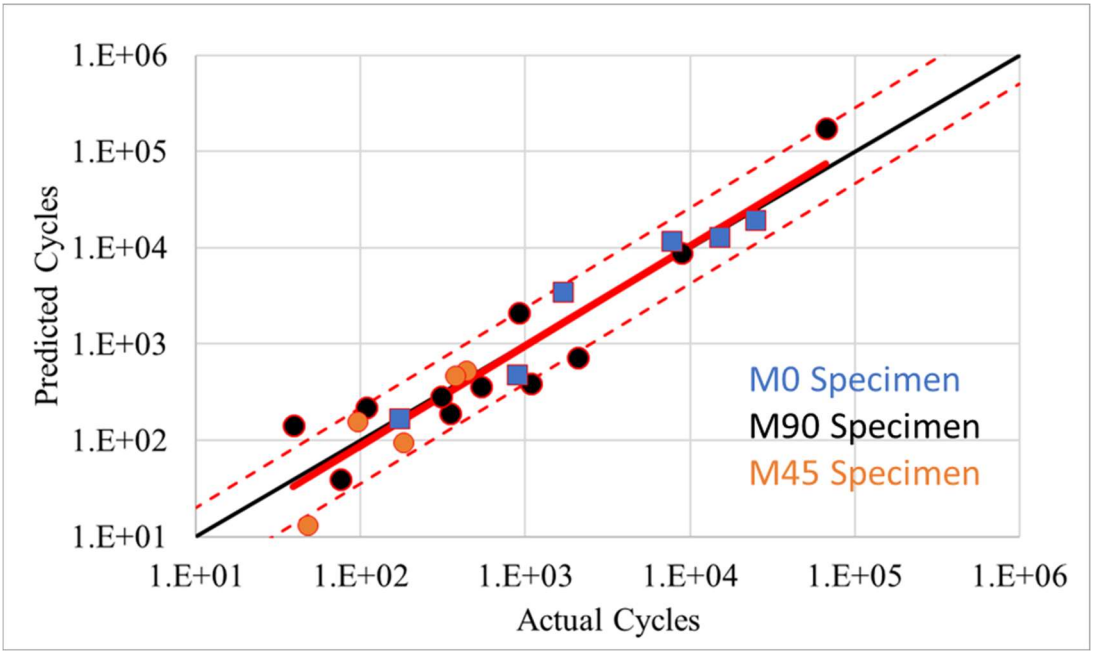

Figure 2-21 Goodness of fit of fatigue life predictions based on the damage model with 90% confidence bounds.

The damage sites predicted by the multiaxial fatigue damage model are presented in Figure 2-22. The damage model reasonably predicts significant uniform bulk solder damage and interfacial damage in diagonal corners in M0 (shear) specimen. In M90 (tensile) specimen, the model predicts significant interfacial damage and negligible bulk solder damage. Therefore, the damage predicted by both specimens is consistent with the failure sites observed in the failure analysis. It should be noted that the constants A_1, m_1 presented in Table 2-1, only capture interfacial damage due to hydrostatic strains at the interface and should only be used to predict interfacial damage. In case, hydrostatic strains are used to model bulk solder damage in different studies in future, the constants would need to be estimated accordingly.

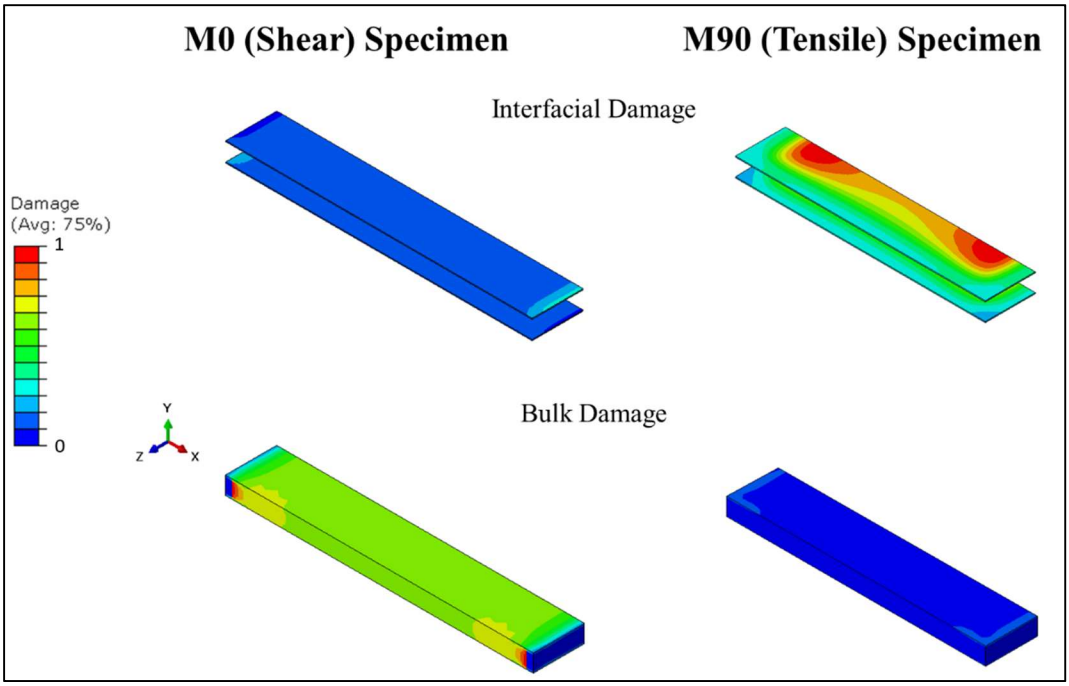

Figure 2-22 Interfacial and bulk damage predicted by the multiaxial damage model.

2.6.Summary and Conclusions

Cyclic mechanical fatigue tests were conducted at room temperature on OFHC-SAC305 microscale solder joint specimens, in tensile, shear and multiaxial loading modes. Cyclic fatigue test results showed that the cyclic tensile loading mode is more damaging than cyclic shear mode in grain-scale SAC joints. The different slopes of the SN curves in the individual (tensile, shear and combined) load cases indicate different deformation and degradation mechanisms. The durability of M0 (shear) specimens is more dependent on solder microstructure compared to durability of M90 (tensile) specimens for comparable deformation levels. Dominant damage mode in tensile M90 mode was brittle failure at interface of IMC and solder, whereas failures in shear M0

loading were dominated by ductile damage (intergranular and transgranular) in the bulk of the solder. M45 (multiaxial) specimens experienced mixed-mode failures with higher degree of ductile bulk solder damage than tensile specimens and higher degree of brittle IMC-solder interfacial damage than shear specimens. Importantly, the differences in the nominal tensile, shear and multiaxial durability curves for same material also indicates that equivalent strain in the solder bulk is not a sufficiently generic metric to properly represent durability of SAC305 solder joints across all stress states. Instead, a simple linear damage superposition method is proposed here to represent the durability under different combinations of stress states. This approach accounts for both interfacial damage at solder-IMC interface as well as transgranular and intergranular damage in the bulk of the solder. The two metrics driving this model are the interfacial hydrostatic strain and the average equivalent strain in the solder bulk. It should be noted that the fatigue curves and the life prediction model constants presented in this work are applicable to solder joints which have similar substrate-solder configuration, in terms of joint geometric length-scales, material combinations, substrate roughness and specimen fabrication protocol. Significant changes in these parameters will lead to a different fatigue behavior under tensile vs. shear loading modes.

Additionally, the fatigue behavior of bulk multi-grained solder dog bone specimens typically used for material characterization will also have different fatigue behavior since those specimens lack the deformation constraints caused by the

substrates and lack the interfacial degradation mechanism caused by the presence of the IMC layer.

In summary, the goal of this work was to provide evidence of potential differences in cyclic fatigue failure mechanisms of solder joints when loaded under tensile, shear and multiaxial loading modes. This work also draws attention to the fact that reliability engineers cannot simply rely on fatigue models developed by shear loaded solder joints and must account for additional detrimental influence of tensile loads. Similarly, fatigue damage models for predicting solder joint failure cannot be developed from cyclic testing of bulk dog-bone solder specimens. While accelerated temperature cycling tests do include some tensile loads caused by warpage, traditional Coffin-Manson fatigue model fitted to the test data for a specific PWA will not be generic enough to predict life accurately when the relative severity of warpage (relative to shear deformation) changes.

The findings of this study will be useful when designing components such as Quad Flat No-Lead Package (QFN), Loss-Free Package (LFPAK), and other similar package geometries which consist of solder joints of high aspect ratios, for high reliability, under combined tensile and shear loads caused by PCB flexure and thermal expansion.

2.7.Discussion

The finite element analysis conducted in this study has some limitations, as the solder material was modeled as a homogenous isotropic material. In contrast, TMM SAC solder joints (as well as functional SAC solder joints) as seen in cross-polarized images in Figure 2-4, consist of few highly anisotropic coarse grains of high aspect ratio (ratio of length in X-direction to height in Y-direction). Consequently, each solder joint has a unique structural force-displacement response. As seen before in Section #2.4, the average isotropic FEA results over-predict the inelastic hardening of the shear specimen (Figure 2-14A) but underpredict the inelastic hardening of the tensile specimen (Figure 2-14B). This difference between tensile and shear behavior is believed to be due to an interaction between: (i) the mechanical anisotropy of SAC grains and; (ii) the high aspect ratio of the solder grains due to the high geometric aspect ratio of TMM solder specimens. The effects of this grain-scale anisotropy (anisotropy in mechanical properties as well as in geometry) are beyond the scope of the present paper and will be further explored in a future paper.

Chapter 3 : Grain-scale Study of SAC305 Oligocrystalline Solder Joints: Part-1 -Anisotropic Elasto-Plastic Constitutive Properties of Single Crystals

3.1.Abstract

This paper focuses on anisotropic elastic-plastic constitutive modeling of SAC solder grains because of their importance in modeling the behavior of oligocrystalline (few-grained) micron-scale solder joints that are increasingly common in heterogeneous integration. Such grain-scale modeling provides detailed information about the stress concentrations caused by grain mismatches in solder joints that are unavailable when modeled as homogenous domains with an average set of isotropic mechanical properties. Grain-scale information about local strain concentrations within the grain and at grain boundaries can provide a more accurate assessment of different damage modes such as intergranular/transgranular damage within the solder joint or damage near interfacial intermetallic compound (IMC) layers. This is the first paper in a 2-part series and presents the anisotropic elastic-plastic behavior of SAC305 solder alloy. The second paper of this 2-part series utilizes these single-crystal properties for parametric finite element modeling of oligocrystalline solder joints to provide insights into the variability of the mechanical fields and the resulting variability of fatigue degradation modes under multiaxial cyclic mechanical loading.

In the present paper, the single-crystal anisotropic elastic-plastic constitutive properties are empirically estimated from monotonic tensile and shear tests on

monocrystalline and oligocrystalline SAC305 solder joints fabricated with different cooling rates. Anisotropic behavior in each grain is represented with an anisotropic continuum plasticity model, which utilizes Hill's anisotropic yield potential along with Holloman's power-law plastic flow rule. Mechanistically motivated scaling factors are proposed to account for the influence of different grain sizes as well as for the different dendritic and eutectic microstructural morphology within the grains in specimens fabricated with varying rates of cooling. These microstructural scale factors within each grain allow scaling of the stress-strain response for different cooling rates and different isothermal aging protocols. Model constants were assessed by conducting grain-scale finite element simulations of each test specimen with microstructurally-informed anisotropic elastic-plastic constitutive models and matching the simulation results to the experimental measurements.

3.2.Introduction

This section discusses background and motivation of the present work and the literature review.

3.2.1. Background and Motivation

The semiconductor industry has opted for heterogeneous integration of different individually designed and manufactured diverse chiplets and components in a single package to maintain the pace of improvement of functionality, performance, and cost. Multiple different dies are integrated into a package either side-by-side or in 3D stacks so that the resulting system in package (SiP) can perform enhanced functions

in a small form factor [35] [56]. Heterogeneous integration inevitably leads to hierarchical interconnection architectures, resulting in a wide range of solder joint characteristic dimensions and pitch ranging from near-10 microns to several 100 microns. This miniaturization has resulted in SAC solder joints with one grain (monocrystalline) or, at most, a few grains (oligocrystalline). At this length scale, the mechanical response of each solder joint is highly sensitive to the grain-scale anisotropic properties, which are very different from the bulk isotropic polygranular solder mechanical properties commonly found in the literature. SAC305 consists of 96.5% β-Sn ,which has a body-centered tetragonal (BCT) crystal lattice (a = 0.58 nm, c = 0.317 nm, and c/a = 0.545), and strong anisotropy of the thermal expansion coefficient and the modulus of elasticity, as shown in Figure 3-1 [18]. The modulus of elasticity in the [001] direction at 20°C is 68 GPa, which is considerably larger than the [100] direction, which has a modulus of elasticity of about 24 GPa. Besides, the coefficient of thermal expansion in the [001] direction is 30 ppm/°C, which is almost twice as large as that in the [100] direction. The anisotropic elastic stiffness constants for β-Sn have been characterized by several researchers in the past and used for modeling Tin-rich SAC solder joints in lieu of SAC properties [19][20]. Jiang et. al [5] quantified the elastic stiffness constants for SAC305 shown in Table 3-1 by incorporating the microstructural variations between SAC grain and Sn grain.

Apart from the highly anisotropic behavior of SAC, another source of variation in SAC305 properties is its heterogeneous microstructure. The entire composition of SAC305 from macro to nano length-scale has been classified in different tiers by

Cuddalorepatta et. al [11] as shown in Figure 3-2. Tier 4 consists of a macroscale package assembly that contains multiple solder interconnects. Tier 3 consists of a single oligocrystalline solder joint. Tiers 0-2 consist of the microstructure within each SAC grain. A SAC grain consists of pro-eutectic β-Sn dendrites surrounded by a eutectic Sn-Ag micro-constituent. There are also embedded Cu_6Sn_5 IMC microconstituents. This micromorphology within each grain is termed Tier 2. The Tier 1 eutectic Ag-Sn micro-constituent consists of nanoscale Ag_3Sn intermetallic compound (IMC) particles distributed in β-Sn matrix. These IMC particles block the dislocation motions, leading to dispersion strengthening in the eutectic micro-constituent. The β-Sn matrix is labeled as Tier 0.

Another challenge in characterizing the uniaxial tensile behavior of solder joints arises from the length scale effect of the solder joint specimen used for testing. As the aspect ratio of solder joints increases, the global triaxial stresses (due to Poisson mismatch with the Cu substrate and the interfacial Cu-Sn IMC layers) significantly increase the extensional forces required to yield the solder joint [16] [17]. Therefore, it is informative to evaluate the mechanical properties of solder joints using specimens whose geometry are representative of functional solder joints.

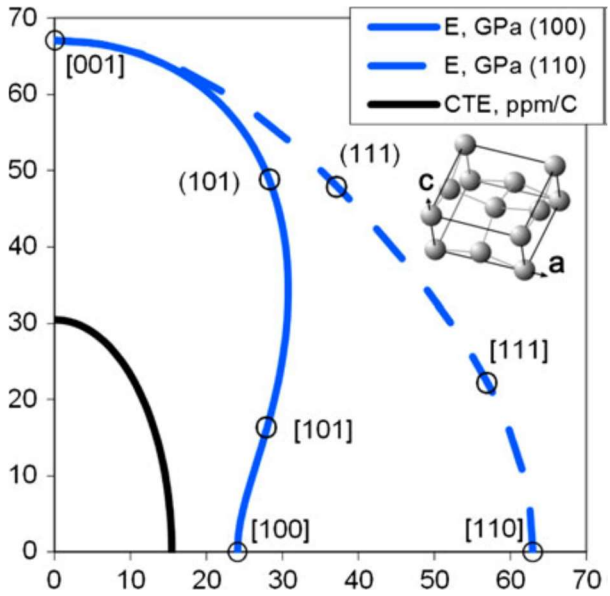

Figure 3-1 Elastic modulus and CTE of Sn in different crystal directions [18]

Table 3-1 Elastic Constants of SAC grain (GPa) [5]

C_{11}	C_{22}	C_{33}	C_{44}	C_{55}	C_{66}	C_{23}	C_{13}	C_{12}
73.2	73.5	89.3	22.3	22.3	24.2	36.4	36.3	59.6

Owing to the severe anisotropy and variability seen in the mechanical behavior of solder joints, many researchers have studied the impact of solder microstructure on failures. Matin et al. investigated deformations in solder joints subjected to thermal cycling and correlated those microscopic observations with stress fields obtained from elastic anisotropic FE analysis [21]. In addition, Park et al. [22][23] characterized strain fields in temperature cycled SAC solder balls with single and multi-grained microstructure using DIC. Cross-polarized microscopy was conducted to correlate the damage sites with the microstructure. The highest strain concentrations and cracking

were along the grain boundaries and Cu pad-solder interfaces in few-grained solder joints.

Arfaei et. al [24] **Error! Reference source not found.** studied the effect of number of grains and their orientation on cyclic mechanical fatigue of solder balls under shear mode. Fatigue lifetimes for multi-grained (2 to 3 grains) solder ball was found to be longer than single grain solder balls. Early failures were observed in single grain solder joint with grain-oriented along [001], [010], and [110] directions. Similarly, Bieler et. al. [12] looked at the effect of Sn grain size and orientation on thermomechanical reliability of solder joints. OIM (orientation imaging microscopy) analysis clearly indicated that the severity of damage correlated with the orientations that had very high CTE values ([001] direction). Maximum CTE mismatch is observed when the crystal c-direction is oriented parallel to the substrate and is a worst-case scenario. Xu et. al [25] examined the grain structure in BGA solder balls and correlated that with fatigue failures. The grain structure of different solder balls within a BGA package was found to be sensitive to the joint location and cooling rate. The fatigue resistance was found to improve as the number of grains increased, possibly due to reduced mismatch at grain boundaries with decreasing grain size.

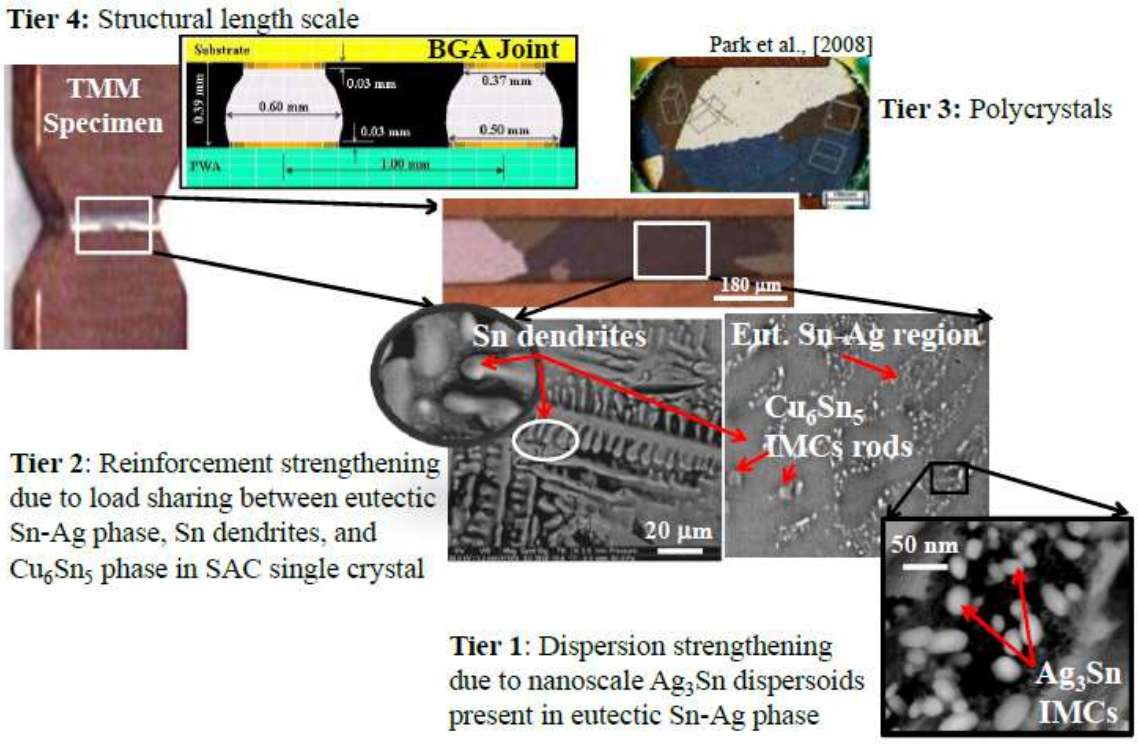

Figure 3-2 SAC solder microstructure classified in different tiers across different length-scales [54]

In conclusion, appropriate understanding and quantification of solder microstructure is needed for modeling anisotropic grain-scale behavior of small oligocrystalline solder joints. However, the present literature on experimental characterization and continuum-modeling of anisotropic properties for SAC305 is very limited. In absence of reliable anisotropic properties of SAC305 and complexities in modeling, engineers have traditionally relied on more approximate homogenous isotropic mechanical properties for estimating stresses and strains in the solder joints. Several factors affect the microstructure of the lead-free solder alloys such as composition, solder cooling rates, time above liquidus, aging conditions and surface

plating materials. Section 3.2.2 presents the effect of cooling rate and isothermal aging on mechanical properties of solder joints.

3.2.2. Effect of cooling rate on constitutive properties of SAC solder alloy

The cooling rate during the assembly process impacts the solder microstructure and thermo-mechanical behavior of solder joints. However, the literature on the effect of cooling rate (and the resulting solidification rate and crystallization rate) on SAC solder behavior is somewhat limited. Wei et. al. [26] studied the effect of cooling rates (0.14 K/s, 1.7 K/s, ~100 K/s) on the microhardness of SAC305 solder joints. The β-Sn pro-eutectic dendrite size and arm spacing was seen to decrease as the cooling rate increased. In addition, faster cooling rates lead to finer eutectic microstructure, consisting of closely spaced and uniformly distributed small Ag_3Sn particles, resulting in severe dispersion strengthening. Conversely, a slower cooling rate leads to significantly coarser Ag_3Sn IMC particles in the eutectic region. Consequently, Vickers microhardness was seen to increase with rapid solidification rates.

Similarly, Lee et. al. [27] studied the SAC305 microstructure under different cooling rates- 2.5°C/s, 9°C/s, 21°C/s, and 63°C/s. The β-Sn dendrite size (620μm^2, 550μm^2, 380μm^2 and 30μm^2) and volume fraction (55.3%, 50.2%, 42.5%, and 27.8%) decreased as the cooling rate increased monotonically. The Ag_3Sn IMC was shaped like a leaf at the lowest cooling rate and changed to ellipsoidal particles at the highest cooling rate. In addition, the tensile strength was seen to reduce by 34% between the highest cooling rate (60.8 MPa) to the lowest cooling rate (39.5 MPa). Mueller et al.

[28] analyzed the effect of cooling rate, composition, and solder volume on the microstructure of lead-free solder joints. Cooling rates used in this study were 0.14K/s, 1.1K/s and 10.9K/s. An increase in cooling rate was seen to reduce the size of IMC particles and spacing between β−Sn dendrites, whereas the area fraction of the eutectic Ag3Sn phase was seen to increase. Mutuku et. al. [29] investigated the effect of cooling rate, aging time on microstructure, and shear fatigue lifetimes of different SAC solder joints. The mechanical properties of lead-free solder joints were found to vary in direct correlation with the distribution of dispersoids in the joint. The solder joint strength and shear fatigue life increased as the number of Ag_3Sn IMC particles increased (with increasing cooling rate).

3.2.3. Effect of aging on constitutive properties of SAC solder alloy

Numerous researchers have reported that post-reflow isothermal aging temperature and duration influences the solder microstructure and mechanical properties, similar to the influences seen for different cooling rates. Solder microstructure continuously evolves throughout its life, starting from the assembly process to its end of life. It's important to understand the evolution of the stress-strain response of SAC305 since its degradation or enhancement can both influence its fatigue durability. Chauhan and Mukherjee, [30] quantified microstructural parameters such as size, volume fraction and spacing of nanoscale Ag_3Sn, Cu_6Sn_5 IMCs and Sn dendrites in SAC305 solder alloy during 24-1000 Hrs. of aging at 100°C. The microstructural parameters were used in mechanical multi-scale creep model to study the effect of aging on creep behavior of SAC305 solder joints. The Ag_3Sn IMC particle size and

spacing was seen to monotonically increase with increasing aging duration. In contrast, evolution of the microscale Cu_6Sn_5 phase wasn't sensitive to aging duration and exhibited a non-monotonic trend. Volume fraction of pure Sn dendrites increased monotonically from 59% to 72% from as soldered condition to 1000 Hrs. of aging. Secondary creep resistance of SAC305 was seen to decrease with aging, since the coarsening of the eutectic phase (increased Ag_3Sn particle spacing) reduced the dispersion strengthening of the alloy. This trend was measured experimentally and also predicted with microstructurally motivated multiscale crystal viscoplasticity models.

Lall et. al. [31] conducted uniaxial tensile tests at different test temperatures (25°C, 75°C, 100°C and 125°C) and at different strain rates (1E-3, 1E-4 and 1E-5 s^{-1}) on SAC305 bulk solder bars aged at 100°C for different durations (0-12 months). The yield strength and ultimate tensile strength of the solder was seen to decrease significantly with the duration of aging and test temperature for a given strain rate. Similar trends were also observed for reflow cooled specimen as well. Fu et. al. [32] studied the effect of long-term aging of SAC305 and SAC405 solder specimen on its cyclic stress-strain response. The tests were conducted at 25 °C and 1E-3 strain rate. The test specimens were subjected to two aging temperatures- 25 °C and 125 °C for various aging periods (0, 5, 10, 20, 30, 45, 60, 80, 110, 150, 200, 260, and 360 days). A microscopic examination of fixed region of a sample was conducted at the end of each aging period. The stress-strain hysteresis area ΔW reduced significantly in first few days of aging and then stabilized. This was correlated with the coarsening of Ag_3Sn IMC particles and weakening of pure tin dendritic structure. Fu and Wu [33] [34] in

different studies have quantified the evolution of microstructure at different intervals during the aging period. The Ag_3Sn particle size and number was measured at a fixed location in the specimen by analyzing the SEM images using image processing tools.

3.2.4. Overall Approach

The present study characterizes the anisotropic plastic behavior of SAC305 solder joints by conducting uniaxial tensile and shear monotonic tests on monocrystalline and oligocrystalline SAC305 specimens. Anisotropic Hill-Holloman continuum plasticity models have been developed, with the model constants calibrated by matching FEA simulations of the tests with the measured stress-strain results. As the microstructure and mechanical behavior of solder joints vary based on the cooling rate and grain size, the microstructure of single and multi-crystal specimens was quantified and its influence on stress-strain behavior was incorporated in Holloman model constants using an Orowan hardening relation.

3.3.Experimental Details and Results

This section provides details about test specimens, test setup, testing method, results and OIM analysis conducted in this study.

3.3.1. Specimen Details

The grain-scale solder specimen used for applying monotonic tensile and shear loads on the solder joints have been traditionally used by this research group in the past [45][46][16]. Schematic drawings of the specimens with low aspect ratio (LAR) and

high aspect ratio (HAR) solder joints are shown in Figure 3-3. Different specimen geometries were used for tensile and shear tests of LAR vs. HAR specimens to ensure uniform tensile and shear stress fields in the solder joint. The soldering profiles used in this study for manual wire-soldering (sample provided in Figure 3-4) are different from those used for reflow-soldering. As a result, extensive microstructural characterization and microstructure-sensitive modeling are combined in this study, to permit the results to be extrapolated to different microstructural morphologies resulting from different soldering profiles. Literature suggested that the low cooling rate during soldering results in the formation of a single grain in an equiaxed solder joints [57]. Therefore, low aspect ratio specimens (shown in Figure 3-3) and low cooling rate (~0.23°C/s) (shown in Figure 3-4) were selected for fabricating single-grained LAR solder joint specimens. In contrast, higher cooling rate (~7°C/s), multi-grained specimens were subjected to temperature profile with used in a previous study [16]. The multi-grained HAR specimens were fabricated with ~200 μm tall solder joints, to make the length-scale of the test specimen approximately comparable with the length-scale of functional solder joints in electronics. This geometric matching is important because the solder joint mechanical response is known to be sensitive to the length-scale. Table 3-2 shows the different types of specimens used in this study, grouped by the cooling rate, aspect ratio and the number of grains. The specimens consist of one or at most 4 grains (depending upon the cooling rate), hence it is referred to as a grain-scale solder specimen.

Table 3-2 Different types of specimens used for monotonic tensile and shear tests

		Cooling Rate	
		Low (~0.23°C/s)	High (~7°C/s)
Aspect Ratio	Low (1.5mm/1mm)	Monocrystalline  (specimen # 1-4)	Oligocrystalline  (specimen # 5, 6)
	High (2.5-3mm/0.2mm)		Oligocrystalline  (specimen # 7-10)

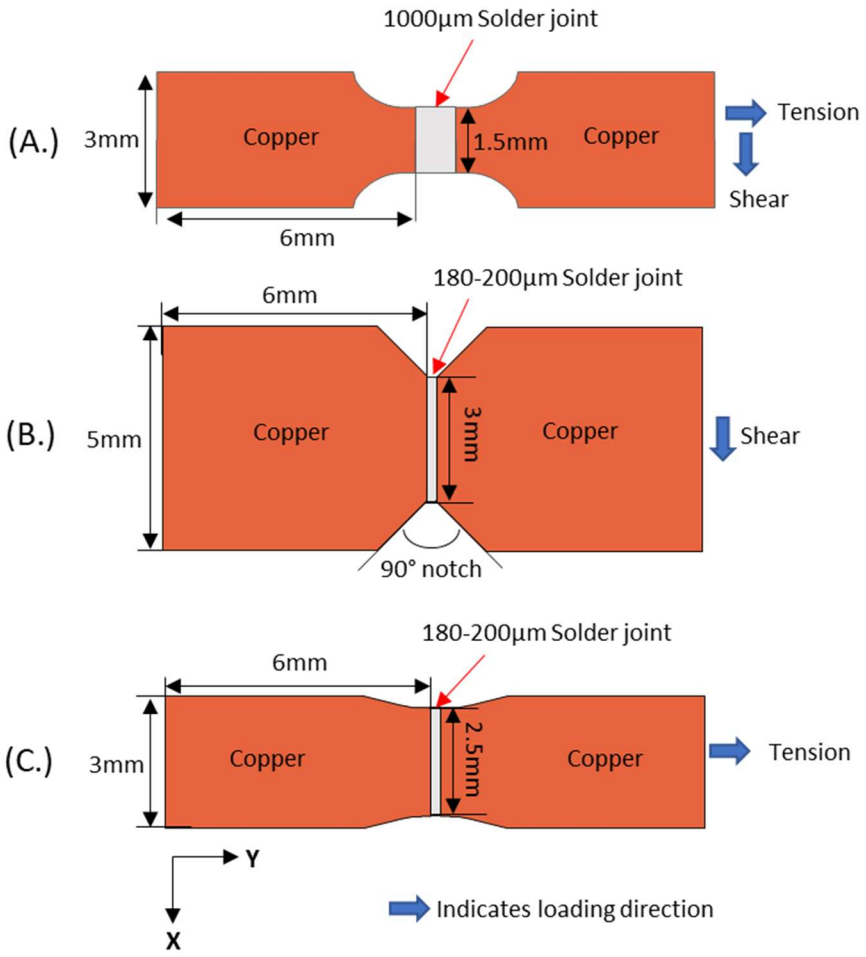

Figure 3-3 (A.) LAR tensile/shear specimen; (B.) HAR shear specimen; (C.) HAR tensile specimen

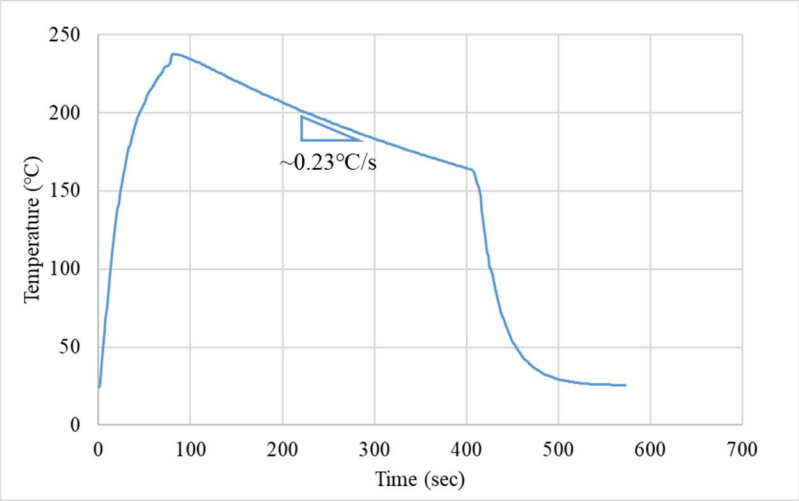

Figure 3-4 Soldering temperature profile for fabricating single-crystal solder joints

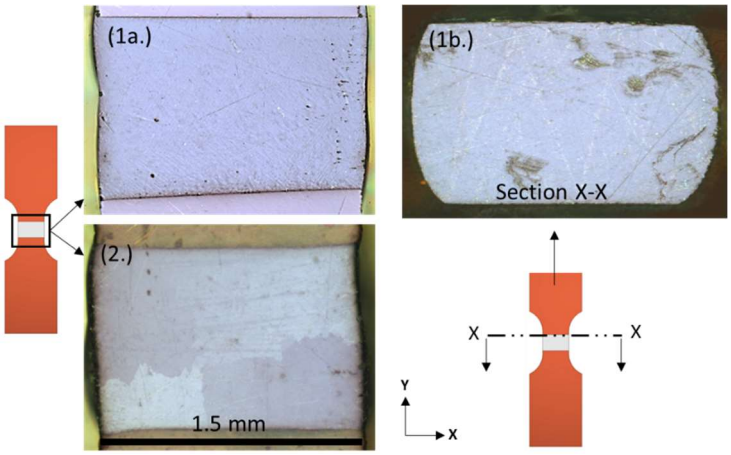

Figure 3-5 Cross-polarized images of SAC305 solder joint: 1a.) Single crystal specimen; 1b.) Sectional view of single crystal specimen; 2.) Multi- crystal specimen.

A spacer is inserted between the two copper platens in order to maintain the joint height for each specimen (1000 μm for LAR specimens and 200 μm for HAR specimens). The specimens are ground to remove the excess pool of solder and the

thickness of the specimens is reduced to approximately 1000 μm. The specimens are isothermally aged for 63-72Hrs at 125°C, to partially stabilize the microstructure and to relieve the residual stresses generated during the fabrication steps. Cross-polarized microscopy is conducted prior to testing to determine whether the solder joints is single grained. As an example, cross-polarized microscope images presented in Figure 3-5 show single-grained and multi-grained solder joint specimens. The front and rear faces as well as selected cross-sections are imaged to verify whether this fabrication process is capable of yielding single-grain specimens. The average grain area for single-grain specimens is ~1.4 mm^2. SEM observations in Figure 3-6 reveal the microstructural differences resulting from the different cooling rates that had to be used for the single and multi-grain solder specimens. The images show dark-grey pro-eutectic β-Sn dendritic lobes surrounded by a matrix of Ag-Sn eutectic mixture. The bright round and elliptical particles in the eutectic region are Ag_3Sn IMCs. The morphological differences (average dendrite volume fraction, average size and spacing of Ag_3Sn IMC particles within the eutectic region) were quantified using a commercial image processing software *Image-Pro*© and the results are provided in Table 3-3. Image processing steps are provided in detail in Section A1 of Appendix. Results clearly show that low cooling rate during soldering resulted in approximately 270% increase in Ag_3Sn particle size, 190% increase in Ag_3Sn particle spacing and 15% decrease in area fraction of dendritic phase. OIM analysis was conducted on the tested specimens using electron back-scatter diffraction (EBSD) to quantify the lattice orientation of each Sn grain in the specimen. As each specimen has a unique mechanical response owing

to the uniqueness in its grain structure. EBSD images of tested specimens along with the Euler angles (Bunge convention [58]) and area for respective grains are presented in Figure 3-7 and Figure 3-8.

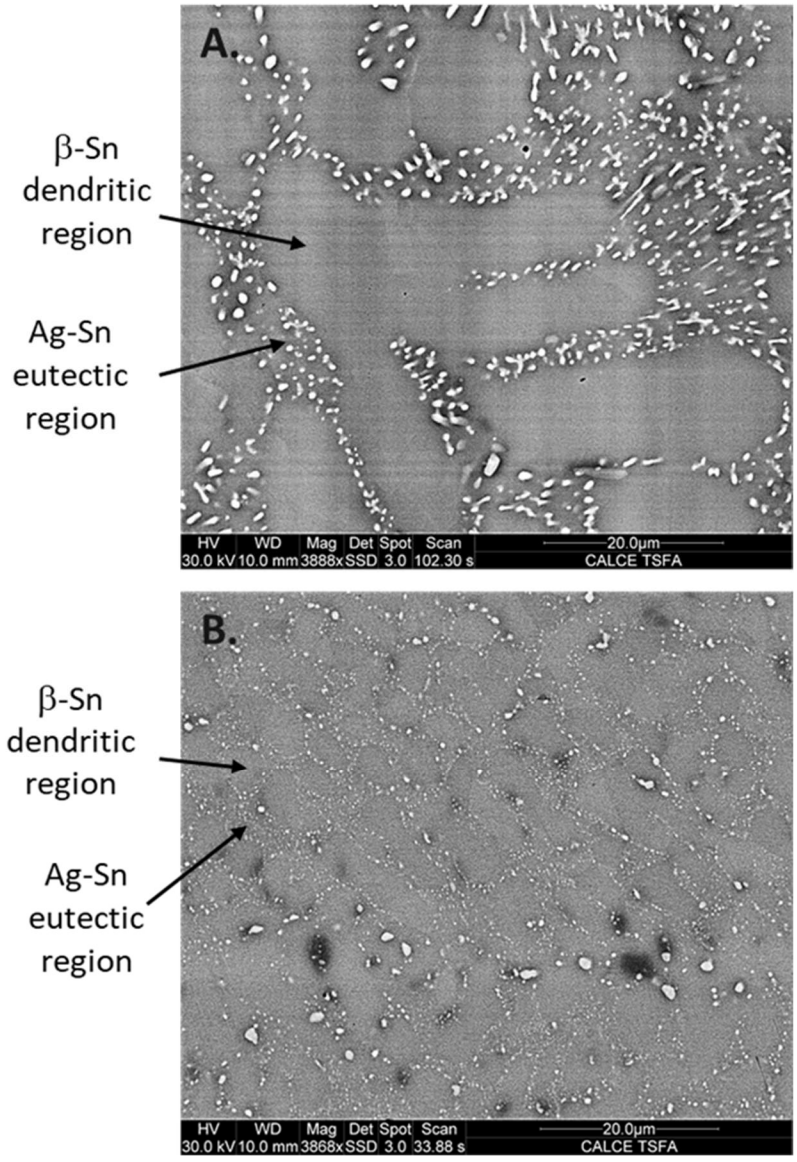

Figure 3-6 SEM Images showing microstructures in specimens soldered using - A.) Low cooling rate; B.) High cooling rate.

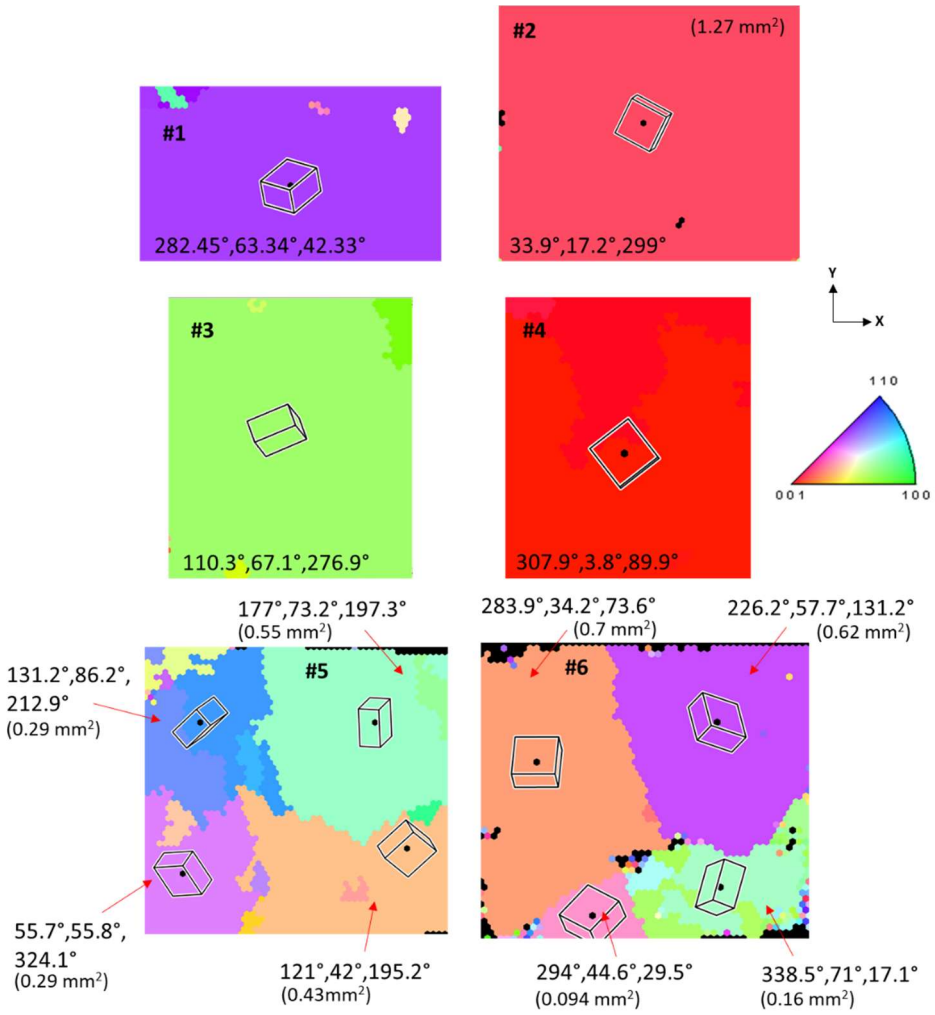

Figure 3-7 EBSD and Euler angles of single (#s 1- 4) and multi-crystal (#s 5 and 6)

LAR solder joint specimens

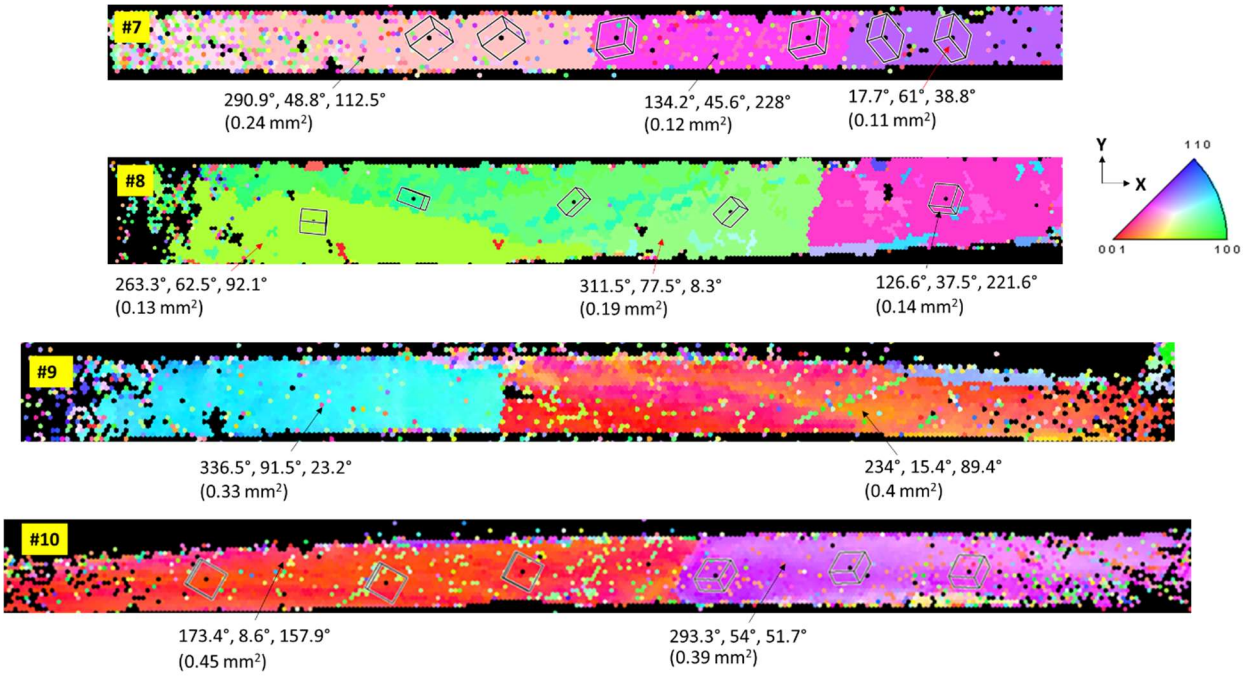

Figure 3-8 EBSD and Euler angles for multi-crystal tensile (#7, 8) and shear (#9, 10) HAR specimens

Table 3-3 Quantification of LCR and HCR intra-crystal microstructure using image processing (see Section A1: Appendix for details)

Cooling Rate (°C/s)	Aging Duration (Hrs.) (at 125°C)	Ag-Sn Particle Size		Ag-Sn Particle Spacing (L) (µm) (mean)	Area Fraction		L-D (µm)
		Area (µm²) (mean)	Diameter (D) (µm) (mean)		Dendrite	Eutectic	
0.23	72	0.38	0.55	1.04	60%	40%	0.5
7	63	0.03	0.15	0.36	71%	29%	0.22

3.3.2. Monotonic Tensile and Shear Test Results

Room temperature monotonic tensile and shear tests were conducted on single-crystal and multi-crystal SAC305 solder joint specimens using a custom Thermo-Mechanical Microscale (TMM) test frame and digital image correlation (DIC) system. The test setup is described in detail in a prior study [16]. Tensile or shear displacements were applied at the rate of 1μm/s. The relative displacement δ, within the solder (between the Copper interfaces) is continuously measured during the test using DIC and the shear or tensile engineering strain in the solder joint is estimated ($\varepsilon = \delta/h$). The load P is measured by the load-cell and the nominal shear or tensile stress is estimated ($\sigma = P/A$). Prior to testing, the cross-sectional area A and the joint height h of each specimen is recorded. Figure 3-9 presents axial stress vs. engineering strain curves generated from uniaxial monotonic tensile tests, whereas Figure 3-10 presents shear stress vs. engineering shear strain curves obtained from uniaxial monotonic shear

tests. The specimen ID's corresponds to the grain orientations provided in Figure 3-7 and Figure 3-8 in section 3.3.1.

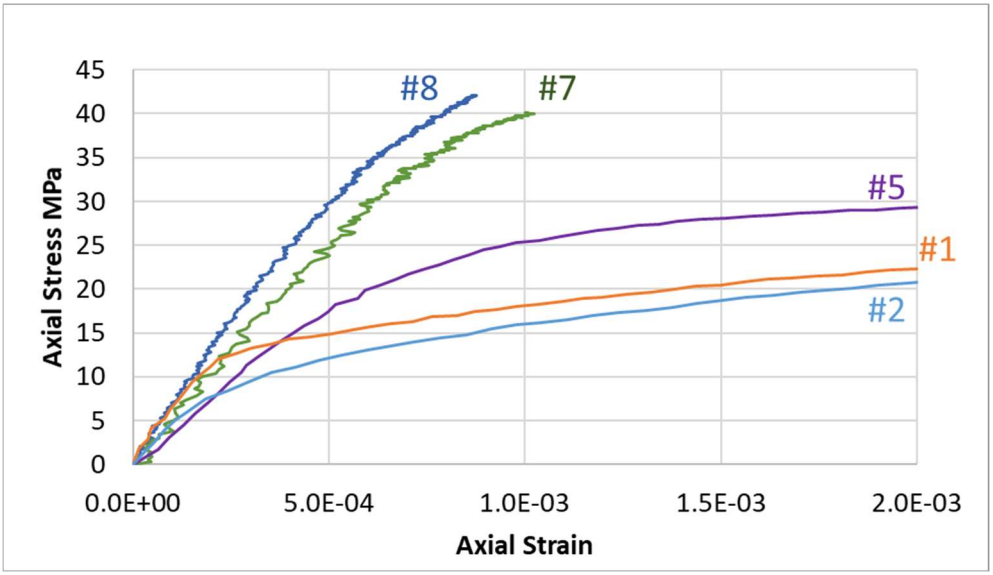

Figure 3-9 Experimental axial stress-strain curves from tensile tests on single-crystal and multi-crystal SAC305 solder joint specimens

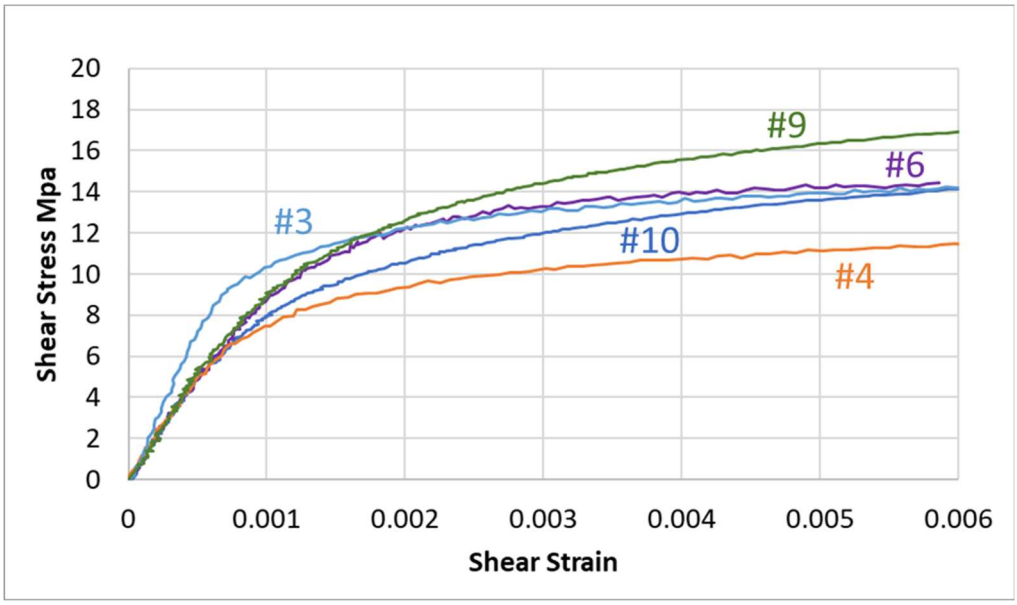

Figure 3-10 Experimental shear stress-strain curves from shear tests on single and multi-crystal SAC305 solder joint specimens

3.4. Anisotropic Elastic-Plastic Constitutive Properties

Anisotropic elasticity is modeled using the elastic stiffness constants for SAC305 (Table 3-1) established in the prior study [5]. Anisotropic Hill-Holloman continuum plasticity models for SAC305 single crystal has been developed in this section. The model constants are calibrated by matching FEA simulations of the uniaxial monotonic tensile and shear tests on single crystal specimens, with the experimentally measured stress-strain results. Two performance metrics used to quantify the accuracy of the anisotropic plasticity model are presented in this section as well.

3.4.1. Anisotropic Hill-Holloman Plasticity Model

The anisotropic behavior of the grain-scale solder joint in this study uses anisotropic continuum Hill's plasticity model as this approach is simple, efficient and faster to implement. Hill's yield criterion [59] and its constants are given in Eq. 3-1- Eq. 3-7 below-

$$\sigma_{Hill} = \sqrt{\begin{matrix} F(\sigma_{22}-\sigma_{33})^2 + G(\sigma_{33}-\sigma_{11})^2 + H(\sigma_{11}-\sigma_{22})^2 \\ +2L\sigma_{23}^2 + 2M\sigma_{13}^2 + 2N\sigma_{12}^2 \end{matrix}} \quad \text{Eq. 3-1}$$

$$F = \frac{1}{2}\left(\frac{1}{{R_{22}}^2} + \frac{1}{{R_{33}}^2} - \frac{1}{{R_{11}}^2}\right) \quad \text{Eq. 3-2}$$

$$G = \frac{1}{2}\left(\frac{1}{{R_{33}}^2} + \frac{1}{{R_{11}}^2} - \frac{1}{{R_{22}}^2}\right) \quad \text{Eq. 3-3}$$

$$H = \frac{1}{2}\left(\frac{1}{{R_{11}}^2} + \frac{1}{{R_{22}}^2} - \frac{1}{{R_{33}}^2}\right) \quad \text{Eq. 3-4}$$

$$L = \frac{3}{2{R_{23}}^2} \quad \text{Eq. 3-5}$$

$$M = \frac{3}{2{R_{13}}^2} \quad \text{Eq. 3-6}$$

$$N = \frac{3}{2{R_{12}}^2} \quad \text{Eq. 3-7}$$

where σ_{Hill} is Hill's stress and F, G, H, L, M and N are Hill constants that define the anisotropy of the yield strength of Sn lattice. R_{11}, R_{22} and R_{33} are anisotropic yield strength ratios in [100], [010] and [001] crystal principal directions whereas, R_{12}, R_{23} and R_{13} are shear yield strength ratios. The Hill's constants are best estimated by conducting uniaxial monotonic tensile and shear tests on single crystal specimens oriented in specific crystal directions. However, fabrication of single crystal specimens with specific orientation is challenging, since the crystals formed during solidification are randomly oriented. Therefore, this paper utilizes experimental stress-strain curves for specimens with randomly oriented grains along with an iterative finite element-based approach to determine the Hill's yield strength ratios. Further details regarding the calibration process are provided in Section 3.4.2. Hill's yield criterion resembles von Mises' yield criterion for isotropic materials when all the yield strength ratios are set to 1.

$$\sigma = K{\varepsilon_p}^n \qquad \text{Eq. 3-8}$$

Holloman's model for deformation plasticity (shown in Eq. 3-8) which relates stress σ to plastic strains ε_p, was used to model the plastic flow behavior of SAC305. Here, K is the strength co-efficient whereas, n is the strain hardening exponent. The anisotropic yield strength ratios and the plasticity model constants have been calibrated using FEA of the tested specimens (listed above in Section 3.3.1). The calibration method and results are presented next in Section 3.4.2.

3.4.2. Calibration of Hill-Holloman Model Constants

Single crystal stress-strain data was used to determine Hill's yield strength ratios using a parametric anisotropic elastic-plastic finite element approach. This is a manually conducted parametric study, for preliminary verification of the viability of using this Hill-Holloman approach for grain-scale modeling of solder joints. Future studies should use more systematic machine-learning optimization approaches to find the best-fit model constants. The tensile and shear single crystal specimen geometries were modeled in FEA along with their corresponding local material axes based on the grain orientations. The FEA model (full, no symmetry) shown in Figure 3-11 comprised of the exposed portion of the specimen that lies between the clamps of the test frame. The solder joint consisted of an anisotropic single-crystal or multi-crystal elastic-plastic block of solder material sandwiched between the two Copper substrates. Elastic stiffness constants shown in Table 3-1 were used to model anisotropic elasticity of SAC305. The bottom surface of the specimen was constrained and a monotonic tensile or shear displacement was applied on the top face. 8-noded linear brick element was used to model the specimen and the Copper substrate was modeled as a linear elastic-isotropic material (Elastic modulus: E=110 GPa, Poisson's ratio: ν=0.35). Cu-Sn interfacial IMC layers were not considered in the FEA model, since the interfacial IMCs are assumed to have negligible impact on the overall average solder constitutive properties. Average applied stress was estimated by summing reaction forces at the fixed end (in the y-direction for axial loading and in the x-direction for shear loading)

and dividing the total reaction force by the cross-sectional area of the solder joint at the narrowest section of the fillet. Average strain was calculated by dividing relative displacement (measured across the top and bottom Copper interfaces; in the y-direction for axial loading and in the x-direction for shear loading) by the height of the solder joint. Engineering stress-strain response curves were constructed using the average stress and average strain.

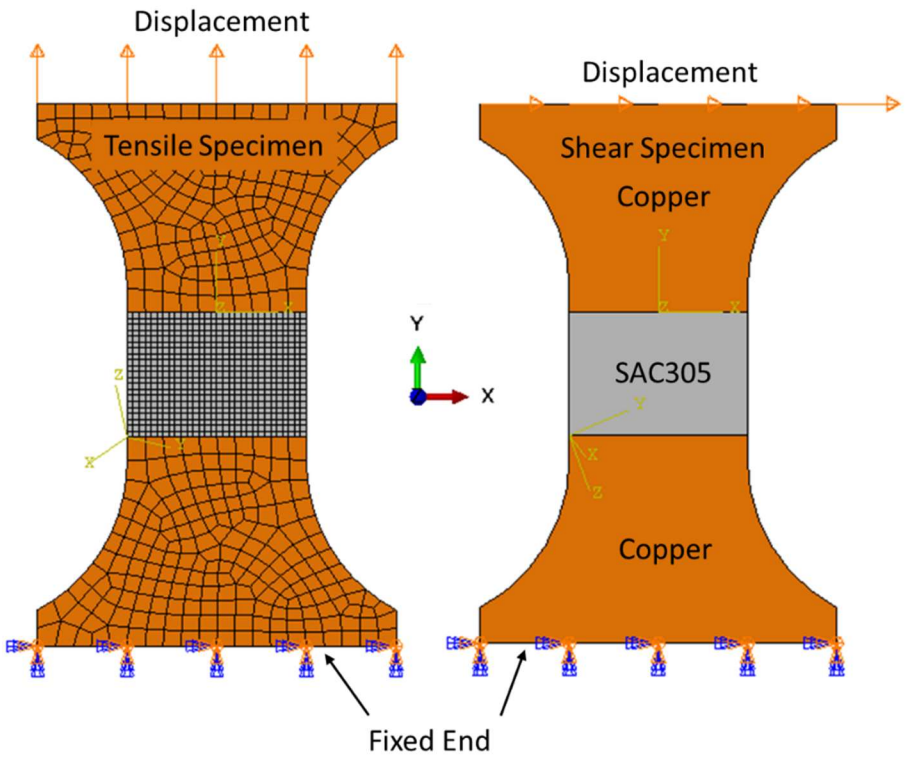

Figure 3-11 FEA model of LAR single crystal specimen

Table 3-4 Parametric variations of Hill's yeild stress ratios

#	Hill's Yield Stress Ratios				Parametric Scheme
	R11, R22	***R33***	***R13, R23***	***R12***	
0	1	1	1	1	**Isotropic condition**
1	0.83	1	1.18	1.16	**Varying tensile yield stress ratios**
2	0.73	1	1.18	1.16	
3	0.63	1	1.18	1.16	
4	0.83	1	1.08	1.06	**Varying shear yield stress ratios**
5	0.83	1	1.18	1.16	
6	0.83	1	1.28	1.26	
7	0.83	1	1.08	1.06	**Varying both tensile and shear yield stress ratios**
8	0.73	1	1.18	1.16	
9	0.63	1	1.28	1.26	
10	0.83	1	1.08	0.99	**Varying ratio between shear yield stress ratios**
11	0.83	1	1.08	1.06	
12	0.83	1	1.08	1.12	

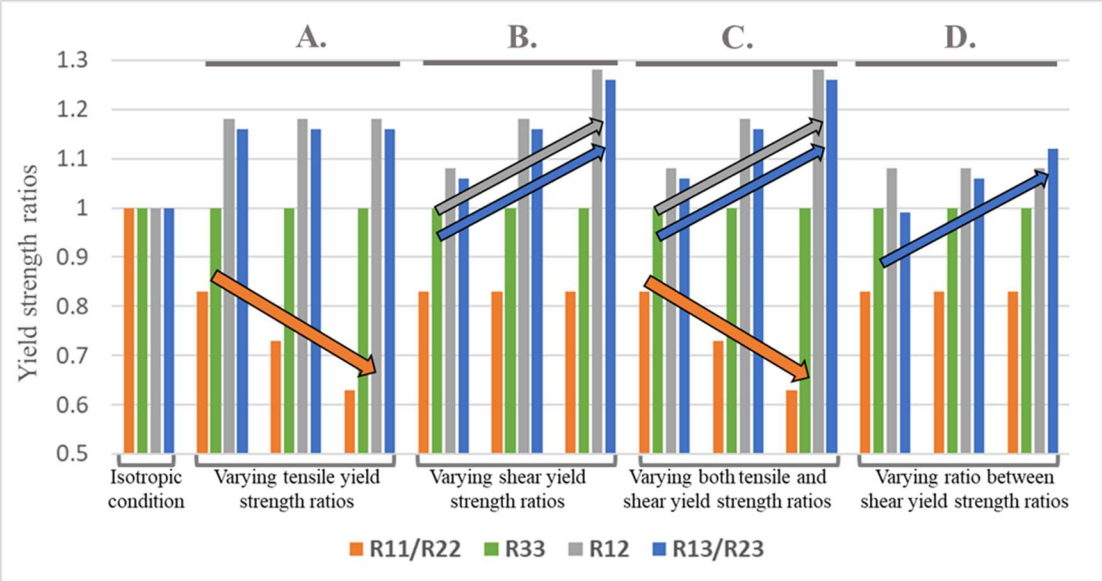

Figure 3-12 Parametric variation scheme for evaluating the effect of yield stress ratios

The yield strength ratios were parametrically varied starting from all R=1 (isotropic condition). Engineering stress-strain responses along the loading direction for each single crystal specimen were recorded and compared with average experimental stress-strain curves for multiple single crystal specimens. The input plasticity properties (Hill's stress-inelastic-strain curves) were simultaneously optimized (by minimum fitting error by maximizing the R^2 value) for each of the parametric cases, to obtain a the most reasonable possible fit of FEA predictions vs. experimental results. Table 3-4 shows different combinations of yield stress ratios used for the parametric study. Based on these combinations, as shown in Figure 3-12, effect of varying following parameters on stress-strain predictions was evaluated: A.) tensile yield stress ratios; B.) shear yield stress ratios; C.) both tensile and shear yield stress ratios; and C.) ratio between shear yield stress ratios. The following simplifications

were made due to the BCT symmetry of the Sn crystal, where [100] and [010] crystallographic directions are similar: $R_{11} = R_{22}$ and $R_{13} = R_{23}$. In this study, all yield strength values have been normalized by R_{33} (which is the stiff [001] direction of the BCT crystal). The corresponding Hill-Holloman plastic stress-strain curve is that measured from uniaxial tensile test in the [001] direction. The goodness of fit of the FEA vs. experimental stress-strain responses was quantified using two metrics, M_1 and M_2:

(i) *Accuracy metric*- ability of anisotropic Hill FEA to predict both average tensile as well as average shear stress-strain responses of all tested single-grained specimens (averaged across multiple grain orientations). This was accomplished by minimizing the RMS difference between average FEA and average experimental stress-strain responses across multiple grain orientations. The R^2 value of the comparison is used as the metric M_1 and M_1=1 represents the best case. R^2 value was picked for M_1 since, it can quantify the deviation of FEA prediction from experimental results.

(ii) *Anisotropy metric* (M_2)- ability of anisotropic Hill FEA to predict severity of anisotropy caused by different grain orientations, in both tensile and shear specimens. The tested specimens with the most dissimilar grain orientations are selected for assessing metric M_2. Thus M_2=1 for the best case (when the FEA predicts the same difference in stress-strain response for the different selected specimens, compared to experiments). M_2<1 implies that FEA lacks sufficient sensitivity to predict the measured anisotropy, while M_2>1 indicates that the

FEA is overly anisotropic. As a default worst case, M_2=0 is for isotropic FEA. Anisotropy metric is defined as follows-

$$Anisotropy\ Metric = \frac{FEA\ \%\ difference\ between\ response\ of\ selected\ specimens}{Experiment\ \%\ difference\ between\ response\ of\ selected\ specimens}$$

M_1 metrics for prediction accuracy study are shown in Figure 3-13 and M_2 metrics for anisotropy sensitivity study are shown in Figure 3-14. Interestingly, isotropic FEA showed the best accuracy among all the cases studies, however, it is intrinsically deficient of course when it comes to predicting the anisotropy between different specimens. Based on the these two metrics for all the cases examined in this preliminary parametric study, constants presented in **Error! Reference source not found.** were found to generate the most reasonable FEA stress-strain response (shown in red boxed area in Figure 3-13 and Figure 3-14). The corresponding Holloman power-law flow rule relating Hill's stress to Hill's equivalent inelastic strain (K = 91 and n = 0.225) is shown in Figure 3-15. These Hill-Holloman model constants are relevant for large SAC305 single crystals with coarse dendritic and eutectic microstructures that are common when the solder is either solidified and crystallized using slow cooling rate, or is isothermally aged for extended periods after solidification. Methods to scale these elastic-plastic properties for finer microstructures and for smaller grains are discussed next in Section **Error! Reference source not found.** . The FEA stress-strain predictions generated by using this set of constitutive properties are compared to experimental results shown in Figure 3-16 and Figure 3-17. The anisotropic Hill FEA

is able to predict the anisotropy between specimens with different orientations reasonably well. However, the M_1 metric (~0.9) is slightly lower than the best case (M_1=1) probably due to the fact that the single power law plasticity behavior was assumed instead of a more complex plasticity behavior as indicated by the experimental stress-strain results.

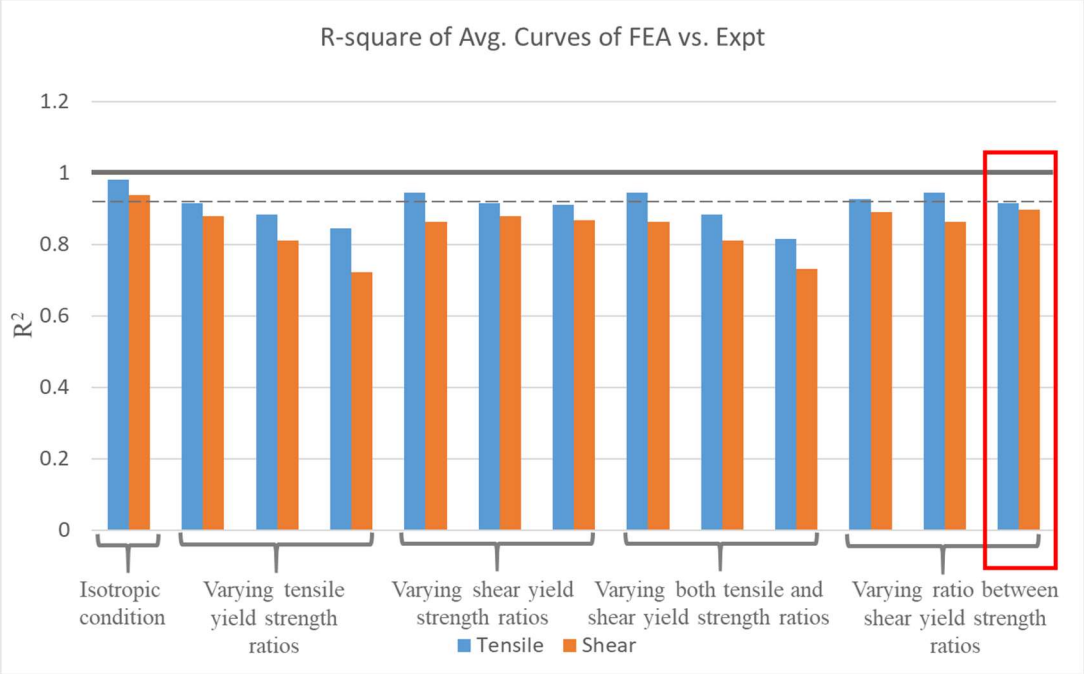

Figure 3-13 M_1 metric for prediction accuracy study for averaged tensile and shear specimens

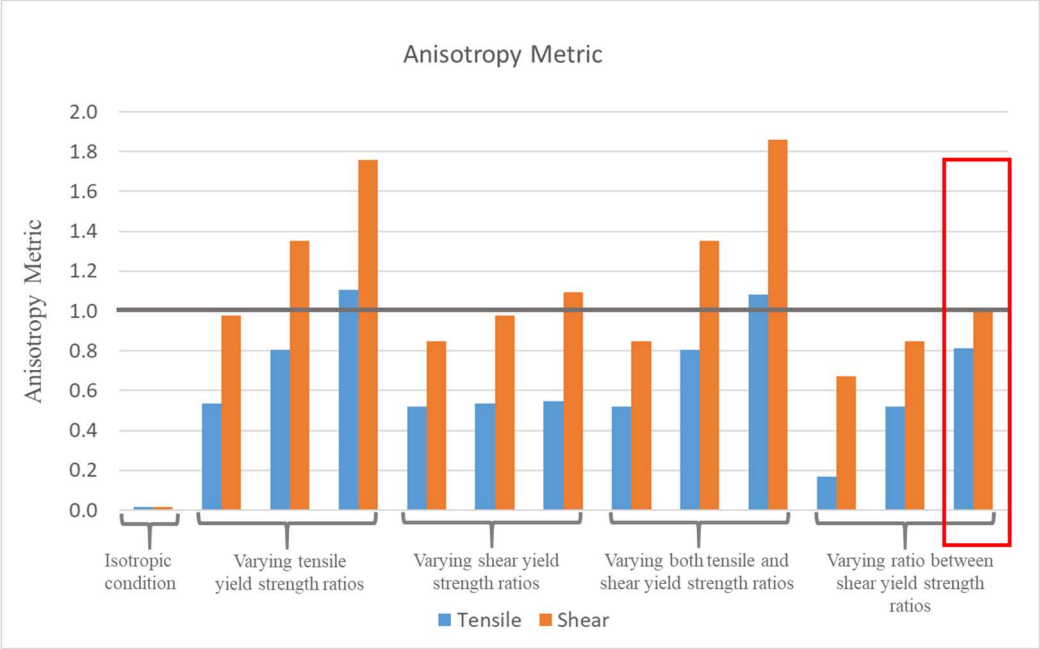

Figure 3-14 M_2 metric for anisotropy sensitivity study for both tensile and shear specimens

Table 3-5 Calibrated Hill's yield strength ratios

R_{33}	R_{11}, R_{22}	R_{13}, R_{23}	R_{12}
1	0.83	1.12	1.08

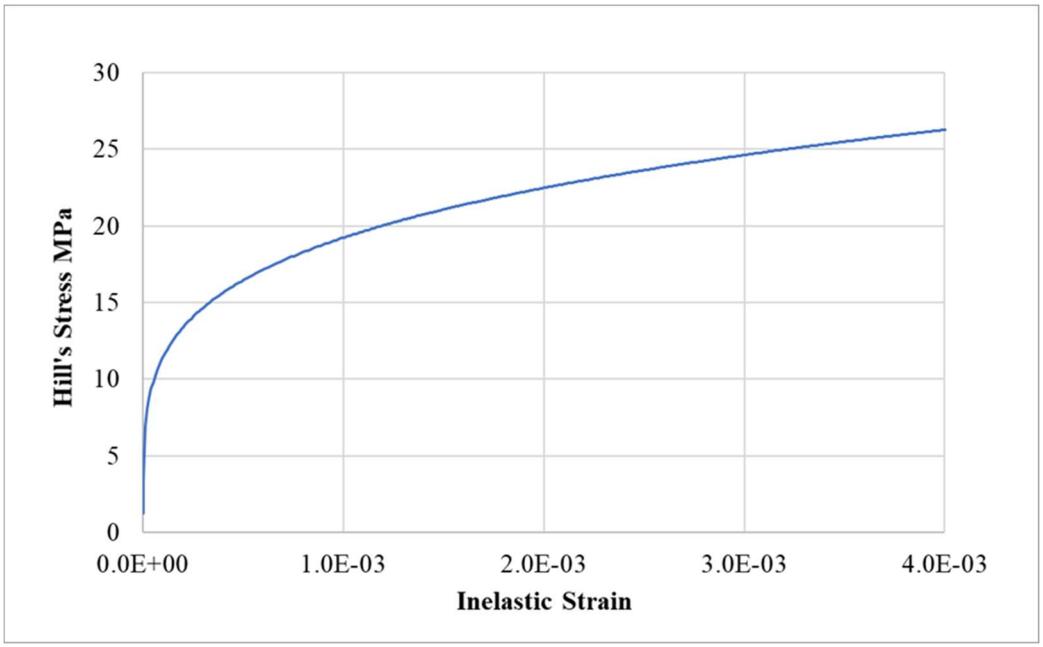

Figure 3-15 Hill's stress-inelastic Hill's strain curve for modeling in FEA (for Hill constants given in Table 3-5). This directly represents the behavior for uniaxial tensile test in the [001] lattice direction for large grains with low cooling rate.

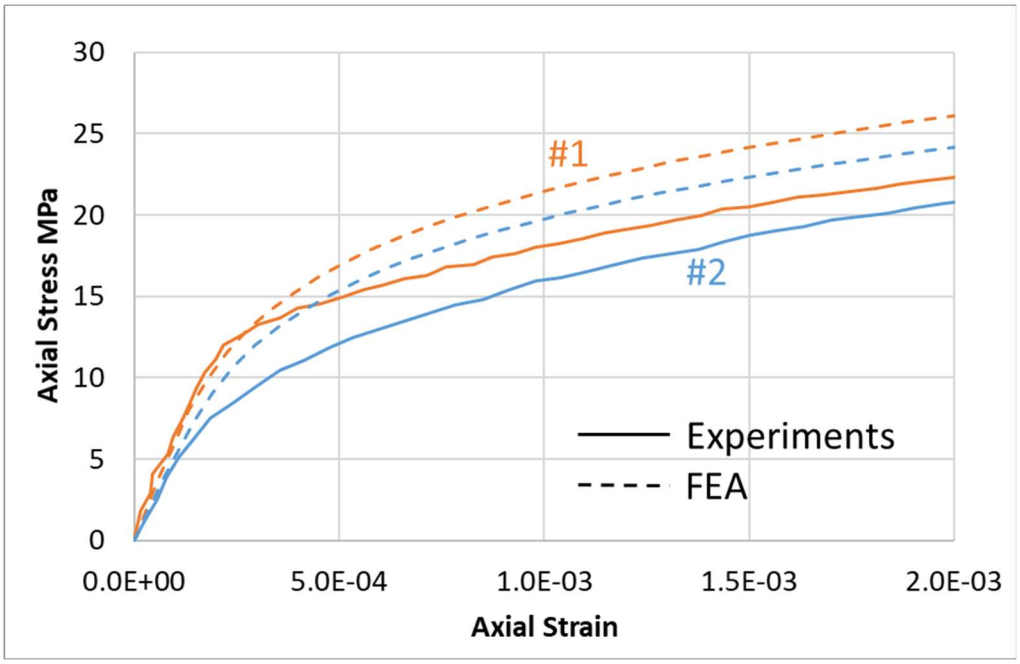

Figure 3-16 Axial stress-strain curve comparison for two selected single-crystal specimens: FEA predictions vs. experimental results

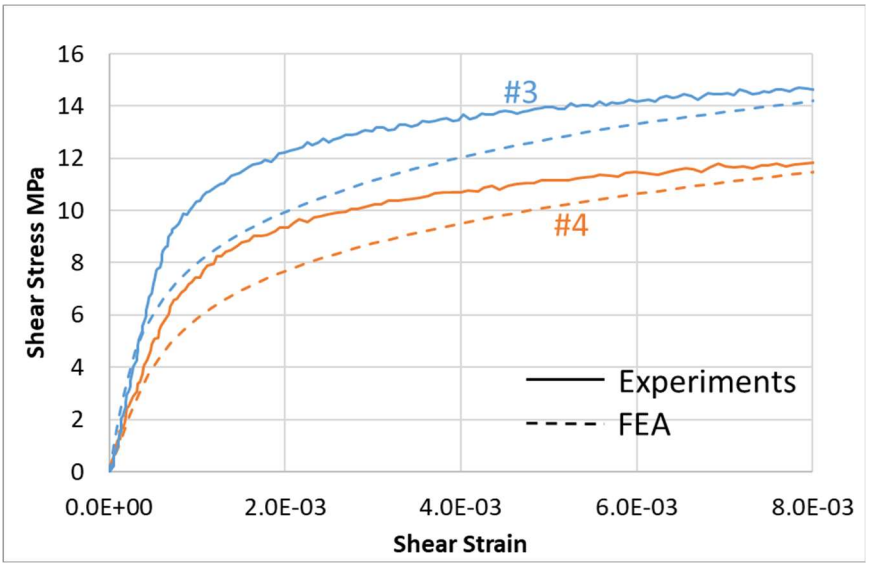

Figure 3-17 Shear stress-strain curves comparison for two selected single-crystal specimens: FEA predictions vs. experimental results

3.5. Dependence of Elastic-Plastic Properties on Grain Size and on Microstructure within the Grain

As discussed in earlier, the cooling rate used during fabrication of single-crystal solder joint specimens was about an order of magnitude lower than that typically used during assembly process of functional electronics. The low cooling rate results in significantly coarser eutectic and dendritic microstructure, when compared to those with high cooling rate specimens. Coarser microstructures are also common under isothermal aging. Another source of differences in mechanical elastic-plastic response can come from grain-size dependence. Therefore, the single crystal elastic-plastic Hill-Holloman elastic-plastic properties presented in Table 3-5 and in Figure 3-15 need to be scaled as a function of microstructural features and grain size in order to estimate

the mechanical behavior across wide range of fabrication and isothermal aging conditions.

Both of the micro-morphological influences discussed above can be modeled as appropriate strengthening mechanisms as the microstructural features (Tiers 1 and 2) or the grain size (Tier 3) shrink and refine. The scaling factors have been determined using top-down approach from Tier 3 scaling factor to Tier 1 scaling factor. The single crystal stress vs. inelastic strain data is scaled based on the Tier 1-3 microstructural parameters. The procedure for estimating the scaling factors is discussed below in Sections 3.5.1-3.5.3.

3.5.1. Scaling Factors for Average Grain Size (Tier 3):

Tier 3 consists of single or multiple SAC grains of different sizes in a single solder joint. The grain boundaries act as barriers for movement of dislocations which causes dislocations to pile up at the grain boundary. This leads to grain boundary strengthening due to Hall-Petch effect. As the grain size decreases, the amount of grain boundaries that block dislocations increases, in turn increasing in the effective yield strength of the material. Hall-Petch relation is defined as-

$$\sigma_y = \sigma_o + k_y d^{-0.5} \qquad \text{Eq. 3-9}$$

Where σ_y is the yield strength, σ_o is the constant, k_y is the strengthening co-efficient and d is the average grain diameter. The average grain diameter d is approximated as $2\sqrt{Area/\pi}$. Figure 3-18 shows the relationship between the solder

yield stress and square root of the average grain diameter. The grain size dependent properties for SAC solder (composite) were iteratively determined by matching grain-scale anisotropic FEA with experimental stress-strain results of HCR multi-crystal specimens #5-10. As shown in Figure 3-7 and Figure 3-8, specimens #5-10 have wide range of grain sizes available for calibration of the Hall-Petch model constants. Details regarding the grain-scale anisotropic FE modeling procedure are provided in Section 3.5.4.

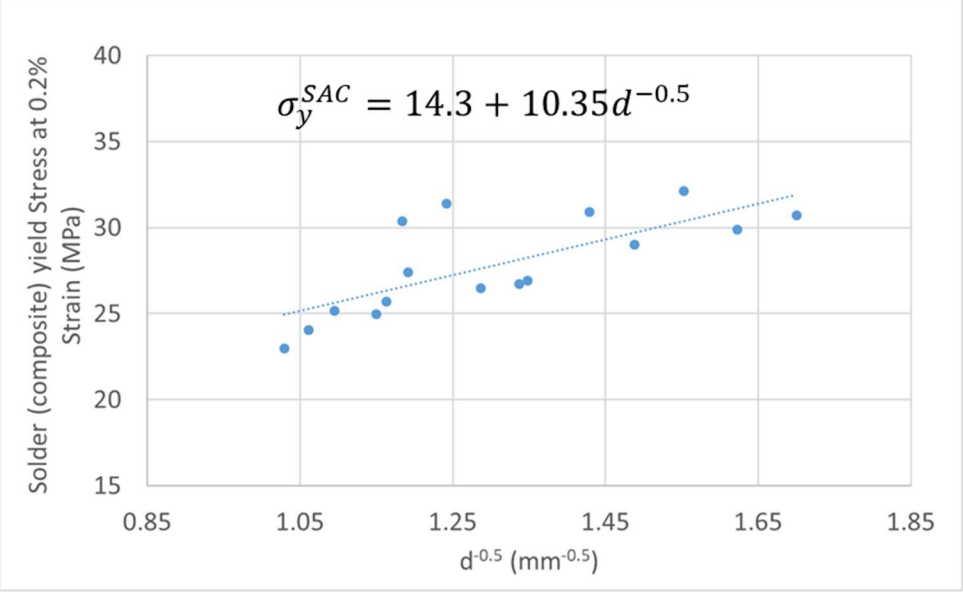

Figure 3-18 Relationship between solder yield strength and average grain diameter 'd'

3.5.2. Scaling Factors for Dendritic (Tier 2) Volume Fraction:

At the next length scale (Tier 2 of Figure 3-2), the heterogeneous microstructure of the SAC solder composite is approximated as ellipsoidal β-Sn dendritic regions

('inclusions') surrounded by the Ag-Sn eutectic region ('matrix'). The average stresses in the solder composite are approximated by considering the load-sharing between the Ag-Sn eutectic phase and β-Sn dendrite using the three-phase sphere model proposed by Christensen [60] (refer to Eq. 4.12 - 4.16 from Christensen's book [60]) for isotropic linear elastic materials. As the cooling rate (or isothermal aging) changes the strength of the eutectic region and the volume fraction of the dendrites (and hence volume fraction of the eutectic region), the effective homogenized strength of the SAC composite alloy also changes. Examples of these changes are shown below in Section 3.5.4.

In addition, as the grain size strengthening mechanism is ideally attributed to Sn and not eutectic Ag-Sn phase of SAC solder, grain size dependent yield strength for Sn was estimated using Christensen's model as shown in Figure 3-19. β-Sn stress-strain curve from the prior work by Kariya et al. [37][38] was treated as a reference stress-strain curve for infinitely large grain which was scaled based on the Tier 1-3 microstructures. $k_y = 22.6$ for Sn is greater than SAC (10.35) indicating that the Sn yield strength has greater sensitivity to grain size than SAC yield strength. The grain size dependence of Sn is muted after homogenization with eutectic Ag-Sn phase which is insensitive to grain size.

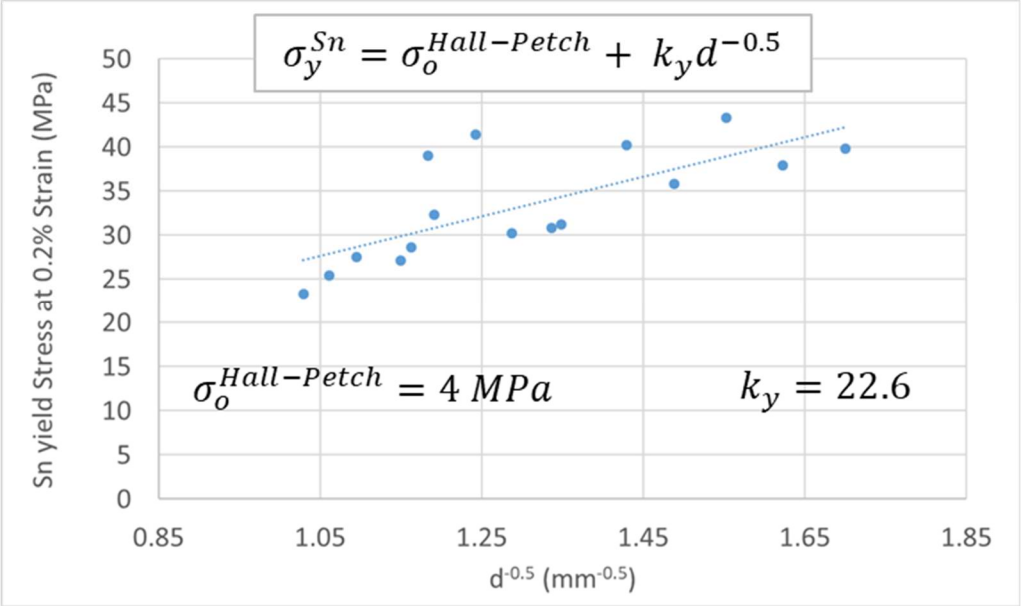

Figure 3-19 Relationship between Sn yield strength and average grain diameter 'd'

3.5.3. Scaling Factors for Eutectic (Tier 1) Microstructure:

In the eutectic microconstituent of SAC solders (Tier 1 of Figure 3-2), Ag_3Sn IMC particles block the dislocation movement causing dispersion strengthening. As the cooling rate is lowered, the Ag_3Sn IMC particles coalesce and coarsen (as they do also under isothermal aging). This leads to larger IMC particles that are more sparsely dispersed in the eutectic phase. The movement of dislocations in eutectic phase is governed by Orowan hardening mechanism [61] where the shear stress required to propagate dislocations through an alloy is defined by the Orowan stress τ_{OR} given below-

$$\tau_{OR} = \frac{aGb}{(L - 2r)} \qquad \text{Eq. 3-10}$$

Where, a is a constant, G is the shear modulus, b is the Burger's vector, L is the interparticle spacing and r is the radius of the dispersed particles. The yield strength of the eutectic region depends on the Orowan stress. Therefore, as the particle size (r) and spacing (L) increase, as in case of slow cooled (or isothermally aged) specimens, the yield strength of the eutectic region reduces in inverse proportion to (L-2r). Figure 3-20 shows Tier 1 scaling factors determined for scaling the eutectic yield strength as a function of cooling rate. Since, this study only consisted of specimens fabricated using two (low and high) cooling rates, the Tier 1 scaling model is assumed to be linear.

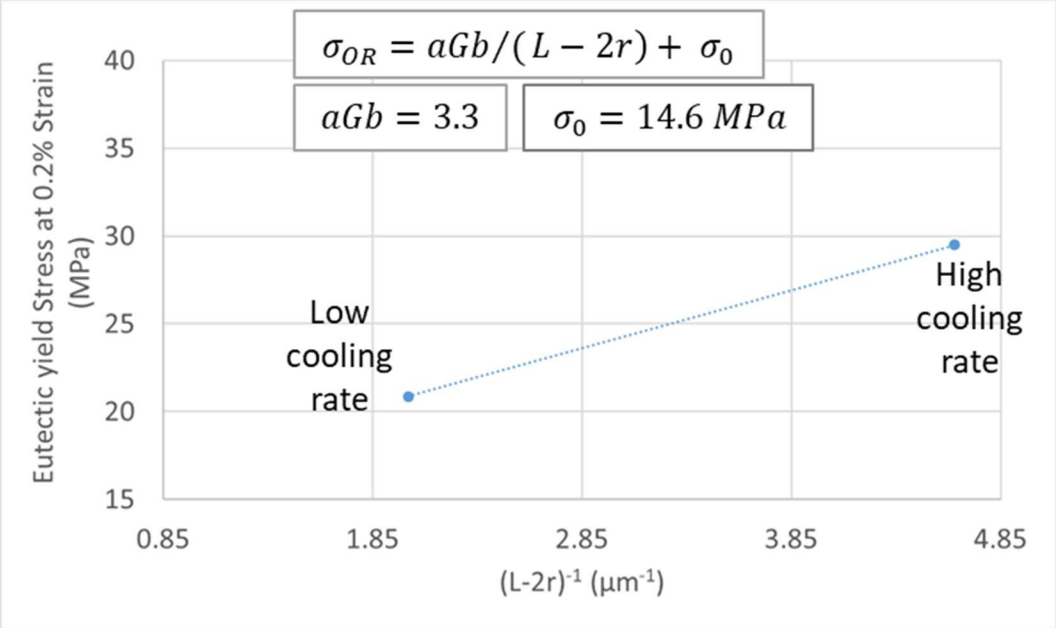

Figure 3-20 Relationship between eutectic yield strength and microstructural parameters

3.5.4. Comparison of Grain-scale FEA Predictions with Homogenous Isotropic FEA:

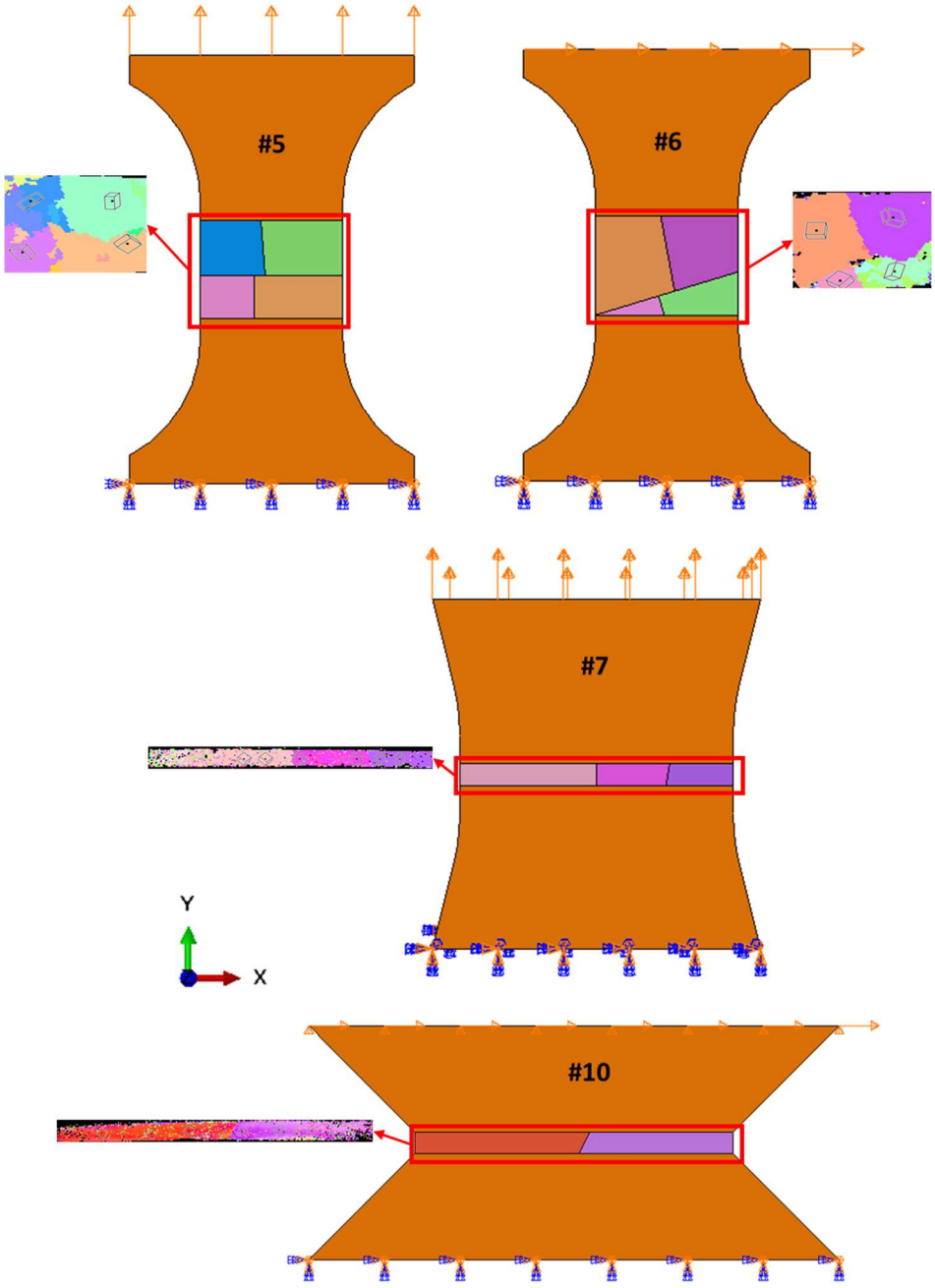

Figure 3-21 Grain-scale anisotropic FEA models of specimens #5, 6, 7 and 10

Grain-scale anisotropic FEA models of multi-crystal HCR specimens (LAR: #5,6; HAR: #7-10) were used to- (i.) calibrate Tier 3 scaling factors and; (ii.) compare the anisotropic Hill FEA predictions with homogeneous isotropic FEA. As mentioned before, multi-crystal HCR specimens #5-10 consist of 16 different grain size variations that are needed for calibration of Hall-Petch equation. As an example, full FEA models (along with mesh) of tensile and shear specimens (LAR and HAR) are provided in Figure 3-21. Displacements and boundary conditions were applied (depending upon tensile or shear specimen) in the same way as discussed in Section 3.4.2 and as shown in Figure 3-11.

At same displacement level, the Hill's stress contour plots for specimens #5, 6, 7 and 10 are compared with von Mises stress distributions in homogeneous isotropic model as shown in Figure 3-21. Clearly, the homogeneous isotropic modeling methodology fails to predict the severity and location of stress concentrations in solder joints when compared with grain-scale anisotropic modeling methodology. The grain-scale anisotropic FEA model predictions for different specimens are compared with homogeneous isotropic FE predictions and the experimental results as shown in Figure 3-23. The prediction accuracy of microstructurally scaled Hill-Holloman anisotropic elastic-plastic grain-scale FEA is compared with that of homogeneous isotropic FEA, in Figure 3-24, for representative multi-crystal tensile and shear specimens. The homogenous isotropic FEA uses average stress-strain properties presented in prior work [16]. The RMS differences between FEA predictions and experimental results shows that the grain-scale anisotropic FEA predicts stress-strain response of solder

joints with better accuracy than the homogenous isotropic FEA. The LAR specimens (#5 and #6) with 2 grains in the direction of loading direction, are less sensitive to grain anisotropy and have almost similar R^2 for grain-scale anisotropic model vs. homogeneous average isotropic model. In contrast, HAR specimens (#7-10), with only one grain along the width (y-direction in Figure 3-8), are much more sensitive to grain anisotropy and therefore have higher RMS discrepancy (lower R^2 value) for homogenous isotropic FEA compared to grain-scale anisotropic FEA. As a result of this study, Figure 3-25 shows Hill's stress vs. Hill's inelastic strain curves for different grain sizes of HCR solder joints. Figure 3-26 shows Hill's stress vs. inelastic strain curves of infinitely large grain for low and high cooling rates. These curves can be used to conduct anisotropic grain-scale FE analysis of oligocrystalline solder joints.

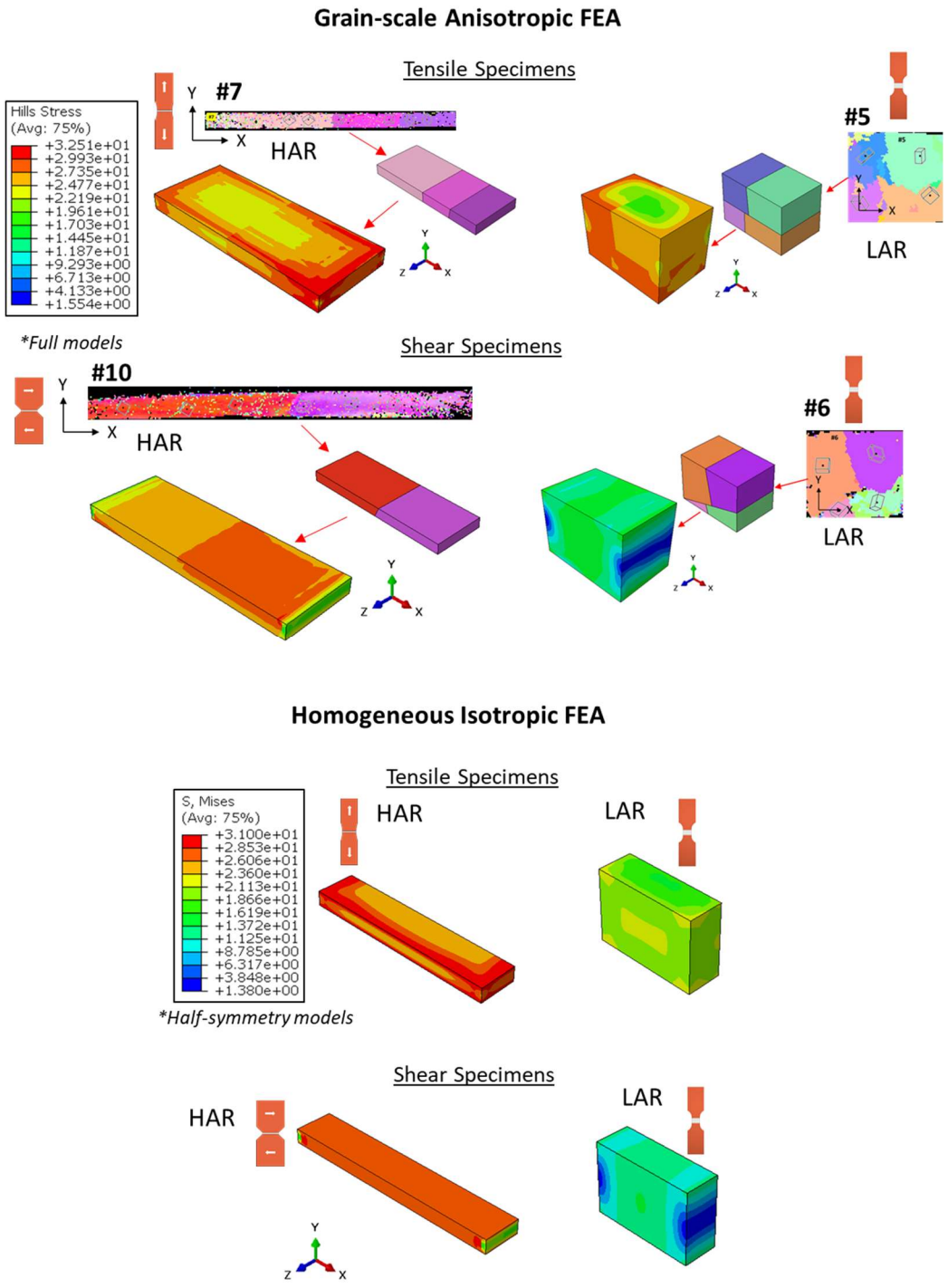

Figure 3-22 Comparison of grain-scale anisotropic FEA results with homogeneous isotropic FEA predictions at same displacement level

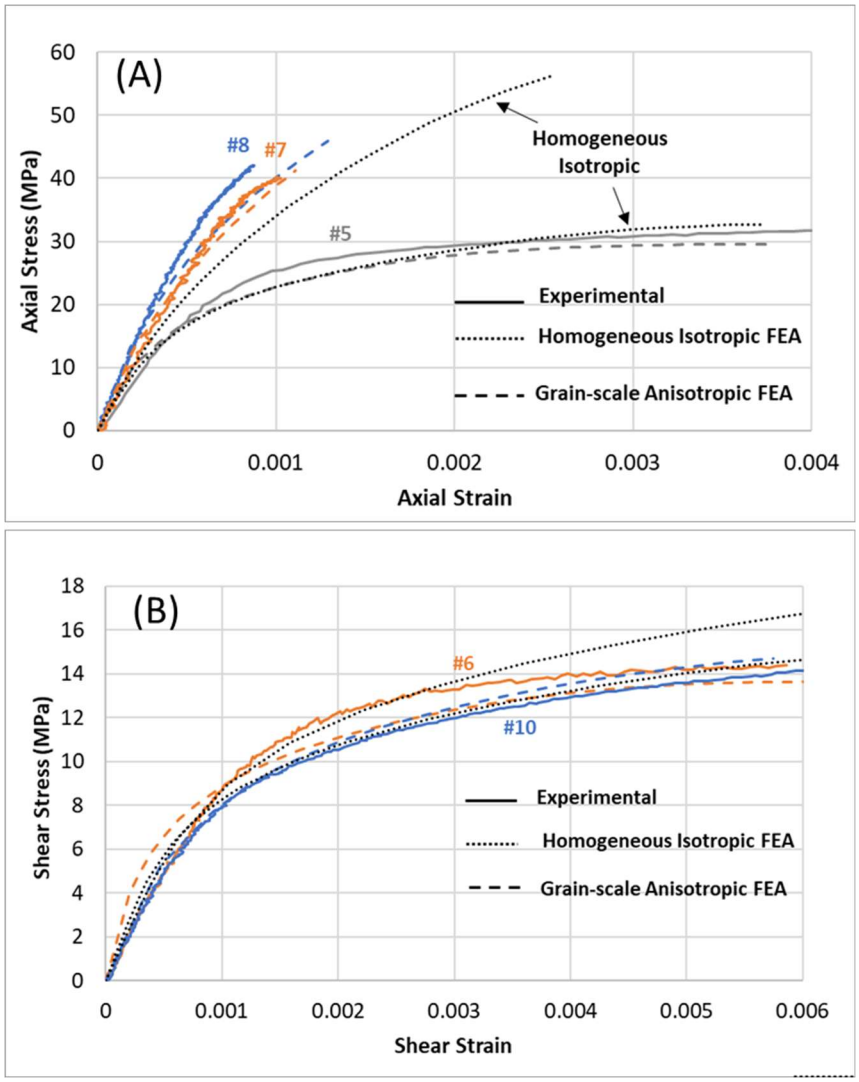

Figure 3-23 Comparison of stress-strain predictions using grain-scale anisotropic model vs. homogenous isotropic model- (A.) Axial stress-strain curves for tensile specimens; (B.) Shear stress-strain curves for shear specimens.

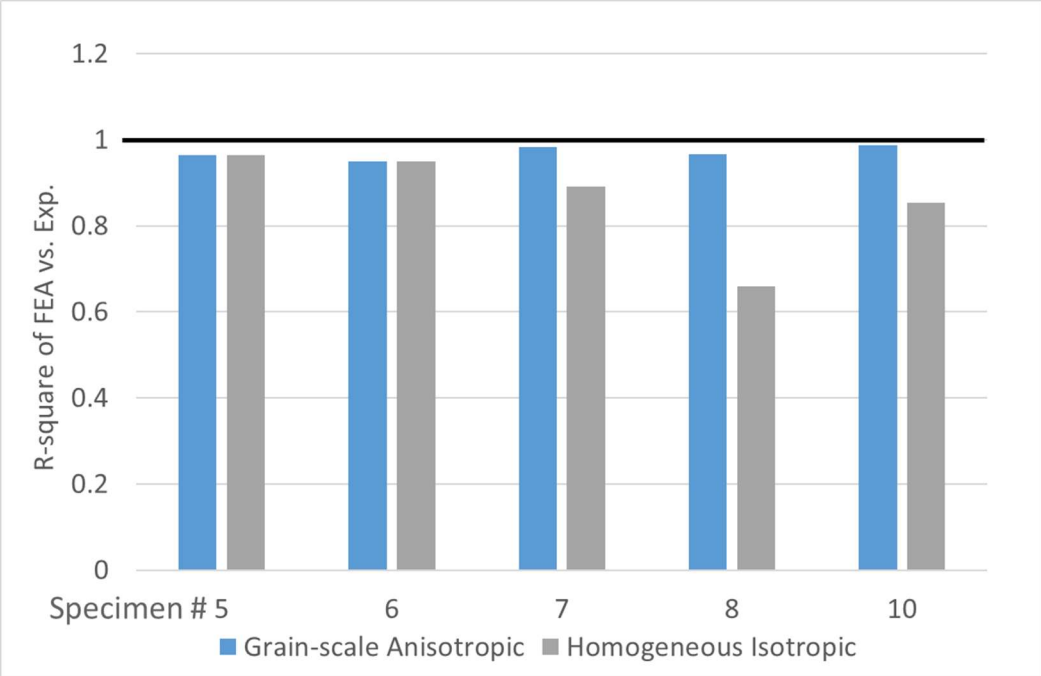

Figure 3-24 Comparison of microstructure based grain-scale anisotropic FEA vs. homogenous isoptropic FEA predictions.

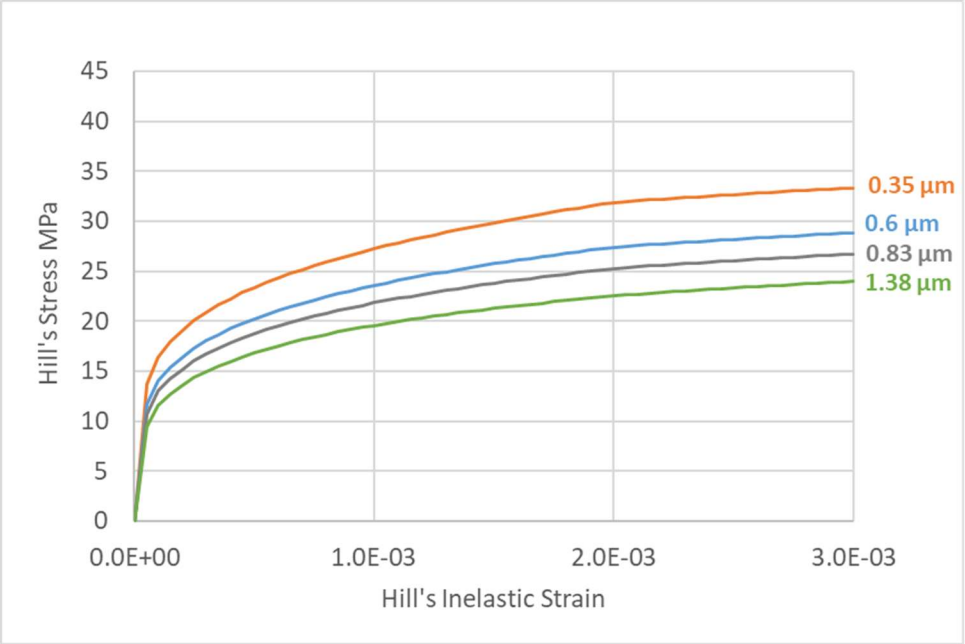

Figure 3-25 Hill's stress vs. inelastic strain curves for HCR specimen as a function of average grain diameter.

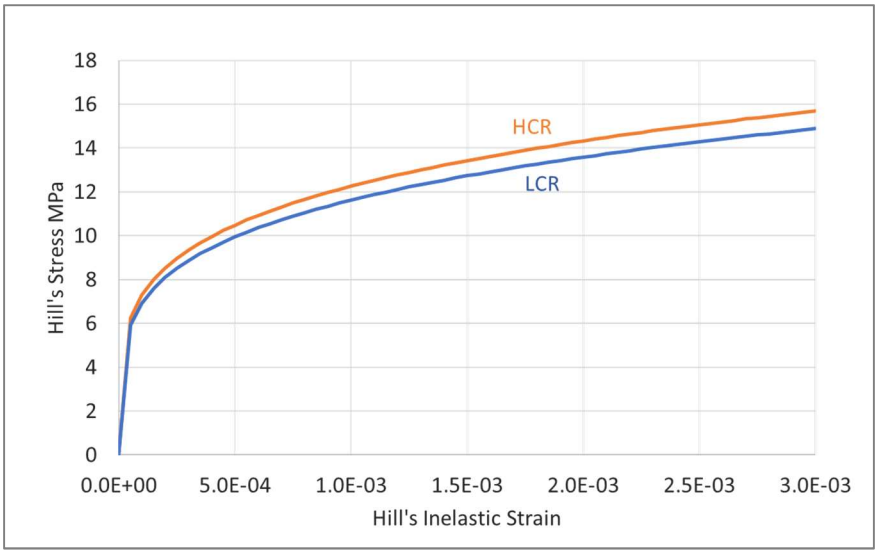

Figure 3-26 Hill's stress vs. inelastic strain curves as a function of cooling rate.

3.6.Summary and Conclusions

Monotonic tensile and shear tests were conducted on single and multi-crystal SAC305 solder joint specimens in order to characterize the anisotropic plastic behavior of SAC305 solder joints. The anisotropic plasticity was modeled using Hill's yield criterion and a Holloman plasticity model. The single grain solder stress-strain results were used to determine the Hill's yield stress ratios and characterize the plastic response of SAC305 solder joints. Each specimen was modeled in FEA and the influence of each yield stress ratio on solder joint stress-strain response was evaluated by parametrically varying the ratios systematically and comparing the engineering stress-strain response with experimental results. The performance of different yield stress ratios was evaluated using a 'Accuracy metric' and an 'Anisotropy metric'. The optimized set of yield stress ratios, that provide a better fit for different specimens across the two metrics, was proposed in this study.

The single grain was attained using low cooling rate during soldering process, which resulted in significant differences in the Tier 1-2 microstructure compared to higher cooling rate specimens. In addition, higher cooling rate leads to formation of multiple grains in the solder joint, resulting in different Tier 3 microstructure compared to low cooling rate specimens. The differences in microstructure lead to higher yield strength in high cooling rate specimens compared to low cooling rate specimens due to a combined contribution from Orowan hardening and Hall-Petch effect. Therefore, an empirical scaling methodology has been proposed to scale the single-crystal stress-strain results (with low cooling rate) to multi-crystal stress-strain curves (with higher

cooling rate). The scaling factors are influenced by parameters such as- the Ag_3Sn particle size and spacing, volume fraction of dendritic and eutectic phases, and grain sizes. The FEA conducted in this paper successfully demonstrates that microstructurally motivated grain-scale anisotropic model predicts stress-strain response of tested specimens more accurately than homogenous isotropic FEA.

The grain-scale anisotropic properties determined in this study can be used by engineers to: (i) assess the variability in mechanical behavior of solder joints which is attributed to grain anisotropy; (ii) supplement the failure analysis of tested joints, by accurately evaluating the stress concentrations at failure sites. The part-II paper essentially showcases these applications.

Chapter 4 : Grain-scale Study of SAC305 Oligocrystalline Solder Joints: Part-2 – Influence of Grain Orientation on Tensile and Shear Mechanical Cycling Durability

Abstract

Functional solder joints experience multiaxial stresses (tensile and shear) as they undergo a combination operational loads such as temperature cycling and out-of-plane PWB flexure/warpage. Researchers often use finite element simulations to quantify stresses and strains in the critical solder joint, by modeling the solder joints homogenous isotropic volumes. Solder strain (or other similar damage metrics, such as work density) is used to construct fatigue durability curves from fatigue test data and to predict failures under life-cycle loading conditions. In reality, each SAC solder joint consists of few highly anisotropic grains and is neither homogeneous nor isotropic. As a result, homogeneous, isotropic finite element models erroneously represent the true material behavior and neglect the resulting stress concentrations at grain boundaries and triple corners between mis-oriented grains and IMC interfaces. Due to piece-to-piece variability in the grain structure of tested joints, a simple homogeneous isotropic representation leads to significant piece-to-piece uncertainty in predicting the strain levels (and hence in the fatigue durability) of each solder joint at any given level of applied loads. A typical approach for dealing with this variability is to test a large number of samples at each loading level and use confidence intervals to determine the

statistical variability. However, such a process is resource-intensive and time-consuming as temperature cycling tests can take few months to complete.

Therefore, this study aims to quantify the role of the grain anisotropy on the variability in fatigue durability predictions, based on a simulation-based 'virtual-testing' alternative. The approach of current paper (which is the second part of the 2-part paper series), consists of parametric, grain-scale, anisotropic FEA simulations - (i) to determine the upper and lower bounds of multiaxial fatigue damage model constants proposed in prior work by the authors; and (ii) to demonstrate variability in fatigue damage of a ball grid array solder ball. The part-1 paper focused on experimental determination of a reasonable set of anisotropic elastic-plastic properties of SAC305 solder joints. Findings of this study can enable more accurate 'digital twins' and empower engineers to obtain more accurate, faster and cheaper a-priori estimates about the variability of fatigue reliability predictions.

4.1.Introduction

4.1.1. Background and Motivation

Solder joint reliability is typically assessed by performing accelerated temperature cycling and harmonic vibration tests. This is because, these accelerated tests expose similar failure mechanisms in a short duration, as the solder joints normally would experience during their operational life. As an example, the solder joints are subjected to multiaxial stresses (tensile and shear) as they undergo a combination of operational loads such as temperature cycling and out-of-plane PWB flexure/warpage.

The strains (or other similar damage metrics) in the solder joints during the accelerated tests are estimated using finite element analysis (FEA). Researchers treat solder joints as homogenous isotropic volumes and use time-dependent plasticity models and unified viscoplasticity models such as Anand's model [1] and Chaboche model [62], to describe monotonic, cyclic and creep loading of homogenous isotropic inelastic solder joints [63][64][65][66]. The solder strains estimated from finite element analysis are used to develop thermo-mechanical or vibration fatigue durability master curves. Engineers use confidence intervals to account for the variability in the solder fatigue SN curves. The fatigue durability curves are then used to predict failures in the solder joints under life-cycle loading conditions. However, this entire process starting from accelerated testing to the development of fatigue curves is expensive and takes significant amount of time.

One reason it takes lot of time to establish probabilistic SN curves is because engineers need to test statistically significant samples to get a reasonable trend, due to inherent piece-to-piece variability in the grain structure of each joint. The variation in the grain structure and hence in the mechanical behavior of solder joints, stems from the fact that the SAC solder joints have few coarse grains which are highly anisotropic. As is well known in the literature, the SAC solder alloy family contains >90% ß-Tin with a body-centered tetragonal crystal structure. The modulus of elasticity of ß-tin in [001] direction (68 GPa) is almost 2.5 times larger than that in [100] direction (24GPa) [5].

However, modeling solder alloy as a homogenous isotropic volume during finite element analysis will incorrectly predict the strains levels in the solder joint. Hence, this paper aims to minimize the time required for reliability testing phase by virtually estimating the variability in solder strains due to differences in grain structure.

4.1.2. Grain-scale Modeling of Solder Joints

Solder joints are traditionally modeled as a homogenous isotropic inelastic volume in finite element analysis to gain understanding of the stresses and strains leading to failure of the joint. Researchers used time-dependent plasticity models and unified viscoplasticity models such as Anand's model and Chaboche model, to describe monotonic, cyclic and creep loading of homogenous isotropic inelastic solder joints. Chaboche model accounts for the influence of stress triaxiality on durability of solder joints and is hence well suited for studying the effect of multiaxial stress states. Modeling the solder joint with this assumption is a common practice, because of the impracticality of obtaining grain orientation information of every single solder joint in actual electronic components. However, coarse-grained lead-free SAC solder joints are far different from homogeneous isotropic structures. Instead, they have few highly anisotropic SnAgCu (SAC) crystals, which creates local mismatches and incompatibilities along the grain boundaries and triple corners, generating stress concentration sites, especially between mismatched grains and interfacial IMC layers. Most of the research studies neglected the influence of such heterogeneities on the observed fatigue failures leading to inaccuracies in quantifying the severity in failures. Therefore, to improve the accuracy of constitutive models, some researchers

implemented crystal-plasticity/crystal-viscoplasticity finite element analysis approach (CPFEA) which accounts for grain orientation and slip system behavior in solder joints [18][35]. For example, Zamiri et. al [35] evaluated the stress-strain response of a solder joint due to thermomechanical load caused by 165°C temperature change using crystal-plasticity modeling. C-axis of the crystal orientated parallel to the solder-IMC interface was seen to have largest thermal expansion mismatch and plastic work. Darbandi et. al [18] presented a crystal plasticity (CP) model to simulate mechanical deformation in a tri-crystal solder ball with different orientations. Lap-shear tests on solder joints were used to calibrate the CPFEA model. The model demonstrated that the CP model was able to simulate deformation in the solder ball in reasonable agreement with the experimental results. Implementing crystal plasticity FEA on every solder joint can be quite challenging and computationally inefficient. Mukherjee [11] and Jiang [36] have provided a hybrid crystal viscoplasticity (CV) based anisotropic continuum modeling approach. This approach uses anisotropic dislocation mechanics based multi-scale crystal viscoplasticity method. The microstructural features of SAC from tiers 0-2 (described in previous section) are used to model anisotropic creep behavior of solder joints. The CV model outputs are converted to continuum creep models (Hill's potentials and Norton power law creep model) for SAC grains. This methodology is relatively simple and computationally efficient to adopt, compared to traditional crystal plasticity finite element analysis.

However, implementing crystal plasticity FEA on every solder joint can be quite challenging and computationally inefficient. As an alternative, researchers have

also attempted to model grain-scale solder joints using anisotropic continuum Hill's plasticity approach. Hill's yield strength ratios for different crystal directions, were determined using Sn single crystal uniaxial tensile test data in selected crystal directions. Hill's model was relatively easy to implement and was able to predict stress-strain response of solder joint reasonably well [37][38]. Unfortunately, corresponding Hill's model and single grain stress-strain experimental data for SAC305 was not present in the literature. Therefore, the part-I paper essentially proposes a set Hill's yield stress ratios and Hill's stress-strain curves, which were calibrated using uniaxial monotonic tensile and shear tests conducted on single grain SAC305 solder joint specimens. Such a grain-scale modeling approach can be used to evaluate the stress concentrations and mechanical response on few-grained solder joints, however, the available literature lacks such information.

4.1.3. Overall Approach

A parametric anisotropic grain-scale finite element analysis is conducted on by varying the grain orientations to simulate best- and worst-case configurations. The solder joint specimens simulated in this study were earlier subjected to mechanical cyclic tensile and shear loading, and a multiaxial fatigue damage model was established in prior work [16]. The parametric FEA results are used to quantify the variability in multiaxial fatigue damage model constants attributed to grain anisotropy. In addition, this paper also aims to shed light on the inaccuracies involved in modeling solder joints as homogenous isotropic material while quantifying their stress and strains. In order to

demonstrate the utility of the variability quantification approach, the parametric grain-scale anisotropic FEA is also conducted on a BGA solder ball.

4.2.Finite Element Approach

This section provides details about the finite element analysis.

4.2.1. Grain-scale Analysis of TMM Specimens

A parametric grain-scale finite element analysis was conducted in this study, to quantify the stochastic variability in fatigue results from a prior study conducted by the authors. Figure 4-1 shows equivalent strain range vs. cycles to failure for solder joints subjected to different cyclic mechanical loading modes. Due to the low number of test samples in shear mode, the scatter bands are much wider than in tensile mode. In addition, the M0 specimens failed by a combination of interfacial cracking and bulk solder damage, compared to failure in M90 specimens, which was dominated at the interface. Hence, the failures in M0 specimens are more likely to be influenced by the piece-to-piece variation in the mechanical response which is attributed to the anisotropy of Sn grain in the bulk solder. Therefore, this section provides a methodology for a realistic assessment of variability in the test results in order to narrow down the confidence intervals.

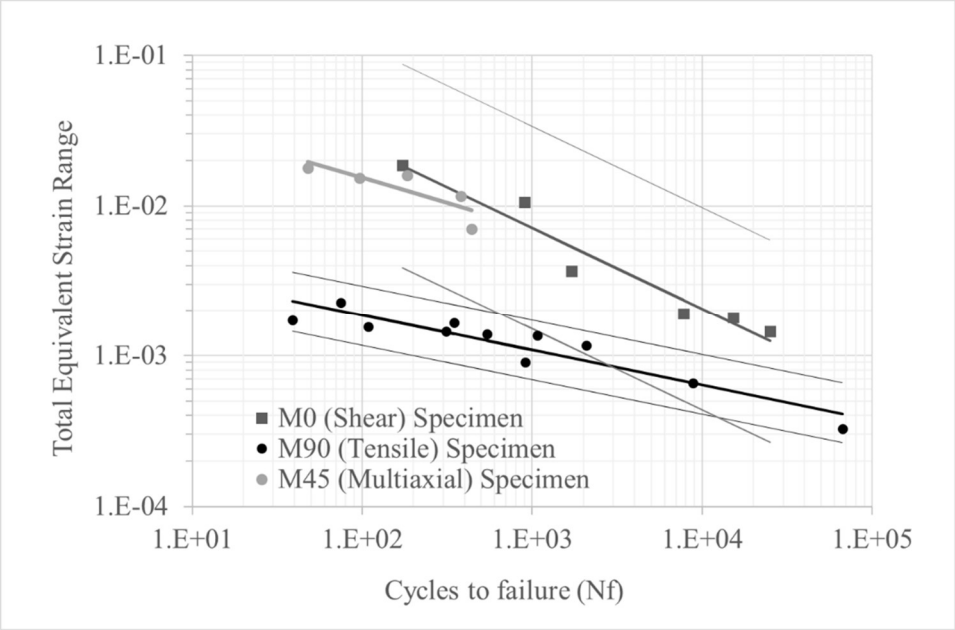

Figure 4-1 Fatigue curves for solder joints under shear, tensile and multi-axial loading mode

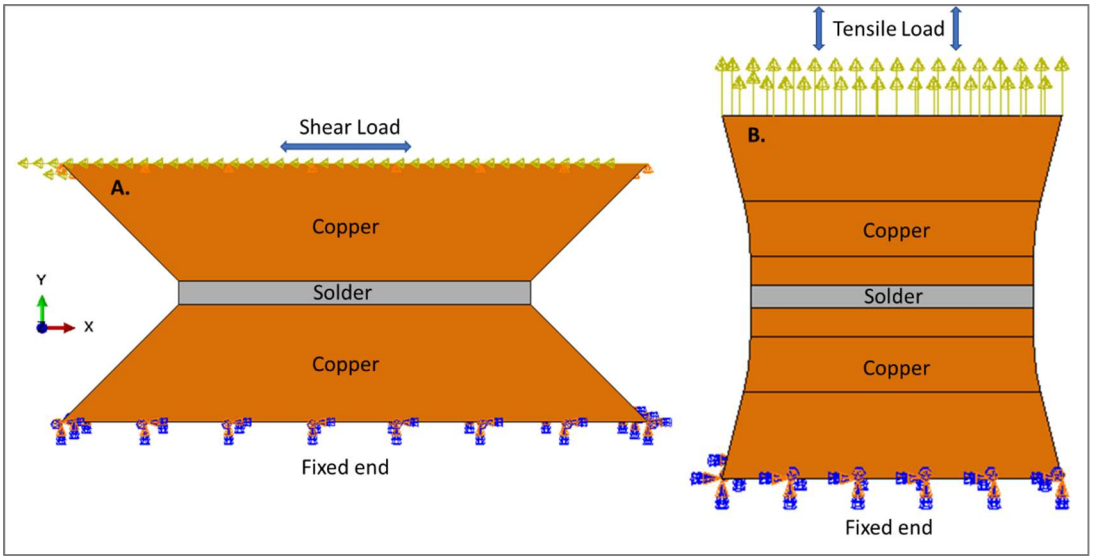

Figure 4-2 FEA Model and Boundary Conditions: A. M0 (shear) specimen; B. M90 (tensile) specimen

Table 4-1 Elastic stiffness constants for SAC305 [5] (Unit: GPa)

C_{11}	C_{22}	C_{33}	C_{44}	C_{55}	C_{66}	C_{23}	C_{13}	C_{12}
73.2	73.5	89.3	22.3	22.3	24.2	36.4	36.3	59.6

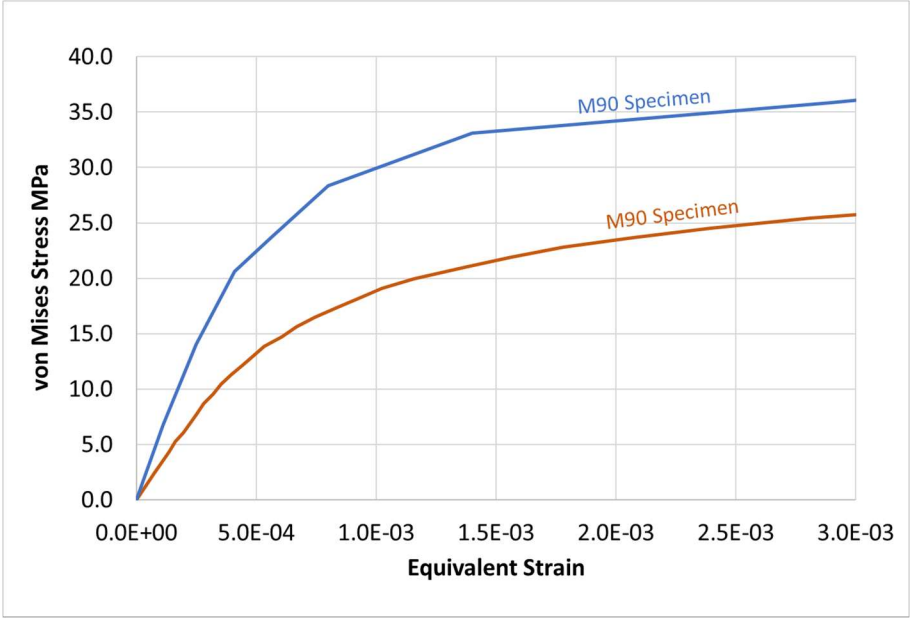

Figure 4-3 von Mises stress-strain curves for M90 and M0 specimen [16]

Half-symmetry models of the M0 (shear) and M90 (tensile) specimens were constructed in FEA. The models represent the exposed portion of the specimen located between the loading grips. Figure 4-2 shows FEA models of the two specimens (M0 and M90 specimens) and boundary conditions applied. The bottom face of the specimen was fixed and a cyclic load (as recorded in experiments) was applied on the top face along appropriate directions, to represent tensile and shear loads. 8-noded linear brick element was used for modeling the entire specimen.

Copper substrate was modelled as a linear elastic isotropic material (E = 110 GPa, ν = 0.35). The solder joint is modeled with anisotropic elastic-plastic properties. The anisotropic elasticity is defined using elastic stiffness matrix constants (provided in Table 4-1) for SAC305 [5], whereas, the anisotropic plasticity is modeled using Hill's anisotropic yield criterion and Hill's stress vs. inelastic strain data presented in the part-I paper [67]. The part-I paper showed different sized grains that are sandwiched between the copper substrates observed in the TMM solder joint. The part-I paper also microstructurally scaled stress-strain curves. Therefore, two extreme scenarios joint configurations considered in this variability analysis were- (i) smallest grain (with high yield strength) and c-axis parallel to Y-axis; (ii) largest grain (with low yield strength) and a-axis or b-axis parallel to Y-axis. In addition, a homogenous isotropic solder joint was modeled using von Mises stress-strain curves shown in Figure 4-3 [16] and the results were compared with parametric grain-scale anisotropic FEA results. Figure 4-5 shows the two best-case and worst-case orientations considered for the parametric grain-scale FEA in this study. Hill's anisotropic yield potentials used for modeling anisotropy in this analysis are listed in Table 4-3. The Hill's stress vs. inelastic strain curves for the smallest and largest SAC305 grains found in M90 (curve-1 & 2) and M0 specimens (curve-2 & 3) are provided in Figure 4-4. Cyclic strain range in the solder is extracted from the different solder grain configurations and compared with the experimental data to determine the variability in fatigue results and the fatigue damage model constants proposed in the prior work by the authors [16]. The details of the fatigue damage model (Eq. 4-1 & Eq. 4-2) are

provided here for completeness. D_t, D_1 and D_2 are total damage, interfacial damage and bulk solder damage terms. The interfacial damage is dependent on hydrostatic strains $\epsilon_h^{interface}$ near the solder-IMC interface, whereas, bulk solder damage is related to deviatoric strains $\Delta\epsilon_{eq}^{bulk}$ in the bulk solder. N_t are the life-cycles to failure. The damage model constants along with 90% confidence limits are presented in Table 4-2.

$$D_t = D_1 + D_2 = \left(\frac{\epsilon_h^{interface}}{A_1}\right)^{\left(\frac{1}{m_1}\right)} + \left(\frac{\Delta\epsilon_{eq}^{bulk}}{A_2}\right)^{\left(\frac{1}{m_2}\right)} \quad \text{Eq. 4-1}$$

$$N_t = \frac{1}{D_t} \quad \text{Eq. 4-2}$$

Table 4-2 Multiaxial fatigue damage model constants [16]

Parameter	**IMC interface damage**		**Bulk solder damage (Intergranular and transgranular damage)**	
A [cycles]^m	6.57E-4	Upper bound: 9.5E-4	3E-1	Upper bound: 10E-1
		Lower bound: 4.5E-4		Lower bound: 0.9E-1
m	0.23		0.54	

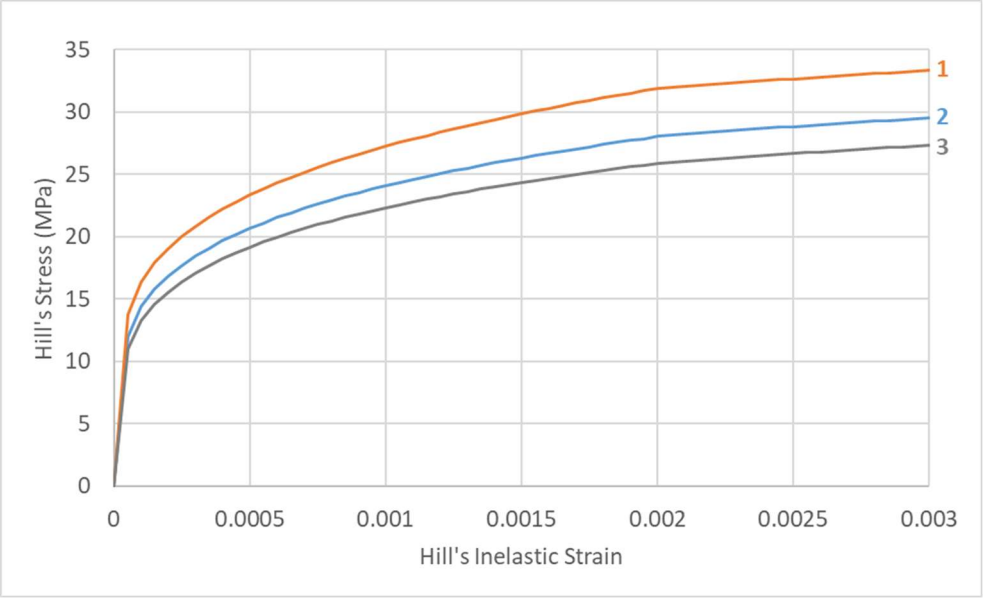

Figure 4-4 Hill's stress vs. inelastic strain curves used for grain-scale FE analysis

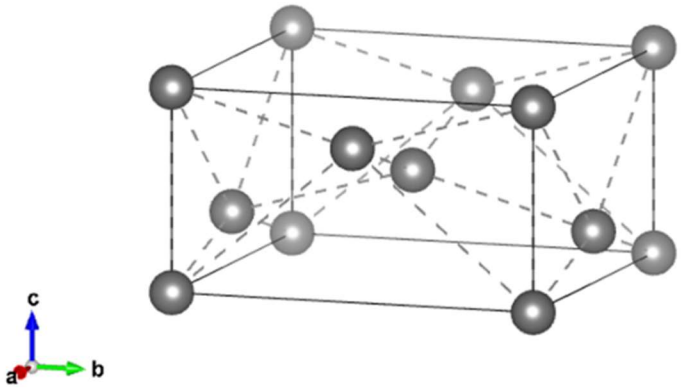

Case#	Configuration
1	c-axis ⊥ to Y-axis
2	c-axis ‖ to Y-axis
3	Isotropic condition

Figure 4-5 Sn crystal lattice [68] and grain orientations considered in this study.

Table 4-3 Hill's anisotropic yield stress ratios for SAC305 [67]

R_{11}	R_{22}	R_{33}	R_{12}	R_{23}	R_{13}
0.83	0.83	1	1.08	1.12	1.12

4.2.2. Grain-scale Analysis of a BGA Solder Joint

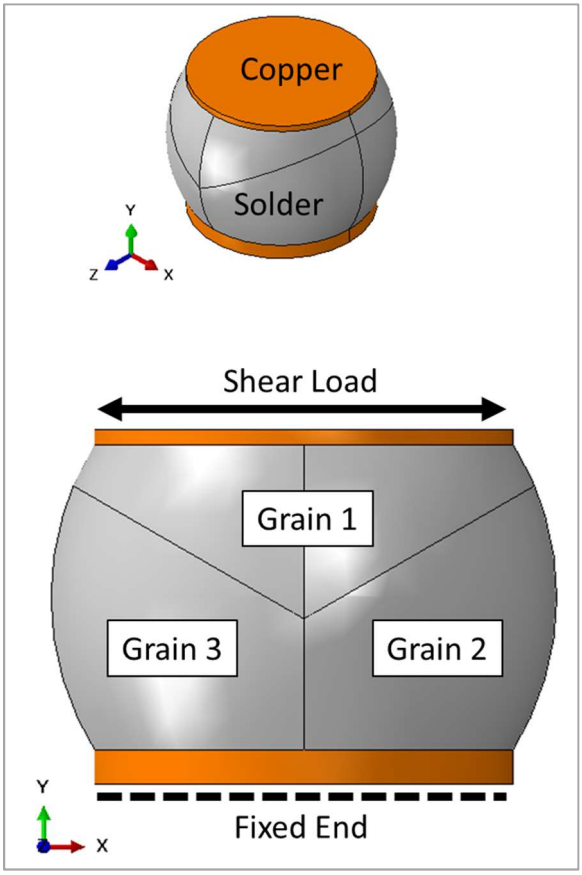

Figure 4-6 Critical BGA solderball with 3 grains

Table 4-4 Grain orientation configurations used for parametric FE analysis

Case#	Configuration
1	Tri-crystal: c-axis ⊥ to each other in all the grains
2	Single grain: c-axis ‖ to Y-axis
3	Single grain: c-axis ‖ to Z-axis
4	Isotropic condition

This section presents an application of grain-scale anisotropic parametric FE methodology in estimating the variability in fatigue life of solder joints. Numerous researchers have reported that the grain morphology in BGA solder ball ranges from single grain to an oligocrystalline beach-ball grain structure [23][24]. The critical corner-most solder ball in BGA package experiences severe stresses and strains during temperature cycling induced thermal expansion mismatch and during mechanical bending of the printed wired assembly. Therefore, as an example, a critical (corner) solder ball of a ball grid array (BGA) package is modeled in this FE analysis as shown in Figure 4-6. The joint is represented with 3 anisotropic, elastic-plastic solder grains. The 3-grained solder ball represents a typical beach-ball grain structure found in functional solder joints. In case-1, the grains are oriented such that the stiffest, strongest

crystal direction [001] (c-axis) of the 3 grains are mutually perpendicular to each other. In addition, extreme single grain configurations are considered where c-axis is parallel to each of the global principal directions. Table 4-4 shows different grain configurations considered in this study.

Anisotropic elastic stiffness constants and Hill's yield stress ratios used for this analysis are presented in Table 4-1 and Table 4-3. Hill' stress-inelastic strain properties used for grain-scale FE analysis is presented in Figure 4-4 (curve-2). Grain boundaries are known to contribute to creep deformation, and therefore, are assumed here to have negligible influence on plastic deformation [69]. Copper pads were assumed to have linear elastic isotropic behavior presented in previous section 4.2.1. A homogeneous isotropic solder ball (Hill's yield stress ratios- R=1) is also modeled for comparison, since engineers in the industry typically model solder balls with homogeneous isotropic assumption. The bottom surface of the PCB side Copper pad is constrained in all degree of freedoms and cyclic mechanical shear load of 0.8 N and 1.25 N is applied on the top of the package side Copper pad. Upper-bound and lower-bound deformation results from this parametric study are used to estimate the variability range for mean durability predictions conducted with the conventional approach of treating the solder as a homogenous isotropic material. The fatigue durability model used for the life cycle predictions in this work was determined in prior investigation on SAC305 solder joints subjected to cyclic mechanical tensile and shear loads. This approach of assessing the fatigue durability of solder joints was introduced in prior work [70].

4.3.Results and Discussion

4.3.1. TMM M90 and M0 Specimens

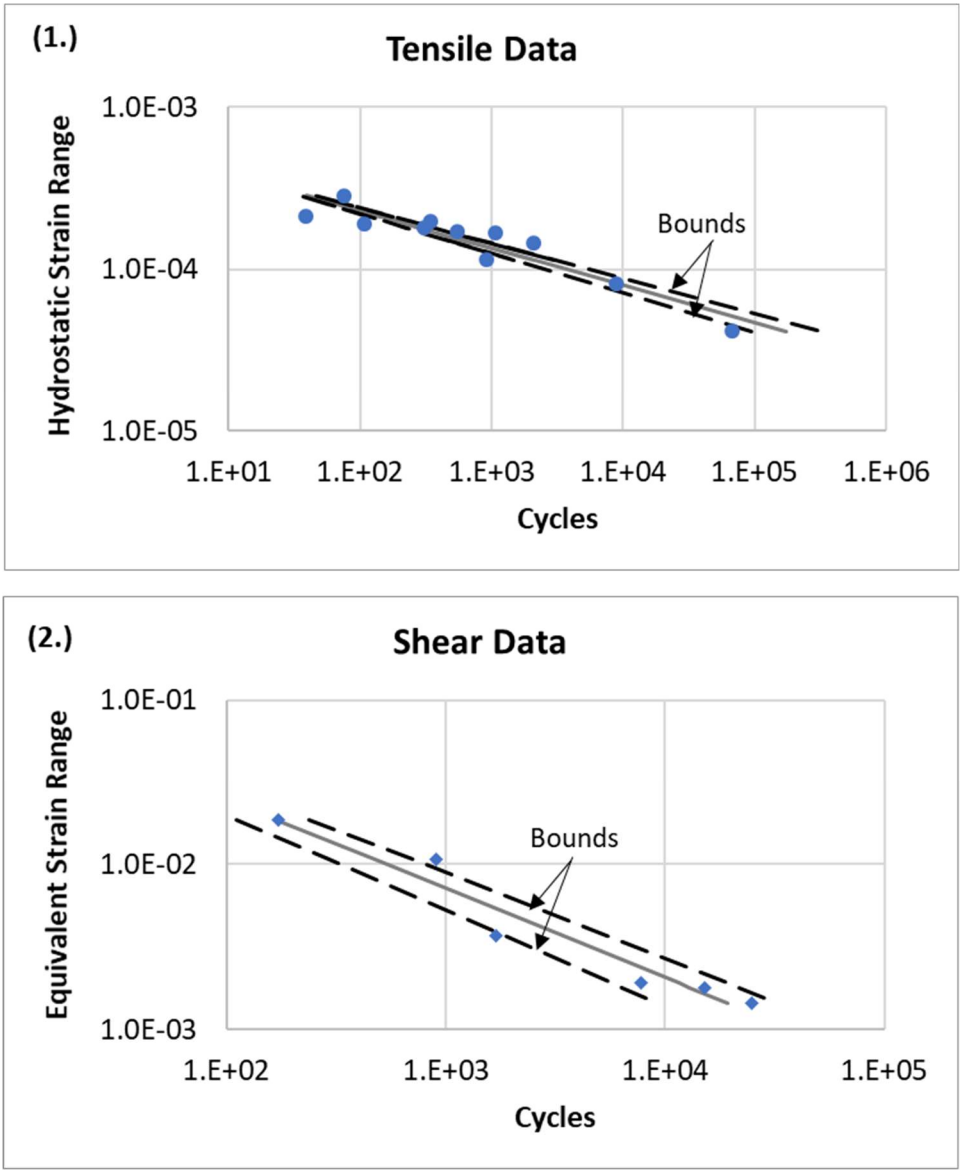

Figure 4-7 (1.) Hydrostatic strain range vs. cycles to failure for M90 tensile specimen; (2.) Equivalent strain range vs. cycles to failure for M0 shear specimen.

Average cyclic tensile and shear strains were extracted from the FEA for each grain configuration. The equivalent strains in the bulk solder and hydrostatic strains in the interfacial region of the solder joint were estimated for different grain structure configurations and plotted against the life-cycles predicted for homogenous isotropic solder ball as shown in Figure 4-7 (1) and (2). The strains extracted from homogenous isotropic FEA are represented by grey curve, whereas the dashed black lines represent the strains extracted from different orientations considered in grain-scale model. The lower dashed line is when c-axis of Sn grain is parallel to Y-axis and it forms the lower limit of the fatigue curve. As expected, the upper dashed line forms the upper limit of the fatigue curves, when c-axis is perpendicular to Y-axis. The bounds of the fatigue damage model constants estimated using the parametric anisotropic grain-scale FE analysis are presented in Table 4-5. The anisotropic grain-scale FE analysis is able to predict the variability in M0 shear specimen specimens, reasonably well, as most of the damage in these specimens was concentrated in the bulk solder (which is in turn dependent on the microstructure). However, as the failure in M90 specimens was concentrated near the solder-IMC interfacial region, the grain-scale analysis predicts that the grain anisotropy plays a negligible role in contributing towards the scatter in the fatigue results.

Table 4-5 Upper and lower bounds of the multiaxial fatigue damage model constants as predicted by grain-scale FE analysis

Constant	A_1	m_1	A_2	m_2
Upper bound	6.48E-04	-0.22	3.27E-01	-0.52
Experimental Least Square Fit	6.57E-04	-0.23	3.00E-01	-0.54
Lower bound	6.69E-04	-0.24	2.88E-01	-0.58

4.3.2. BGA Critical Solder Ball

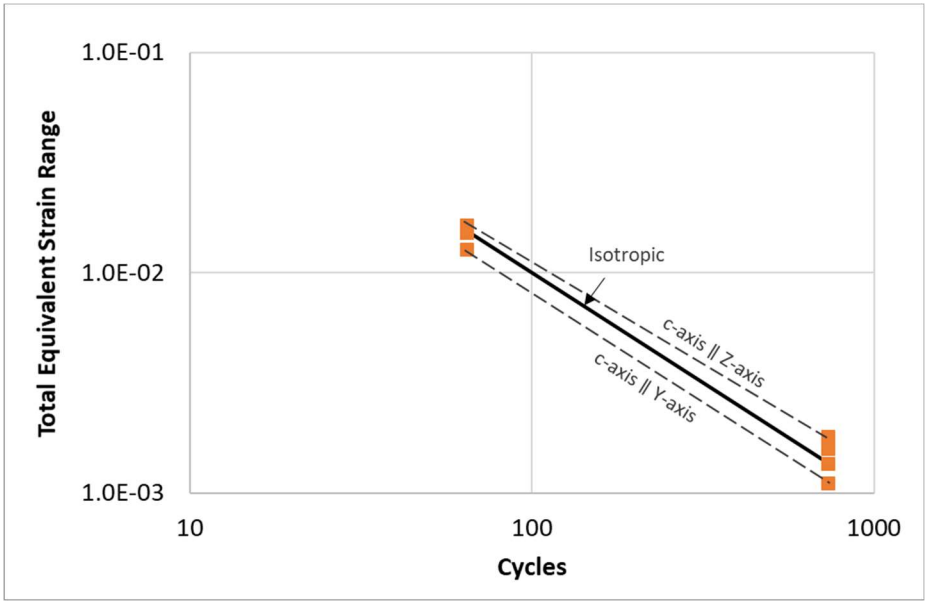

Figure 4-8 Life-cycle predictions for different solder grain configurations

Based on traditional approach that engineers follow, cyclic total equivalent strain range for homogenous isotropic solder ball was used to predict cycles to failure (solid line), as shown in Figure 4-8. Next, cyclic total equivalent strains extracted from different grain structure configurations were plotted against the life-cycles predicted for homogenous isotropic solder ball. This is done to point out that, even though isotropic homogenous FEA approach inaccurately outputs single value of strain, in reality the strain response has a variable range, depending on the grain structure. The dashed lines which represent the stiffest (c-axis parallel to Y-axis) and the most compliant (c-axis parallel to Z-axis) grain structure configurations provide bounds for the SN curve. As expected, the strains in the tri-crystal solder ball (with c-axis of each grain oriented mutually perpendicular to each other) lies between the upper and lower bound SN curves. Therefore, variability and confidence bounds can be easily estimated through this parametric grain-scale modeling methodology.

4.4.Summary and Conclusions

This paper primarily focuses on demonstrating the applications of micro-structurally motivated grain-scale anisotropic FEA modeling methodology in quantifying the variability in fatigue damage model constants and fatigue curves. The variability in mechanical behavior of coarse-grained solder joints is attributed to the grain anisotropy.

In the first example, anisotropic grain-scale modeling approach was used to quantify the upper and lower bounds of fatigue damage model constants presented in prior study. The damage model was developed to predict fatigue life of solder joints

subjected to cyclic tensile and shear mechanical loading. TMM tensile and shear solder joint specimens were modeled as a single grain with best-case and worst-case grain orientations. The worst-case consists of a smallest grain (with high yield strength) and c-axis parallel to Y-axis, whereas the best-case consists of largest grain (with low yield strength) and a-axis or b-axis parallel to Y-axis. The grain-scale modeling methodology is able to predict variability in M0 shear specimens reasonably well. However, for M90 tensile specimens, the methodology proved to be limited, because the interfacial failures in tensile specimens are probably less dependent on grain anisotropy. Based on the grain-scale FEA results, upper and lower bounds of fatigue damage model were estimated.

The grain-scale methodology provides a time and computationally efficient virtual testing approach to conduct parametric sensitivity studies on solder joints with different orientations. The second example demonstrates a similar virtual testing approach to quantify the variability in fatigue curves. A critical BGA solder ball is modeled in FEA with different best-case and worst-case grain orientations and upper and lower limits of fatigue curves are estimated. The proposed virtual testing approach is efficient and inexpensive, compared to traditional approach of generating durability models by testing large number of samples and using confidence bounds to quantify the scatter. Therefore, to save time and costs associated with experiments, this paper recommends testing few samples to identify the trends and then conducting parametric virtual tests to quantify the variability in the durability data for solder joints.

Chapter 5 : Summary, Contributions, Limitations and Future work

This chapter outlines the summary of work, dissertations contributions, limitations and future work.

5.1.Summary of Dissertation

This section provides summary of work completed in Chapters 2-4 of this dissertation.

5.1.1. Role of Nominal Stress State on Cyclic Fatigue Durability of SAC305 Grain-scale Solder Joints

i. Cyclic mechanical elastic-plastic fatigue tests were conducted at room temperature on OFHC-SAC305 microscale solder joint specimens, in tensile, shear and multiaxial loading modes.

ii. Cyclic fatigue test results showed that the cyclic tensile loading mode is more damaging than cyclic shear mode in grain-scale oligocrystalline SAC joints.

iii. The different slopes of the SN curves in the individual (tensile, shear and combined) load cases indicate different deformation and degradation mechanisms.

iv. Failure analysis revealed that dominant damage mode in tensile (M90) mode was brittle failure at interface of IMC and solder, whereas damage in shear (M0) loading was dominated by ductile damage (intergranular and transgranular) in

the bulk of the solder. Multiaxial (M45) specimens experienced mixed-mode failures with more ductile bulk solder damage than tensile specimens and more brittle IMC-solder interfacial damage than shear specimens.

v. The differences in the nominal tensile, shear and multiaxial durability curves for the same material indicate that equivalent strain in the solder bulk is not a sufficiently unified metric to properly represent durability of SAC305 solder joints across all stress states.

vi. A simple linear damage superposition method is proposed to represent the durability under different damage-mode contributions from different combinations of stress states. The approach accounts for both interfacial damage at solder-IMC interface as well as transgranular/intergranular damage in the bulk of the solder. The two metrics driving this model are the interfacial hydrostatic strain and the average equivalent strain in the solder bulk.

5.1.2. Grain-scale Study of SAC305 Oligocrystalline Solder Joints: Part-2 – Influence of Grain Orientation on Tensile and Shear Mechanical Cycling Durability

i. Monotonic tensile and shear tests were conducted on monocrystalline and oligocrystalline test specimens of two different aspect ratios (length-to-width ratio), in order to characterize anisotropic plastic properties of SAC305 as a function of different cooling rates and grain size.

ii. Monocrystalline specimens were used to determine continuum anisotropic Hill plastic yield criterion constants. A systematic parametric FEA was conducted

and the effect of different Hill's yield stress ratios was evaluated using two metrics- a prediction error metric and an anisotropy metric. A suitable set of yield strength ratios that perform well with respect to both metrics was established. Holloman's plasticity model constants for modeling plasticity in single-grain SAC305 solder joint specimens are also proposed.

iii. As the cooling rates were very different for monocrystalline specimens vs oligocrystalline specimens, the dendritic and eutectic microstructure within the grains were significantly different based on cooling rates. The Ag_3Sn IMC particle size & spacing and dendrite size was much higher in low cooling rate specimens compared with high cooling rate specimens. In addition, the volume fractions of Sn dendritic phase vs. eutectic Ag_3Sn phase were different in specimens with low vs. high cooling rates. Furthermore, higher cooling rates during soldering resulted in oligocrystalline specimens rather than monocrystalline specimens. As a result of these microstructural variations, the effective single-grain elastic-plastic behavior was very different in monocrystalline vs. oligocrystalline cooling rate) specimens. Therefore, a methodology was proposed for scaling the mechanical behavior of solder joints specimens across different microstructures (produced by different cooling rates) and different grain sizes.

5.1.3. Grain-scale Study of SAC305 Oligocrystalline Solder Joints: Part-2 – Influence of Grain Orientation on Tensile and Shear Mechanical Cycling Durability

i. A parametric anisotropic grain-scale elastic-plastic FEA was conducted to quantify the stochastic variability (attributed to grain anisotropy and variations in grain structure) in cyclic mechanical (elastic-plastic) fatigue results presented in Chapter 2.

ii. In order to bound the variability, two extreme monocrystalline solder joint configurations were modeled in this study: (i) a compliant configuration that has the [100] or [010] direction of SAC grain oriented along the loading axis (a-axis or b-axis parallel to loading direction); and (ii) a stiff configuration that has [001] direction of SAC grain aligned with the loading axis (c-axis parallel to loading direction). Anisotropic elastic-plastic properties for SAC305 obtained in Chapter 3 were used in this analysis.

iii. The tensile and shear cyclic fatigue tests described in Chapter 2 were simulated using FEA with grain-scale anisotropic elastic-plastic constitutive models obtained in Chapter 3. Cyclic strain range was extracted from FEA and compared with the experimental data. Finally, the upper and lower bounds of the fatigue constants were estimated, using the parametric variation of grain orientation, described above in Step (ii).

iv. Similar parametric grain-scale FEA-based variability assessment was conducted on BGA solder interconnect subjected to mechanical loading, to demonstrate the utility of this methodology.

5.2.Contributions

i. Tensile mode fatigue characterization of grain-scale solder joints along with its comparison with shear mode fatigue has been performed for the first time.

ii. Demonstrated the differences in failure modes and severity of fatigue damage in solder joints subjected to cyclic tensile vs. shear loads.

iii. Drawback of using the traditional Coffin-Manson fatigue model for modeling multiaxial fatigue in solder joints is demonstrated. A simple bi-modal multi-axial fatigue damage model, that accounts for damage contributions from deviatoric and hydrostatic strains, is developed.

iv. Demonstrated differences in solder joint elastic-plastic constitutive properties under shear vs. tensile monotonic loading modes for low and high aspect-ratio solder joints.

v. Monotonic tensile and shear stress-strain properties for monocrystalline SAC305 solder joints have been characterized in this study.

vi. Yield stress ratios for Hill's anisotropic yield criterion for SAC305 have been proposed using comparison between systematic parametric anisotropic grain-scale finite element study and experimental results.

vii. Differences in constitutive properties of SAC305 as a function of soldering cooling rates and grain sizes have been demonstrated. A methodology to scale

the constitutive stress-strain properties depending on the cooling rates and grain size has been presented and validated.

viii. Parametric sensitivity study has been developed to understand and quantify the stochastic variability in mechanical response of oligocrystalline solder joints because of grain anisotropy.

ix. The variability in fatigue damage predictions for oligocrystalline SAC305 solder joints due to grain anisotropy has been estimated using parametric grain-scale anisotropic FE analysis.

5.3.Limitations and Future work

i. The room temperature cyclic mechanical fatigue tests were conducted using a limited number of specimens. Expanding the current study with more samples can help in better calibration of the model. In addition, the cyclic mechanical fatigue tests at different strain rates, specimen aging conditions and test temperature is required for understanding the impact of tensile mode fatigue on functional solder joints in printed circuit assemblies.

ii. The cyclic mechanical fatigue tests in this study were conducted using a displacement control mode due to the current limitations of the test setup. However, fatigue tests are better conducted using strain control mode to maintain a constant strain level throughout the test. Therefore, further testing is suggested to validate the fatigue results obtained in this study.

iii. The multiaxial fatigue damage model proposed in this study uses hydrostatic strain term to estimate the interfacial damage. It should be noted that the power

law fatigue damage constants were only calibrated using hydrostatic strains at the interface. Hydrostatic strains in the bulk solder shouldn't be used for estimating bulk solder damage using the proposed model.

iv. The uniaxial monotonic tensile and shear tests were conducted on a limited number of SAC305 solder joint specimens in this study. Further testing is suggested to gather more data, which can help in better calibration of Hill's yield stress ratios and stress-strain curves.

v. The anisotropic Hill's yield strength ratios and Hill's stress-strain curves developed in this study were determined using a simple, easy to implement, manual, purely empirical ad hoc approach. Machine-learning based least square optimization methods may be used along with more experimental data to get better estimates of Hill's yield strength ratios. More accurate multi-scale crystal plasticity modeling should be implemented to determine the Hill's yield stress ratios and stress-strain curves.

vi. The anisotropic Hill's plastic stress-strain curves in this study were approximated to have a single power law dependence. This assumption turned out to have a limited accuracy in predicting the stress-strain behavior of solder joints. Therefore, the modeling strategy needs to be improved by using double power-law plasticity model.

vii. Christensen's 3-phase sphere model was used to determine the composite solder stress-strain curves. This model assumes spherical shapes for inclusions and was developed for isotropic materials. In contrast, β-Sn dendrites are ellipsoidal

in shape and anisotropic in nature. Similarly, the Sn matrix in the eutectic is not isotropic. Although the results achieved in this study were qualitatively reasonable, a more sophisticated computational anisotropic Mori-Tanaka homogenization approach can be explored for better accuracy in predicting composite solder stress-strain curves.

viii. The reinforcement strengthening due to Cu-Sn IMCs dispersed in Tier 2 is not accounted in this study due to the fact that- (a) Cu-Sn IMCs weren't observed in the bulk solder; (b) Cu-Sn IMCs are usually sparsely dispersed in bulk solder and are known to have minimal influence on the strengthening of the solder. Future study should investigate the effect of Cu-Sn IMCs on mechanical behavior of SAC305 solder.

ix. The EBSD was conducted on one of the surfaces of test specimen and not at different sections through the thickness. Therefore, grain structure through the thickness should be verified by rigorous cross-sectioning.

x. The hydrostatic stresses generated in the solder joint were found to differences in the yield strength of the solder joint, causing each solder joint to have different stress-strain relations. This needs to be examined further by modeling the solder joints using elastic-plastic properties that are dependent on the hydrostatic stress.

xi. The multiaxial fatigue damage model and grain-scale anisotropic plasticity models obtained in this study were calibrated using specimens made from unplated pure copper platens and SAC305 solder. Therefore, further

characterization with different solder materials, plating and platen materials is needed for expanding the usefulness of this model. In addition, the monotonic and fatigue characterization should also be expanded to include test parameters such as elevated temperatures and strain rates.

xii. The fatigue variability study only considers the stochastic variability due the grain anisotropy of solder joints. Sources of mechanical constitutive and fatigue variability other than grain orientation and microstructure should be better quantified.

APPENDICES

A1. Quantification of Microstructure using Image Processing

The differences in the solder microstructure resulting from variation in cooling rates during soldering and post-soldering aging duration were quantified using a commercial image processing software Image-Pro. The comparison of SEM images of different specimens presented in Figure 3-6, clearly showed variation in- a) Sn dendrite size; b) Ag_3Sn particle size and spacing and; c) Area fractions of Sn-dendrite and eutectic phases. Therefore, each SEM image was processed to measure these microstructural parameters which were used in the material models. The specimens were polished with 0.05µm colloidal silica suspension for 30-45 minutes to polish and slightly etch the surface to reveal Ag_3Sn IMC particles. Each SEM image was scanned at about 4500x magnification and saved in a high quality .tiff format, as the quality of the image is important for accuracy of measurements.

The SEM image is calibrated by setting scale provided at the bottom right side of each image. 'Smart Segmentation' tool was used to measuring the area fractions of Sn-dendrites and Ag_3Sn eutectic phase. At first, the tool is trained by manually locating the object region and the background region as a reference. The 'Smart Segmentation' tool then isolates the object regions from the background in the SEM image and measures the area of object regions in the image as shown in Figure 0-1.

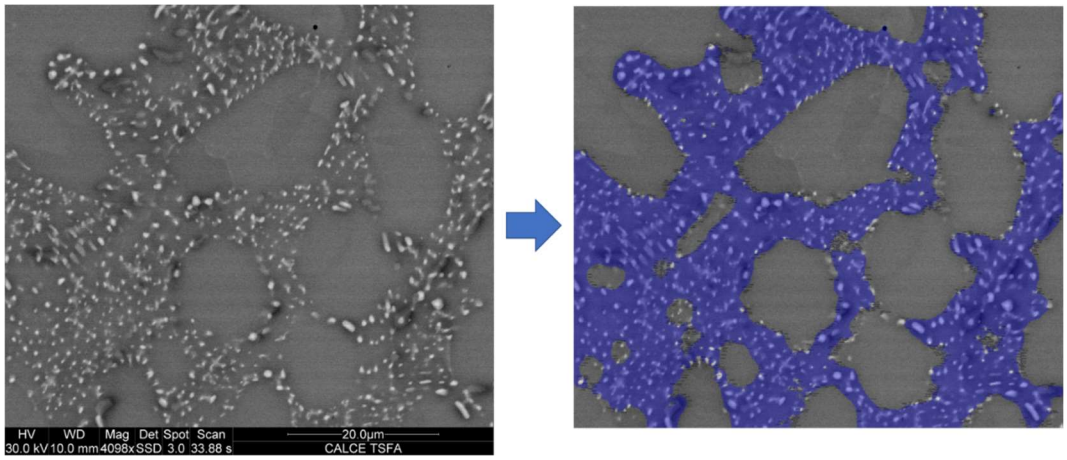

Figure 0-1 Segmentation of original SEM image to identify Ag-Sn eutectic region

The low-pass and watershed filters were applied to threshold and segment the image. Thresholding reduced the images to two intensity levels. This operation converted the gray-scale image to the binary image such that the background was changed to black and the Ag_3Sn particles were set to white as shown in Figure 0-2. The Ag3Sn particles were then selected and their size was recorded.

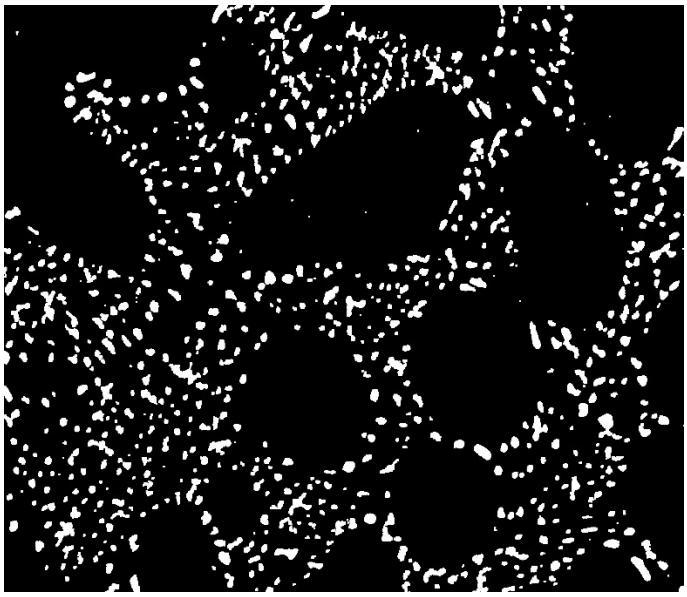

Figure 0-2 Isolation of Ag_3Sn particles using different filters

A Voronoi diagram was used to quantify the spatial characteristic of Ag_3Sn particles such as particle spacing. As shown in Figure 0-3, the Voronoi diagram divides the image into different regions (Voronoi cell) surrounding the reference object (Ag3Sn particles). Each cell consists of set of point that are closest to the object than to other object. Minimum center to center distance between each object can be extracted using this tool. The circular regions represent the corresponding distance between the Ag3Sn particle and its closest neighbor.

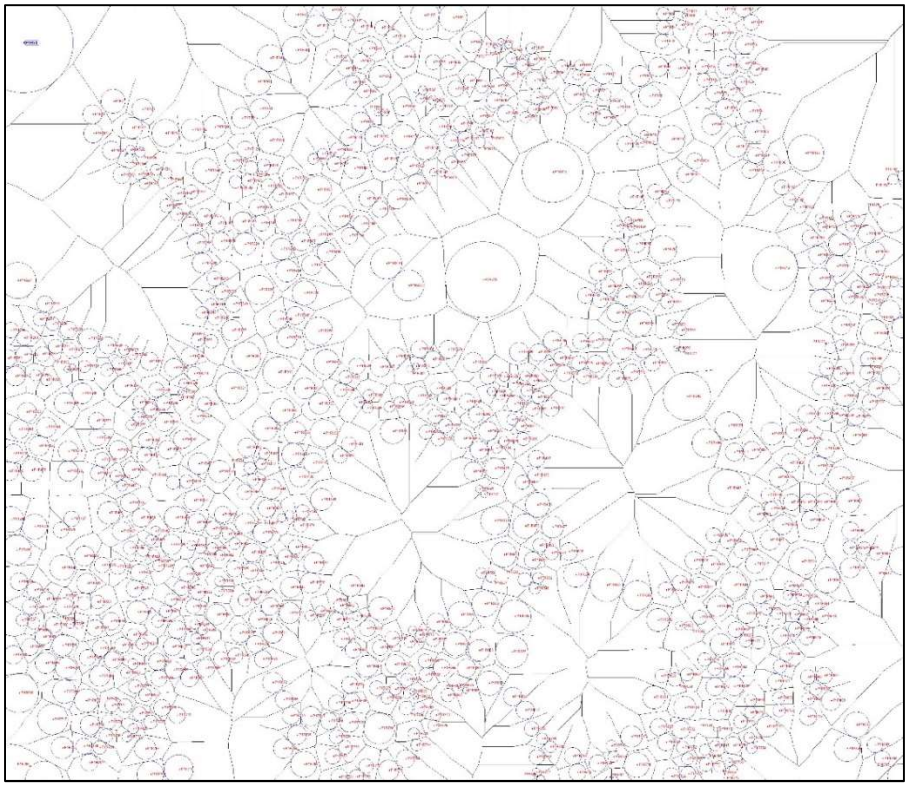

Figure 0-3 Voronoi diagram to measure center to center distance of Ag3Sn particles

A2. MATLAB Code to Convert Euler Angles to Abaqus Coordinate System

```
%%%%%%%%%%% Code to determine input coordinates for a point on X axis
%%%%%%%%%%% and a point in new xy plane using euler  angles zxz from ebsd
clc
clear all
eulergngles = [79.4, 135.0, 129.7];
angz = eulergngles(1)*pi/180;
angx = eulergngles(2)*pi/180;
angz1 = eulergngles(3)*pi/180;
Rz = [cos(angz) sin(angz) 0; -sin(angz) cos(angz) 0; 0 0 1];
Rx = [1 0 0; 0 cos(angx) sin(angx); 0 -sin(angx) cos(angx)];
Rz1 = [cos(angz1) sin(angz1) 0; -sin(angz1) cos(angz1) 0; 0 0 1];
% Rotated by 90deg clockwise...(counter-clockwise being positive)
Rz90 =[cos(-pi/2) sin(-pi/2) 0; -sin(-pi/2) cos(-pi/2) 0; 0 0 1];
```

```
Rotmat= Rz1*Rx*Rz;
x = Rz90'*Rotmat'*[1;0;0]
xy = Rz90'*Rotmat'*[1;1;0]
```

A3. MATLAB Code to Convert Euler Angles to Abaqus Coordinate System

```
%%%%% Estimate stress-strain curve of eutectic using 3-phase sphere model %%%%%%%%%%%%%%%%%%%%%%%%%%%%
%%%%%%%%%% 3-phase sphere model: inclusion:- B-Sn; matrix:- eutectic %%%%%%%%%%%%%%%%%%%%%%%%%%%%
clc
clear all
%% Volume Fraction of Sn dendrites %%%%%%%%%%
% a = 1;          % radius of inlusion
% b = 1.4;        % radius of matrix
a = 0.61;         % area fraction of inclusions (B-Sn dendrite) 0.61
c = (sqrt(a))^3;    % volume fraction of inclusions (B-Sn dendrite)

%% Import composite (experimental single xtal) hill's stress-strain data %%%%%%%%%%%%%%%% and inclusion (beta-Sn) hill's stress-strain data %%%%%%%%
strain1 = xlsread('D:\Abhishek Thesis\FEA\Grain size dependent stress-strain curves from FEA.xlsx','Pure Sn properties from kariya','G3:G50');  % inclusion (beta-Sn)
stress1 = xlsread('D:\Abhishek Thesis\FEA\Grain size dependent stress-strain curves from FEA.xlsx','Pure Sn properties from kariya','H3:H50');  % inclusion (beta-Sn)
strain2 = xlsread('D:\Abhishek Thesis\FEA\Grain size dependent stress-strain curves from FEA.xlsx','Scaling factor work_v3','n17:n77');  % composite (SAC305 xtal crystal)
stress2 = xlsread('D:\Abhishek Thesis\FEA\Grain size dependent stress-strain curves from FEA.xlsx','Scaling factor work_v3','s17:s77'); % composite (SAC305 xtal crystal)
si = 0:0.00005:0.003;

for i=1:length(si)
e = si(i);
stress_i(i) = interp1(strain1,stress1,e,'linear');
stress_c(i) = interp1(strain2,stress2,e,'linear');
end
stress_i = stress_i';
stress_c = stress_c';
strain_i = si';  % inclusion (beta-Sn)
strain_c = strain_i;  % composite (SAC305 xtal crystal)
```

```
%% Estimate eutectic stress-strain curve %%%%%
stress_m(1) = 0; % initial stress for matrix (eutectic)
i =1;
for i = 1 : (length (stress_i)-1)

   mu_i(i) = (stress_i(i+1)-stress_i(i))/(strain_i(i+1)-strain_i(i));   % Tangent modulus
of inclusion (beta-Sn)
   mu_c(i) = (stress_c(i+1)-stress_c(i))/(strain_c(i+1)-strain_c(i));        % Tangent
modulus of composite
   mu_m(i) =  (mu_i(i)+mu_c(i))/2;    % Initial guess of tangent modulus of matrix
(eutectic) (mu_i(i)+mu_c(i))/2

%     if (strain_i(i)>0.002)
       v_i = 0.5;      % Poisson's ratio of inclusion (beta-Sn) after yielding
       v_m = 0.5;      % Poisson's ratio of matrix (eutectic) after yielding
%     else
%        v_i = 0.35;     % Poisson's ratio of inclusion (beta-Sn) before yielding
%        v_m = 0.27;     % (Approximation) Poisson's ratio of matrix (eutectic) before
yielding
%     end
%
   j(i)=1; % initialize j

   while 1 %((mu(i) > (mu_c(i)-10000)) & (mu(i) < (mu_c(i)+10000)))

      eta1   =   (49-50*v_i*v_m)*((mu_i(i)/mu_m(i))-1)+35*(mu_i(i)/mu_m(i))*(v_i-
2*v_m)...
            +35*(2*v_i-v_m);
      eta2 = 5*v_i*((mu_i(i)/mu_m(i))-8)+7*((mu_i(i)/mu_m(i))+4);
      eta3 = (mu_i(i)/mu_m(i))*(8-10*v_m)+(7-5*v_m);

      A = 8*((mu_i(i)/mu_m(i))-1)*(4-5*v_m)*eta1*c^(10/3)...
         -2*(63*((mu_i(i)/mu_m(i))-1)*eta2+2*eta1*eta3)*c^(7/3)...
         +252*((mu_i(i)/mu_m(i))-1)*eta2*c^(5/3)...
         -50*((mu_i(i)/mu_m(i))-1)*(7-12*v_m+8*v_m^2)*eta2*c...
         +4*(7-10*v_m)*eta2*eta3;

      B = -2*((mu_i(i)/mu_m(i))-1)*(1-5*v_m)*eta1*c^(10/3)...
         +2*(63*((mu_i(i)/mu_m(i))-1)*eta2+2*eta1*eta3)*c^(7/3)...
         -252*((mu_i(i)/mu_m(i))-1)*eta2*c^(5/3)...
         +75*((mu_i(i)/mu_m(i))-1)*(3-v_m)*eta2*v_m*c...
         +(3/2)*(15*v_m-7)*eta2*eta3;
```

```
        C = 4*((mu_i(i)/mu_m(i))-1)*(5*v_m-7)*eta1*c^(10/3)...
            -2*(63*((mu_i(i)/mu_m(i))-1)*eta2+2*eta1*eta3)*c^(7/3)...
            +252*((mu_i(i)/mu_m(i))-1)*eta2*c^(5/3)...
            +25*((mu_i(i)/mu_m(i))-1)*(v_m^2-7)*eta2*c...
            -(7+5*v_m)*eta2*eta3;

        p = roots ([(A/(mu_m(i)^2)) (2*B/mu_m(i)) C]);

        mu(i) = p(p>=0);    % Estimated tangent modulus of composite

        if ((mu(i) > (mu_c(i)-10)) & (mu(i) < (mu_c(i)+10)))
            mu_m(i) = mu_m(i);
            break
        elseif ((mu(i)-mu_c(i))<10)
            mu_m(i) = mu_m(i)+ 2;
        elseif ((mu(i)-mu_c(i))>10)
            mu_m(i) = mu_m(i) - 2;
        end

        j(i) = j(i)+1;  % count iterations

    end

    strain_m = (strain_c + strain_i)/2;       % Eutectic (matrix) Strain
    stress_m(i+1) = stress_m(i) + mu_m(i)*(strain_m(i+1)-strain_m(i)); % Eutectic
(matrix) Stress
end
stress_m = stress_m';
```

Bibliography

[1] Anand, L (1985) Constitutive equations for hot-working of metals. International Journal of Plasticity 1(3): 213–231.

[2] Darveaux, R, Banerji, K (1992) Constitutive relations for tin-based-solder joints. In: *IEEE 42nd Electronic components and technology conference, ECTC 1992*, San Diego, CA, USA, 18–20 May, pp.538–551. USA: IEEE.

[3] Lee, Y, Basaran, C (2011) A creep model for solder alloys. Journal of Electronic Packaging 133(4): 044501.

[4] McDowell D, Miller M and Brooks D (1994) A Unified Creep-Plasticity Theory for Solder Alloys. Fatigue of Electronic Materials ASTM STP 1153: 42–59.

[5] Q. Jiang, A. Deshpande and A. Dasgupta, "Elastic Behavior of Coarse Grained SnAgCu (SAC) Solder Joints Based on an Anisotropic Multi-scale Predictive Modeling Approach", J. Electron. Mater., vol. 48, no. 12, pp. 8076-8088, 2019.

[6] R. Darveaux, "Shear deformation of lead-free solder joints," Proceedings Electronic Components and Technology, 2005. ECTC '05., Lake Buena Vista, FL, 2005, pp. 882-893 Vol. 1. doi: 10.1109/ECTC.2005.1441377

[7] J. H. L. Pang, Kwang Hong Tan, Xunqing Shi and Z. P. Wang, "Thermal cycling aging effects on microstructural and mechanical properties of a single PBGA solder joint specimen," in IEEE Transactions on Components and Packaging Technologies, vol. 24, no. 1, pp. 10-15, March 2001. doi: 10.1109/6144.910796

[8] H. Lau, John. (1991). Solder Joint Reliability: Theory and Applications. 10.1007/978-1-4615-3910-0.

[9] N. Fu, J. C. Suhling, S. Hamasha and P. Lall, "Evolution of the cyclic stress-strain and constitutive behaviors of SAC305 lead free solder during fatigue testing," 2017 16th IEEE Intersociety Conference on Thermal and Thermomechanical Phenomena in Electronic Systems (ITherm), Orlando, FL, 2017, pp. 1353-1360. doi: 10.1109/ITHERM.2017.7992639

[10] C. Andersson, Z. Lai, J. Liu, H. Jiang, Y. Yu, Comparison of isothermal mechanical fatigue properties of lead-free solder joints and bulk solders, Materials Science and Engineering: A, Volume 394, Issues 1–2, 2005, Pages 20-27, ISSN 0921-5093, https://doi.org/10.1016/j.msea.2004.10.043.

[11] S. Mukherjee, B. Zhou, A. Dasgupta, T.R. Bieler, Multiscale modeling of the anisotropic transient creep response of heterogeneous single crystal SnAgCu solder, International Journal of Plasticity, Volume 78, 2016, Pages 1-25, ISSN 0749-6419.

[12] T. R. Bieler, H. Jiang, L. P. Lehman, T. Kirkpatrick, E. J. Cotts and B. Nandagopal, "Influence of Sn Grain Size and Orientation on the Thermomechanical Response and Reliability of Pb-free Solder Joints," in IEEE Transactions on Components and Packaging Technologies, vol. 31, no. 2, pp. 370-381, June 2008.

[13] Zimprich P., Betzwar-Kotas A., Khatibi G., Weiss B., Isper H., J Mater Sci: Mater Electron (2008) 19: 383. https://doi.org/10.1007/s10854-007-9349-7.

[14] Ranieri, J.P., Lauten, F.S. & Avery, D.H. JEM (1995) 24: 1419. https://doi.org/10.1007/BF02655458

[15] Zhang Q.K., Zou H.F., Zhang Z.F. Journal of Electronic Materials (2009) 38: 852.

[16] Deshpande, A., Jiang, Q., Dasgupta, A., and Becker, U. (September 15, 2021). "Role of Nominal Stress State on Cyclic Fatigue Durability of SAC305 Grain-Scale Solder Joints." ASME. J. Electron. Packag. September 2022; 144(3): 031006. https://doi.org/10.1115/1.4051647

[17] Wang, S., Yao, Y. & Long, X. Size effect on microstructure and tensile properties of Sn3.0Ag0.5Cu solder joints. J Mater Sci: Mater Electron 28, 17682–17692 (2017). https://doi.org/10.1007/s10854-017-7706-8

[18] Darbandi, P., Bieler, T., Pourboghrat, F. et al. Crystal Plasticity Finite-Element Analysis of Deformation Behavior in Multiple-Grained Lead-Free Solder Joints. Journal of Elec Materi 42, 201–214 (2013). https://doi.org/10.1007/s11664-012-2339-4

[19] Bridgman, P. W., "Certain Physical Properties of single crystals of W, Sb, Bi, Te, Cd, Zn and Sn", Proc. Amer. Acad. Arts and Sciences 60 (1925) 305.

[20] J.A. Rayne and B.S. Chandrasekhar, Elastic Constants of β Tin from 4.2°K to 300°K, Phys. Rev. 120, 1658 (1960).

[21] M.A. Matin, W.P. Vellinga, M.G.D. Geers, Thermomechanical fatigue damage evolution in SAC solder joints, Materials Science and Engineering: A, Volumes

445–446, 2007, Pages 73-85, ISSN 0921-5093, https://doi.org/10.1016/j.msea.2006.09.037.

[22] Seungbae Park, Ramji Dhakal, Lawrence Lehman, Eric Cotts, Measurement of deformations in SnAgCu solder interconnects under in situ thermal loading, Acta Materialia, Volume 55, Issue 9, 2007, Pages 3253-3260, ISSN 1359-6454, https://doi.org/10.1016/j.actamat.2007.01.028.

[23] Park, S., Dhakal, R. & Gao, J. Journal of Elec Materi (2008) 37: 1139. https://doi.org/10.1007/s11664-008-0481-9

[24] B. Arfaei et al., "The effect of Sn grain number and orientation on the shear fatigue life of SnAgCu solder joints," 2008 58th Electronic Components and Technology Conference, 2008, pp. 459-465, doi: 10.1109/ECTC.2008.4550012.

[25] H. Xu, T. Lee and C. Kim, "Grain structure evolution and its impact on the fatigue reliability of lead-free solder joints in BGA packaging assembly," 2013 IEEE 63rd Electronic Components and Technology Conference, 2013, pp. 740-747, doi: 10.1109/ECTC.2013.6575655.

[26] G. Wei and L. Wang, "Effects of cooling rate on microstructure and microhardness of lead-free Sn-3.0Ag-0.5Cu solder," 2012 13th International Conference on Electronic Packaging Technology & High-Density Packaging, 2012, pp. 453-456, doi: 10.1109/ICEPT-HDP.2012.6474657.

[27] Lee, HT., Huang, KC. Effects of Cooling Rate on the Microstructure and Morphology of Sn-3.0Ag-0.5Cu Solder. Journal of Elec Materi 45, 182–190 (2016). https://doi.org/10.1007/s11664-015-4189-3

[28] M. Mueller, S. Wiese, M. Roellig and K. -. Wolter, "Effect of Composition and Cooling Rate on the Microstructure of SnAgCu-Solder Joints," 2007 Proceedings 57th Electronic Components and Technology Conference, 2007, pp. 1579-1588, doi: 10.1109/ECTC.2007.374006.

[29] Mutuku, F., Arfaei, B. & Cotts, E.J. The Influence of Processing on Strengthening Mechanisms in Pb-Free Solder Joints. Journal of Elec Materi 46, 2067–2079 (2017). https://doi.org/10.1007/s11664-016-5130-0

[30] Chauhan, P, Mukherjee, S, Osterman, M, Dasgupta, A, Pecht, M. "Effect of Isothermal Aging on Microstructure and Creep Properties of SAC305 Solder: A Micromechanics Approach." Proceedings of the ASME 2013 International Technical Conference and Exhibition on Packaging and Integration of Electronic and Photonic Microsystems. Burlingame, California, USA. July 16–18, 2013. V001T07A009. ASME. https://doi.org/10.1115/IPACK2013-73164

[31] M. M. Basit, M. Motalab, J. C. Suhling and P. Lall, "The effects of aging on the Anand viscoplastic constitutive model for SAC305 solder," Fourteenth Intersociety Conference on Thermal and Thermomechanical Phenomena in Electronic Systems (ITherm), 2014, pp. 112-126, doi: 10.1109/ITHERM.2014.6892272.

[32] N. Fu, J. C. Suhling, S. Hamasha and P. Lall, "Long term isothermal aging effects on the cyclic stress-strain behavior of Sn-Ag-Cu solders," 2017 16th IEEE Intersociety Conference on Thermal and Thermomechanical Phenomena in Electronic Systems (ITherm), 2017, pp. 1337-1345, doi: 10.1109/ITHERM.2017.7992637

[33] Fu, N, Wu, J, Ahmed, S, Suhling, JC, & Lall, P. "Investigation of Aging Induced Evolution of the Microstructure of SAC305 Lead Free Solder." Proceedings of the ASME 2017 International Technical Conference and Exhibition on Packaging and Integration of Electronic and Photonic Microsystems collocated with the ASME 2017 Conference on Information Storage and Processing Systems. ASME 2017 International Technical Conference and Exhibition on Packaging and Integration of Electronic and Photonic Microsystems. San Francisco, California, USA. August 29–September 1, 2017. V001T01A010. ASME. https://doi.org/10.1115/IPACK2017-74266

[34] J. Wu, J. C. Suhling and P. Lall, "Microstructural Evolution in SAC+X Solders Subjected to Aging," 2019 IEEE 69th Electronic Components and Technology Conference (ECTC), 2019, pp. 1087-1098, doi: 10.1109/ECTC.2019.00170.

[35] Zamiri, A., Bieler, T. & Pourboghrat, F. Anisotropic Crystal Plasticity Finite Element Modeling of the Effect of Crystal Orientation and Solder Joint Geometry on Deformation after Temperature Change. Journal of Elec Materi 38, 231–240 (2009). https://doi.org/10.1007/s11664-008-0595-0

[36] Jiang Q., “Anisotropic Multi-scale Modeling for Steady-state Creep Behavior of Oligocrystalline SnAgCu (SAC) Solder Joints,” PhD Dissertation, University of Maryland, College Park, MD, USA, 2021.

[37] Kariya, Y., Tajima, S., & Yamada, S. (2012). Influence of crystallographic orientation on fatigue reliability of β-Sn and β-Sn micro-joint. Materials Transactions, 53(12), 2067-2071. https://doi.org/10.2320/matertrans.MB201204

[38] Sasaki, T., Yanase, A., Okumura, D., Kariya, Y., Koganemaru, M., & Ikeda, T. (2019). Measurements and FEM analyses of strain distribution in small Sn specimens with few crystal grains. Materials Transactions, 60(6), 868-875. https://doi.org/10.2320/matertrans.MH201808

[39] Perkins, Andrew E., and Sitaraman, Suresh K. Solder Joint Reliability Prediction for Multiple Environments. Germany, Springer US, 2008.

[40] B. Métais, M. Kuczynska, A. Kabakchiev, S. Wolfangel, P. Buhl and S. Weihe, "Experimental and numerical investigation of fatigue damage development under multiaxial loads in a lead-free Sn-based solder alloy," 2016 17th International Conference on Thermal, Mechanical and Multi-Physics Simulation and Experiments in Microelectronics and Microsystems (EuroSimE), 2016, pp. 1-7, doi: 10.1109/EuroSimE.2016.7463378.

[41] P. Rajmane, Multi-Physics Design Optimization Of 2D And Advanced Heterogenous 3d Integrated Circuits, University Of Texas At Arlington, Texas, 2018.

[42] P. Rajmane, Chip Package Interaction Study To Analyze The Mechanical Integrity Of A 3-D TSV Package, University of Texas at Arlington, Texas, 2015.

[43] Daniel T Rooney, N Todd Castello, Mike Cibulsky, Doug Abbott, Dongji Xie, Materials characterization of the effect of mechanical bending on area array package interconnects, Microelectronics Reliability, Volume 44, Issue 2, 2004, Pages 275-285, ISSN 0026-2714, https://doi.org/10.1016/S0026-2714(03)00193-8.

[44] Liang, J., Downes, S., Dariavach, N. et al. Effects of load and thermal conditions on Pb-free solder joint reliability. Journal of Elec Materi 33, 1507–1515 (2004). https://doi.org/10.1007/s11664-004-0092-z.

[45] Haswell, P., “Durability Assessment and Microstructural Observations of Selected Solder Alloys,” PhD Dissertation, University of Maryland, College Park, MD, USA, 2001.

[46] A. Deshpande, Q. Jiang and A. Dasgupta, "A Joint-Scale Test Specimen for Tensile Properties of Solder Alloys," 2018 17th IEEE Intersociety Conference on Thermal and Thermomechanical Phenomena in Electronic Systems (ITherm), San Diego, CA, 2018, pp. 1309-1313. doi: 10.1109/ITHERM.2018.8419581

[47] A. Deshpande, H. Kaeser and A. Dasgupta, "Effect of Stress State on Fatigue Characterization of SAC305 Solder Joints," 2019 20th International Conference on Thermal, Mechanical and Multi-Physics Simulation and Experiments in Microelectronics and Microsystems (EuroSimE), 2019, pp. 1-3, doi: 10.1109/EuroSimE.2019.8724547.

[48] S. Mukherjee, A. Dasgupta, “An evaluation of a modified Iosipescu specimen for measurement of elastic-plastic-creep properties of solder materials,” , pp 159-161, May 2011, doi: https://doi.org/10.1007/978-1-4614-0213-8_24

[49] B. Arfaei et al., "Improving the thermomechanical behavior of lead free solder joints by controlling the microstructure," 13th InterSociety Conference on Thermal and Thermomechanical Phenomena in Electronic Systems, 2012, pp. 392-398, doi: 10.1109/ITHERM.2012.6231456.

[50] A. Deshpande, et.al, Fatigue Life of Joint-Scale SAC305 Solder Specimens in Tensile and Shear Mode, 2019 18th IEEE Intersociety Conference on Thermal and Thermomechanical Phenomena in Electronic Systems (ITherm), 2018.

[51] M. Kuczynska et al., "The role of stress state and stress triaxiality in lifetime prediction of solder joints in different packages utilized in automotive electronics," 2016 17th International Conference on Thermal, Mechanical and Multi-Physics Simulation and Experiments in Microelectronics and Microsystems (EuroSimE), Montpellier, 2016, pp. 1-10. doi: 10.1109/EuroSimE.2016.7463328.

[52] H. Ma, J. C. Suhling, Y. Zhang, P. Lall and M. J. Bozack, "The Influence of Elevated Temperature Aging on Reliability of Lead Free Solder Joints," 2007 Proceedings 57th Electronic Components and Technology Conference, Sparks, NV, USA, 2007, pp. 653-668, doi: 10.1109/ECTC.2007.373867.

[53] D. B. Barker, J. Vodzak, A. Dasgupta and M. Pecht, "Combined vibrational and thermal solder joint fatigue: A generalized strain versus life approach", Trans. Amer. Soc. Mech. Eng. J. Electron. Packag., vol. 112, pp. 129-134, Jun. 1990.

[54] S. Mukherjee, Multiscale Modeling of the Anisotropic Creep Response of SnAgCu Single Crystal, PhD Dissertation, University of Maryland, College Park, Maryland, USA, 2015.

[55] Lau, J.H.; Li, M.; Qingqian, M.L.; Chen, T.; Xu, I.; Yong, Q.X.; Cheng, Z.; Fan, N.; Kuah, E.; Li, Z.; et al. Fan-out wafer-level packaging for heterogeneous integration. IEEE Trans. Compon. Packag. Manuf. Technol. 2018, 8, 1544–1560.

[56] P. Rajmane, K. Dhandapani, M. Schwarz and A. Syed, "Investigation of the Factors Affecting the Warpage Prediction of Multi-Chip Package," 2021 IEEE 71st Electronic Components and Technology Conference (ECTC), 2021, pp. 1514-1520, doi: 10.1109/ECTC32696.2021.00240.

[57] B. Wu, Advancement of Moiré Interferometry For Rate-Dependent Material Behavior And Micromechanical Deformations, PhD Dissertation, University of Maryland, College Park, Maryland, USA, 2018.

[58] Bunge, H.J., 2013. Texture analysis in materials science: mathematical methods. Elsevier.

[59] Hill, R. (1950). The Mathematical theory of plasticity, by R. Hill. Oxford: The Clarendon Press.

[60] Christensen, R. M. (2005). Mechanics of composite materials. Mineola, N.Y: Dover Publications.

[61] Dieter, G. E., Mechanical Metallurgy, 3rd Edition, McGraw Hill, 1986.

[62] J.L. Chaboche, "Constitutive equations for cyclic plasticity and cyclic viscoplasticity", Int. Journal of Plasticity, pp. 247-302, 1989.

[63] P. Rajmane, Multi-Physics Design Optimization Of 2d And Advanced Heterogenous 3d Integrated Circuits, Arlington, Texas: University of Texas At Arlington, 2018.

[64] A. Deshpande, H. Khan, F. Mirza and D. Agonafer, "Global-local finite element optimization study to minimize BGA damage under thermal cycling," Fourteenth Intersociety Conference on Thermal and Thermomechanical Phenomena in

Electronic Systems (ITherm), Orlando, FL, USA, 2014, pp. 483-487, doi: 10.1109/ITHERM.2014.6892321.

[65] A. Syed, "Accumulated creep strain and energy density based thermal fatigue life prediction models for SnAgCu solder joints," 2004 Proceedings. 54th Electronic Components and Technology Conference (IEEE Cat. No.04CH37546), Las Vegas, NV, USA, 2004, pp. 737-746 Vol.1. doi: 10.1109/ECTC.2004.1319419

[66] Ghaffarian, R. (March 30, 2000). "Accelerated Thermal Cycling and Failure Mechanisms for BGA and CSP Assemblies." ASME. J. Electron. Packag. December 2000; 122(4): 335–340. https://doi.org/10.1115/1.1289627.

[67] Deshpande, A., Jiang, Q., Dasgupta, A., Constitutive Properties for Modeling Anisotropic Plasticity in Grain-Scale SAC305 Solder Joints: Part-1, 2022.

[68] K. Momma and F. Izumi, "VESTA 3 for three-dimensional visualization of crystal, volumetric and morphology data," J. Appl. Crystallogr., 44, 1272-1276 (2011).

[69] Jiang, Q.; Deshpande, A.N.; Dasgupta, A. Grain-Scale Anisotropic Analysis of Steady-State Creep in Oligocrystalline SAC Solder Joints. Materials 2021, 14, 5973. https://doi.org/10.3390/ma14205973

[70] A. Deshpande, Q. Jiang and A. Dasgupta, "Variability of Mechanical Cycling Durability of SAC305 Solder Joints: Model-Based Assessment using Grain-scale Modeling of Cyclic Shear Loading," 2021 22nd International Conference on Thermal, Mechanical and Multi-Physics Simulation and Experiments in

Microelectronics and Microsystems (EuroSimE), 2021, pp. 1-4, doi: 10.1109/EuroSimE52062.2021.9410828.